NTIS #

SSC-433

INTERACTIVE BUCKLING TESTING of STIFFENED STEEL PLATE PANELS

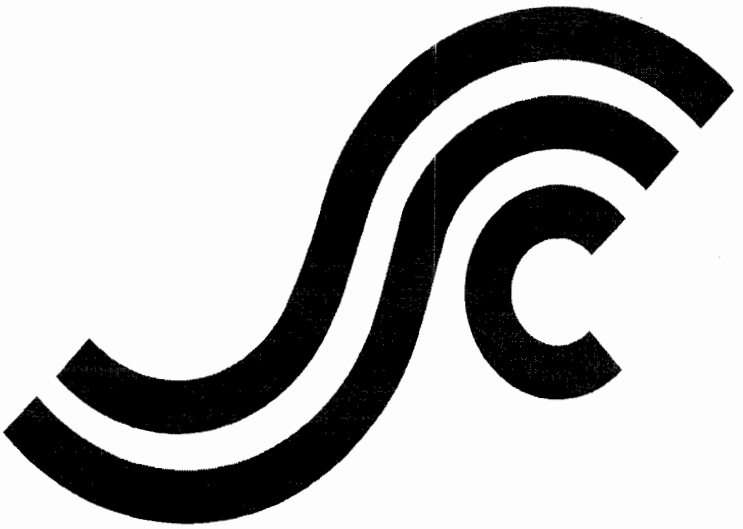

This document has been approved
For public release and sale; its
Distribution is unlimited

SHIP STRUCTURE COMMITTEE
2004

SHIP STRUCTURE COMMITTEE

RADM Thomas H. Gilmour
U. S. Coast Guard Assistant Commandant,
Marine Safety and Environmental Protection
Chairman, Ship Structure Committee

Mr. W. Thomas Packard
Director,
Survivability and Structural Integrity Group
Naval Sea Systems Command

Dr. Donald Liu
Senior Vice President
American Bureau of Shipping

Mr. Joseph Byrne
Director, Office of Ship Construction
Maritime Administration

Mr.Gerard A. McDonald
Director General, Marine Safety,
Safety & Security
Transport Canada

Mr. Thomas Connors
Director of Engineering
Military Sealift Command

Dr. Neil Pegg
Group Leader - Structural Mechanics
Defence Research & Development Canada - Atlantic

CONTRACTING OFFICER TECHNICAL REP.
Lieutenant Eric M. Cooper / Ms. Dinah Mulligan
U.S. Coast Guard R & D Center

EXECUTIVE DIRECTOR
Lieutenant Eric M. Cooper
U. S. Coast Guard

SHIP STRUCTURE SUB-COMMITTEE

AMERICAN BUREAU OF SHIPPING
Mr. Glenn Ashe
Mr. Yung Shin
Mr. Phil Rynn
Mr. William Hanzalek

DEFENCE RESEARCH & DEVELOPMENT ATLANTIC
Dr David Stredulinsky
Mr. John Porter

MARITIME ADMINISTRATION
Mr. Chao Lin
Mr. Carlos Setterstrom
Mr. Richard Sonnenschein

MILITARY SEALIFT COMMAND
Mr. Joseph Bohr
Mr. Rick A. Anderson
Mr. Michael W. Touma

NAVAL SEA SYSTEMS COMMAND
Mr. Jeffery E. Beach
Mr. Edward E. Kadala
Mr. Allen H. Engle
Mr. Charles L. Null

TRANSPORT CANADA
Mr. Jacek Dubiel

UNITED STATES COAST GUARD
Mr. Rubin Sheinberg
Mr. Robert Sedat
Commander Ray Petow

CANADIAN COAST GUARD
Mr. Daniel Gauvin

Member Agencies:

American Bureau of Shipping
Defence Research Development Canada
Maritime Administration
Military Sealift Command
Naval Sea Systems Command
Society of Naval Architects & Marine Engineers
Transport Canada
United States Coast Guard

Ship
Structure
Committee

Address Correspondence to:

Executive Director
Ship Structure Committee
U.S. Coast Guard (G-MSE/SSC)
2100 Second Street, SW
Washington, D.C. 20593-0001
Website: http://www.shipstructure.org

SSC – 433
SR – 1431

May 2004

INTERACTIVE BUCKLING TESTING OF STIFFENED STEEL PLATE PANELS

Interactive buckling is the interaction of two buckling modes, which results in reduced load carrying capacity of a design. The objectives of this project were to design and test stiffened plate specimens that are susceptible to interactive buckling, and collect experimental data to facilitate the development of design criteria that address interactive buckling.

Full-scale specimens that resembled stiffened plate panels in ship structures were fabricated using welded or hot-rolled T-stiffeners. A test matrix consisting of four test series was developed to examine the effect of bending moment, interaction index and damage on interactive buckling (interaction of plate buckling and overall column buckling).

An evaluation of existing design methods concluded that the load carrying capacity of a design under interactive buckling could be predicted using overall buckling strength calculations with a reduced plate width to account for the effect of plate buckling. An alternative design method that combines the reduced plate width and the Perry-Robertson beam-column equation was proposed. A comparison with test results shows that the alternative approaches give better predictions than current methods.

T. H. GILMOUR
Rear Admiral, U.S. Coast Guard
Chairman, Ship Structure Committee

CONVERSION FACTORS

(Approximate conversions to metric measures)

To convert from	to	Function	Value
LENGTH			
inches	meters	divide	39.3701
inches	millimeters	multiply by	25.4000
feet	meters	divide by	3.2808
VOLUME			
cubic feet	cubic meters	divide by	35.3149
cubic inches	cubic meters	divide by	61,024
SECTION MODULUS			
$inches^2$ $feet^2$	$centimeters^2$ $meters^2$	multiply by	1.9665
$inches^2$ $feet^2$	$centimeters^3$	multiply by	196.6448
$inches^4$	$centimeters^3$	multiply by	16.3871
MOMENT OF INERTIA			
$inches^2$ $feet^2$	$centimeters^2$ meters	divide by	1.6684
$inches^2$ $feet^2$	$centimeters^4$	multiply by	5993.73
$inches^4$	$centimeters^4$	multiply by	41.623
FORCE OR MASS			
long tons	tonne	multiply by	1.0160
long tons	kilograms	multiply by	1016.047
pounds	tonnes	divide by	2204.62
pounds	kilograms	divide by	2.2046
pounds	Newtons	multiply by	4.4482
PRESSURE OR STRESS			
$pounds/inch^2$	$Newtons/meter^2$ (Pascals)	multiply by	6894.757
kilo $pounds/inch^2$	mega $Newtons/meter^2$ (mega Pascals)	multiply by	6.8947
BENDING OR TORQUE			
foot tons	meter tons	divide by	3.2291
foot pounds	kilogram meters	divide by	7.23285
foot pounds	Newton meters	multiply by	1.35582
ENERGY			
foot pounds	Joules	multiply by	1.355826
STRESS INTENSITY			
kilo $pound/inch^2$ $inch^{1/2}$ ($ksi\sqrt{in}$)	mega Newton $MNm^{3/2}$	multiply by	1.0998
J-INTEGRAL			
kilo pound/inch	$Joules/mm^2$	multiply by	0.1753
kilo pound/inch	kilo $Joules/m^2$	multiply by	175.3

NOTICE

1. This Report was prepared as an account of work conducted at C-FER Technologies on behalf of the Ship Structure Committee. All reasonable efforts were made to ensure that the work conforms to accepted scientific, engineering and environmental practices, but C-FER makes no other representation and gives no other warranty with respect to the reliability, accuracy, validity or fitness of the information, analysis and conclusions contained in this Report. Any and all implied or statutory warranties of merchantability or fitness for any purpose are expressly excluded. The Ship Structure Committee acknowledges that any use or interpretation of the information, analysis or conclusions contained in this Report is at its own risk. Reference herein to any specified commercial product, process or service by trade-name, trademark, manufacturer or otherwise does not constitute or imply an endorsement or recommendation by C-FER.

2. Any authorized copies of this Report distributed to a third party shall include an acknowledgement that the Report was prepared by C-FER and shall give appropriate credit to C-FER and the authors of the Report.

3.

Technical Report Documentation Page

1. Report No.	2. Government Accession No.	3. Recipient's Catalog No.
4. Title and Subtitle Interactive Buckling Testing of Stiffened Steel Plate Panels		5. Report Date October 2003 6. Performing Organization Code S017
7. Author(s) Qishi.Chen, Ryan.S. Hanson, Gilbert. Y. Grondin		8. Performing Organization Report No. SR-1431
9. Performing Organization Name and Address C-FER Technologies, 200 Karl Clark Road, Edmonton, AB T6N 1H2, Canada		10. Work Unit No. (TRAIS) 11. Contract or Grant No. DTCG32-02-C-R0001
12. Sponsoring Agency Name and Address Ship Structure Committee U.S. Coast Guard (G-MSE/SSC) 2100 Second Street, SW Washington, D.C. 20593-0001		13. Type of Report and Period Covered Final Report 14. Sponsoring Agency Code G-M
15. Supplementary Notes Sponsored by the Ship Structure Committee. Jointly funded by its member agencies.		

16. Abstract

A test matrix consisting of four test series was developed to examine the effect of bending moment, interaction index and damage on interactive buckling, or the interaction of plate buckling and overall column buckling. Full-scale specimens that resembled stiffened plate panels in ship structures were fabricated using welded or hot-rolled T-stiffeners. Ten tests, including eight for "as-built" specimens and two for "damaged" specimens, were carried out in a high-capacity testing system. This unique system was developed during a previous SSC project (SSC-399) to study multiple buckling modes of stiffened plates under combined in-plane and out-of-plane loads, while maintaining an accurate representation of the boundary conditions applicable to a unidirectional stiffened plate within a grillage system.

In six tests of as-built specimens, plate buckling preceded and interacted with overall buckling. Overall bending and interaction of plate buckling and stiffener tripping were observed in the other two tests of as-built specimens. During the tests of two damaged specimens, pre-bending deformations caused a bending failure, and a web defect led to a sudden failure at the short section where the defect was located.

An evaluation of existing design methods concluded that the load carrying capacity associated with interactive buckling can be predicted based on overall buckling strength calculations that use a reduced plate width to account for the effect of plate buckling. An alternative design method that combines the reduced plate width and the Perry-Robertson beam-column equation was proposed. A comparison with test results shows that the alternative approach gives better predictions than the current methods.

17. Key Words Stiffened plate, buckling, testing, stability, design	18. Distribution Statement Distribution is available to the public through: National Technical Information Service U.S. Department of Commerce Springfield VA 22151 Tel. (703) 487-4650		
19. Security Classif. (of this report) Unclassified	20. Security Classif. (of this page) Unclassified	21. No. of Pages 83	22. Price $100,000

ACKNOWLEDGEMENTS

Mr. Nat Nappi of U.S. Naval Sea Systems Command (NAVSEA) represented the Project Technical Committee and provided guidance through the course of this project. In particular, his valuable contribution to the development of the test plan is greatly appreciated.

The authors would like to acknowledge the contribution of C-FER's Technical Services Department, in particularly Paul Erickson, Jennifer Strasser, Tim Roth, Richard Wayken and Raymond Christenson, for assembling the test set-up and data acquisition system, preparing the test specimens and conducting the tests.

TABLE OF CONTENTS

LIST OF ILLUSTRATIONS

LIST OF TABLES

LIST OF SYMBOLS

A	=	cross-sectional area of the stiffened plate
A_e	=	effective area of the stiffened plate
A_p	=	cross-sectional area of the plate
A_s	=	cross-sectional area of the stiffener
b	=	width of the plate
b_f	=	width of the flange
B_e	=	effective plate width
c	=	distance to the centroid
D	=	bending rigidity for a unit width of plate
e	=	axial load eccentricity
E	=	Young's modulus of elasticity
f	=	stress applied on the plate
f_{max}	=	overall buckling stress
f_u	=	ultimate buckling stress
F_{cr}	=	elastic buckling stress of the plate
F_e	=	elastic buckling stress of a column
F_y	=	yield stress of the plate
F_{yf}	=	yield stress of the flange
F_{ys}	=	yield stress of the stiffener
F_{yw}	=	yield stress of the web
h_w	=	height of the web
I_s	=	moment of inertia of the stiffener
k	=	plate buckling coefficient
K	=	effective length factor
L	=	length of the stiffened steel plate
l_u	=	unsupported length
M	=	bending moment
M_u	=	ultimate moment
P	=	applied axial force
P_{eu}	=	elastic overall buckling force

P_u	=	ultimate axial force
r	=	radius of gyration
r_e	=	radius of gyration of the effective cross-section
r_z	=	radius of gyration about the z-z axis
t	=	thickness of the plate
t_f	=	thickness of the flange
t_w	=	thickness of the web
u_1	=	maximum out-of-straightness deflection of the stiffener
u_2	=	maximum plate deflection from the best-fit plane
u_3	=	maximum torsional displacement of the web to flange junction
u_4	=	maximum out-of-straightness deflection of the web to plate junction
u_x	=	axial displacement
u_y	=	lateral in-plane plate displacement
u_z	=	lateral out-of-plane plate displacement
U_1	=	moment amplification factor
v	=	Poisson's ratio
Z_p	=	distance to the centroid of the effective cross-section of the plate mid-thickness
β_1	=	plate slenderness
γ	=	stiffness ratio between stiffener and plate
δ	=	initial deflection
θ_x	=	tangential rotation along the edge
θ_y	=	free out-of-plane flexural rotation
θ_z	=	in-plane rotation
λ	=	elastic plate slenderness ratio
$\bar{\lambda}$	=	dimensionless slenderness
λ_c	=	column slenderness ratio
ρ	=	effective width factor
σ_{max}	=	maximum stress

1. INTRODUCTION

1.1 Terms of Reference

This report summarizes the results of a project entitled "Experimental Identification of Non-Conservative Designs in Stiffened Steel Panels", which was carried out by C-FER Technologies (C-FER) for the Ship Structure Committee (SSC). The non-conservative designs refer to cases for which design checks based on individual buckling modes overestimate the load-carrying capacity due to the interaction of two buckling modes, or interactive buckling. The objectives of this project were to design and test stiffened plate specimens that are susceptible to interactive buckling, and collect experimental data to facilitate the development of design criteria that address interactive buckling.

1.2 Work Scope

Objectives of this project were accomplished by carrying out the following tasks:

- preparation of a test matrix and a detailed testing plan;
- acquisition and preparation of test specimens;
- measurement of initial imperfections, material properties and residual stresses;
- assembly of test set-up and instrumentation;
- execution of full-scale tests;
- analysis of test data;
- research of design methods; and
- preparation of a final report.

Ten full-scale tests were carried out using a unique, high-capacity testing system, which was developed during a previous SSC project (SSC-399) to study the buckling response of stiffened steel plates under combined in-plane and out-of-plane loads, while maintaining an accurate representation of the boundary conditions applicable to a unidirectional stiffened plate within a grillage system.

This report consists of six sections. Following this introduction section, Sections 2 to 5 deal with test specimens, test set-up, test results and design methods, respectively. The summary of findings is presented in Section 6.

1.3 Interactive Buckling of Stiffened Steel Plates

When the applied load is predominantly axial compression, the strength of a stiffened panel in ship structures is affected by three basic buckling modes: plate buckling, stiffener buckling (or tripping), and overall buckling, in which stiffener and plating buckle together like a beam-

column. Factors, such as the direction and magnitude of lateral load, cross-sectional geometry, material properties, boundary restraints, initial imperfections and residual stresses, influence which of the buckling modes governs.

In cases where the failure loads associated with two buckling modes are nearly identical, the interaction of two buckling modes may cause the structure to fail at a load level that is less than the lower of the two failure loads corresponding to individual buckling modes. In other cases where local buckling (e.g. plate buckling) precedes overall buckling, the capacity associated with overall buckling is likely to decrease due to the interaction of two buckling modes.

During project SSC-399, plate buckling and stiffener tripping were observed in "as-built" specimens which were representative of mid-section deck plates used in a frigate. This was expected according to the design of the specimen geometry and load combination (Chen et al. 1996). However, it was noticed during some tests that deformations associated with overall buckling increased significantly as the result of plate buckling. The interaction of different buckling modes suggested that interactive buckling could occur in stiffened panels with dimensions and materials that are typical of ship structures. Subsequent to SSC-399, such an interactive buckling mode was investigated analytically utilizing the finite element method, and then experimentally verified by Grondin et al. (2002).

The interaction of two buckling modes generally reduces the load-carrying capacity corresponding to a single buckling mode, as illustrated in Figure 1.1. The interaction of plate buckling and overall buckling reduces overall buckling capacity and could potentially lead to an unstable post-buckling behavior similar to the tripping of stiffener.

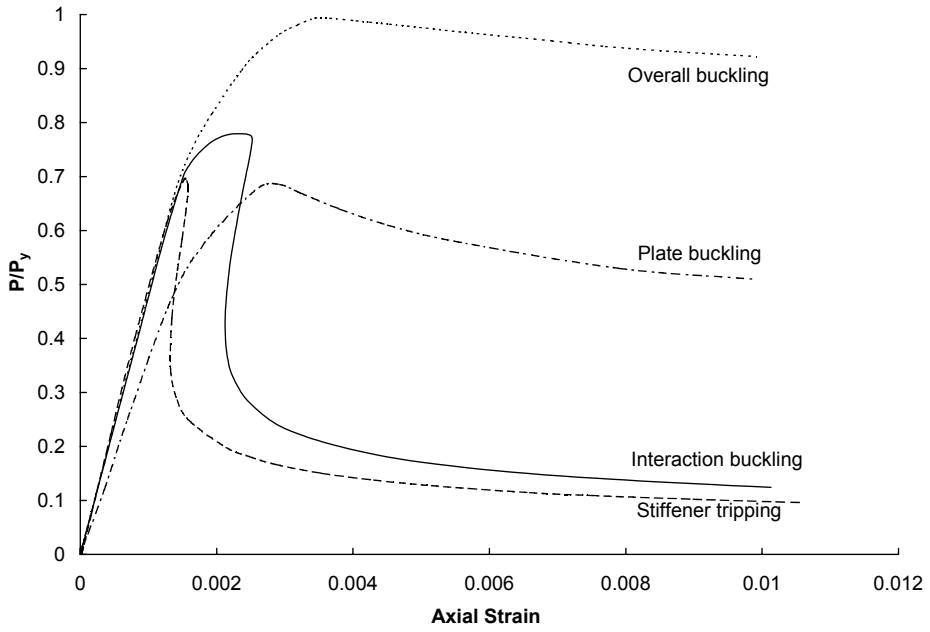

Figure 1.1 Load versus Displacement Responses of Various Buckling Modes

1.4 Tests at the University of Alberta

Using the boundary restraint apparatus developed in SSC-399, four stiffened steel plate panels were tested under axial compression at the University of Alberta (Grondin et al. 2002). Specimen dimensions and test results are summarized in Tables 1.1 and 1.2, with symbols for dimensions illustrated in Figure 1.2. As shown in Table 1.2, interactive buckling was observed in three of the four tests. Figure 1.3 shows that unstable post-ultimate behavior, represented by a sudden loss of load-carrying capacity, occurred in SSP2 due to stiffener tripping and in SSP3 and SSP4 due to interactive buckling.

Specimen	Plate			Web			Flange			Interaction Index
	b (mm)	t (mm)	F_y (MPa)	h_w (mm)	t_w (mm)	F_{yw} (MPa)	b_f (mm)	t_f (mm)	F_{yf} (MPa)	
SSP1	799	12.8	342	152	4.68	294	75	7.8	301	1.16
SSP2	569	9.5	407	88	2.91	202	38	6.2	331	1.53
SSP3	420	9.3	407	101	2.91	202	51	6.2	331	1.08
SSP4	500	12.6	342	126	3.21	285	63	7.8	301	1.00

Table 1.1 Dimensions of Specimens Tested at the University of Alberta

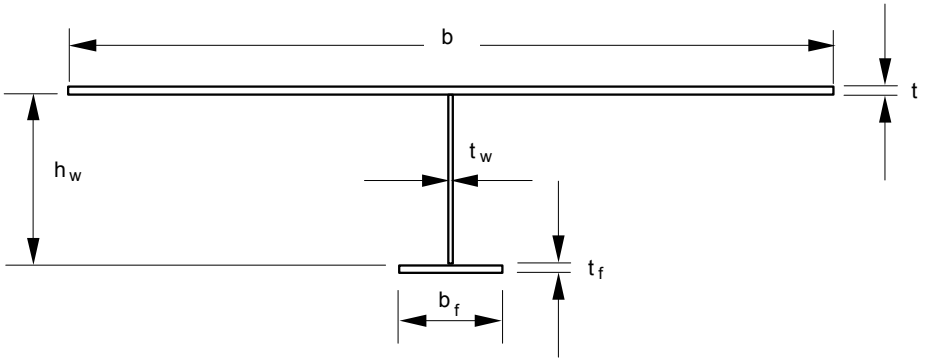

Figure 1.2 Test Specimen Dimensions

Specimen	Eccentricity (mm)	Peak load (kN)	Failure mode
SSP1	-10.0	1934	Interactive buckling
SSP2	+3.4	680	Stiffener tripping
SSP3	-5.0	1158	Interactive buckling
SSP4	-5.0	1866	Interactive buckling

Note: The plate is in flexural tension due to a positive eccentricity, and in flexural compression for a negative eccentricity

Table 1.2 Tests Results Reported by the University of Alberta

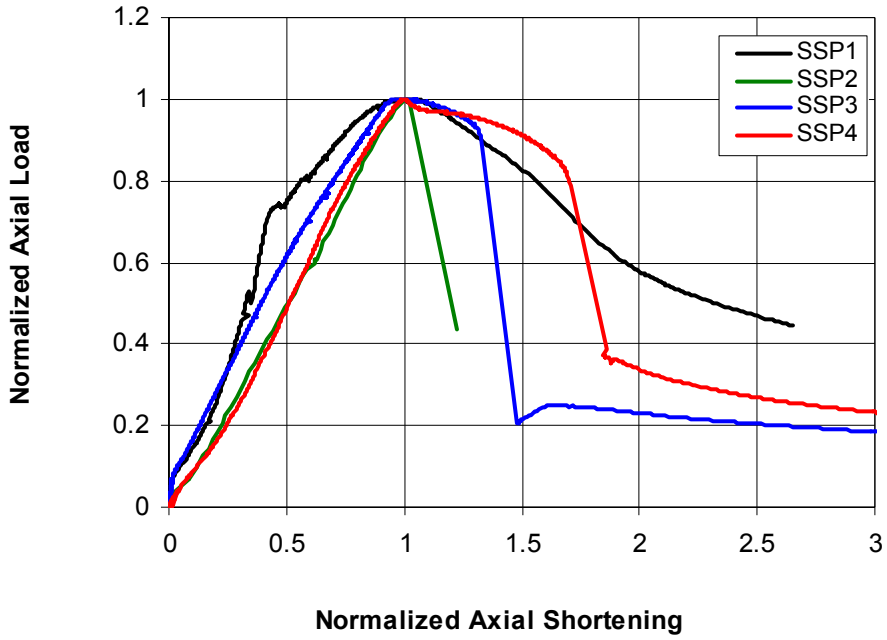

Figure 1.3 Load versus Displacement Response of University of Alberta Tests

The ability of design codes to predict the load-carrying capacity associated with interactive buckling was assessed by Sheikh et al. (2000) using finite element analysis results. It was found that the design equations for individual buckling modes presented in API Bulletin 2V (API 2000) and DNV Classification Note 30.1 (DNV 1995) were not able to offer reasonable predictions. By taking the capacity from the buckling mode that gave the least capacity as the capacity for interactive buckling failure, Sheikh et al. found that the codes gave very low capacities and a large scatter in comparison to finite element results. In their work, Sheikh et al. did not use the effective plate width provided by DNV to account for the reduced plate stiffness due to plate buckling, likely because the plate buckling load was nearly identical to the overall buckling load in those cases and plate buckling deformation was not evident at the failure.

1.5 Interaction Index

Based on an extensive investigation of stiffened plate buckling using a finite element model validated during project SSC-399, Sheikh et al. proposed an equation to define the condition for interactive buckling. Such a condition was characterized by the so-called interaction index. Interactive buckling is predicted to occur if this index is equal to or greater than 1.0, or

$$\text{Interaction index} = 0.5\,\beta_1 + 0.7\,\beta_4 - 3.6\,\beta_5 \geq 1.0 \qquad [1.1]$$

Non-dimensional parameters β_1, β_4 and β_5 are determined according to the geometry and yield stress of the stiffened plate panel:

$$\beta_1 = \frac{b}{t}\sqrt{\frac{F_y}{E}} \qquad [1.2]$$

$$\beta_4 = \frac{l_u t}{r_z b}\sqrt{\frac{F_{ys}}{F_y}} \qquad [1.3]$$

$$\beta_5 = A_s / A_p \qquad [1.4]$$

where

A_p = cross-sectional area of the plate;

A_s = cross-sectional area of the stiffener;

b = width of the plate;

E = Young's modulus of elasticity;

F_y = yield stress of the plate;

F_{ys} = yield stress of the stiffener;

l_u = unsupported length;

r_z = radius of gyration about the centroidal z-z axis of the stiffener; and

t = thickness of the plate.

Table 1.2 shows that interactive buckling occurred in specimens with an index value between 1.0 and 1.16, if a small eccentricity is applied towards the plate. It is noticed that specimen SSP2 failed by stiffener tripping despite an index value of 1.53. This was attributed to the eccentricity that was applied towards the stiffener. The connection between eccentricity and failure mode suggests that bending moment influences whether interactive buckling takes place, even though the effect of bending moment was not the focus of investigation in these tests.

2. TEST SPECIMENS

2.1 Test Matrix

In order to collect experimental data to study the interaction of local plate buckling and overall column buckling, a test matrix was constructed to guide the design of test specimens and the selection of load condition. The development of the test matrix focused on the effect of the following variables on interactive buckling:

- Bending moment. Stiffened plate panels in a ship structure are subjected to the combination of axial load and bending, which is caused by lateral loads and eccentricities associated with geometric imperfections and end restraint.
- Interaction index. The interaction index given in Equation [1.1] to define the condition of interactive buckling was verified by three tests at the University of Alberta. Further experimental verification is required for interaction index values outside the tested range.
- Structural damage. In-service ship structures may sustain structural damage due to localized metal loss defects (e.g. corrosion or erosion) or overall deformation (e.g. out-of-flatness of a plate, or out-of-straightness of a member). Interactive buckling of a damaged stiffened plate panel may differ from that of an as-built structure.

The previous tests at the University of Alberta described in Section 1.3 were under axial compression without lateral load, and the interaction index for the three specimens that failed by interactive buckling varied from 1.0 to 1.16 (Tables 1.1 and 1.2). In comparison, the test matrix developed for the current project introduced bending moment and structural damage as new variables, in addition to extending the interaction index beyond the 1.0 to 1.16 range.

Table 2.1 presents the test matrix developed to study the above-mentioned effects. As shown in the table, the test matrix consists of four series and each series consists of three new tests. This matrix allowed the effects of bending moment, interaction index and damage to be examined individually. Series SP-A and SP-B were designed to observe the effect of bending moment on two specimen designs corresponding to different interaction index values. Three tests in series SP-C were under axial compression without lateral load, and were expected to show the effect of interaction index in the range of 0.6 to 1.5. Finally, series SP-D was intended to examine interactive buckling of damaged specimens. In total, there were ten new tests. Some tests, such as SP-A1, are shown in more than one series since they are used to assess the effects of different variables.

Also included in Table 2.1 are three as-built specimens tested by C-FER during SSC-399 (SP1.1, SP1.2 and SP1.3), and three tests by the University of Alberta (SSP1, SSP3 and SSP4). All of these tests showed some form of interaction between local plate buckling and overall column buckling. SP1.1, SP1.2 and SP1.3 have the same design as the new SP-B specimens, but were subjected to different lateral loads varying from 0 to 25 kN. They were included in the SP-B series to assess the effect of bending moment. SP1.2 was the only specimen of the SP-B series that was tested in axial compression without lateral load. It was therefore included in series SP-C and SP-D where all specimens were axially loaded to study the effect of interaction index or damage, respectively. In addition, two damaged specimens tested in SSC-399 (SP3.1 with a

web defect and SP3.2 with two symmetric flange defects) were included in the SP-D series, because plate buckling interacted with overall buckling during these tests.

Series	Objective	New Tests	Previous Tests	Variable	Constant
SP-A	Assess bending moment effect for interaction index > 1.0	SP-A1, SP-A2, SP-A3	—	Bending moment	Same specimen design
SP-B	Assess bending moment effect for interaction index <1.0	SP-B1, SP-B2, SP-B3	SP1.1, SP1.2, SP1.3	Bending moment	Same specimen design
SP-C	Assess effect of interaction index	SP-C1, SP-C2, SP-A1	SP1.2, SSP1, SSP3, SSP4	Interaction index =0.6-1.5	All in axial compression
SP-D	Assess effect of previous damage	SP-DA, SP-DB, SP-A1	SP1.2, SP3.1, SP3.2	Damage	All in axial compression. Two designs (SP-A & SP-B).

Table 2.1 Test Matrix

2.2 Design and Fabrication

Figure 2.1 shows an isometric view of a typical test specimen and the test set-up used to apply axial and lateral loads. All specimens consisted of a 2000 x 500 mm plate with a T-stiffener welded along the centerline of the plate. Both ends of each specimen were welded to a 25 mm thick end plate to distribute the applied axial load. This configuration represents a single plate panel in a ship hull or deck element with multiple stiffeners, where the longitudinal edges match the centerlines between stiffeners, and both ends of the panel are bounded by grillage girders.

All test specimens were designed using variations of a basic geometry and material combination representative of stiffened plate panels used in ship structures. Dimensions and materials of the SP-B series, which were identical to the specimens used in SSC-399, were similar to a typical deck plate for the mid-section of a frigate (Chen et al. 1996). These dimensions were varied to form the SP-A and SP-C series to satisfy the required interaction index values and other design requirements.

Design of test specimens based on the test matrix was an iterative process that involved several preliminary designs based on available steel grades and plate thickness, as well as design checks to satisfy the requirements of achieving the desired failure mode. In order for the specimen to fail by interaction of plate buckling and overall buckling, the following design constraints were imposed:

- web and flange not to develop plate buckling;
- stiffener not to trip;
- plate buckling stress to be similar to overall buckling stress; and
- plate buckling to occur prior to yielding.

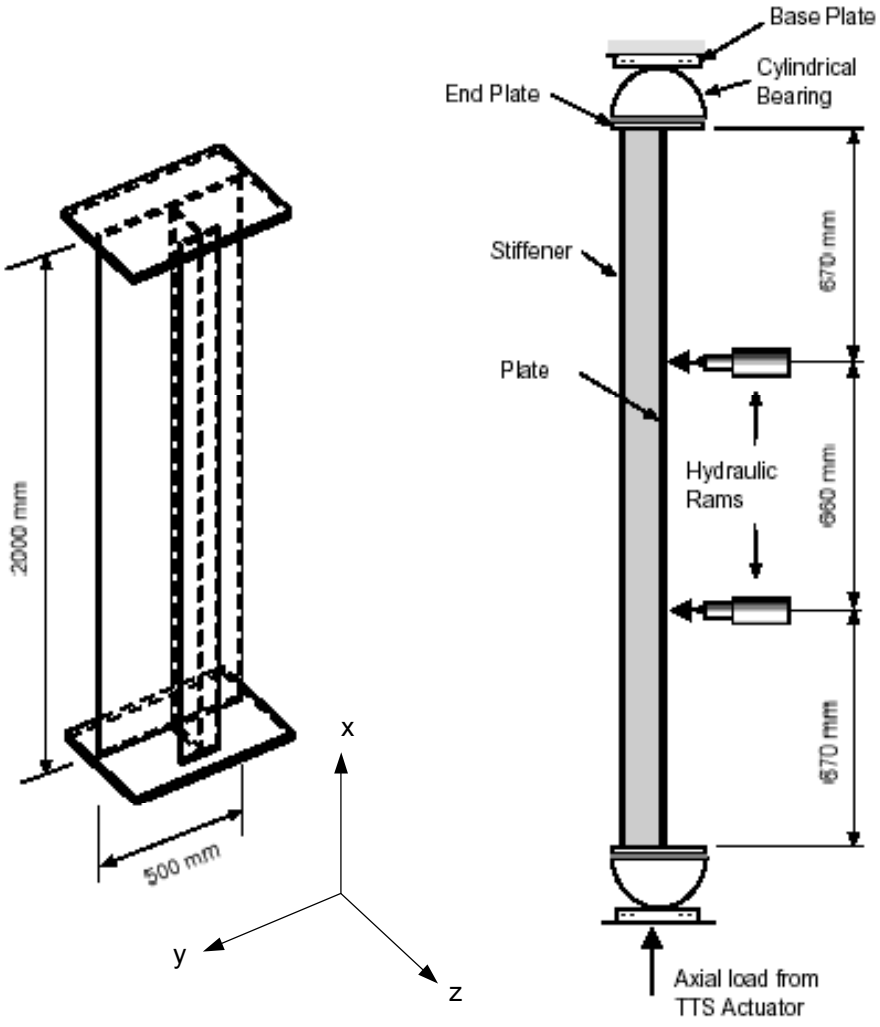

(a) Test Specimen **(b) Test Set-Up**

Figure 2.1 Schematic of Test Specimen and Set-Up

The first two constraints were intended to avoid undesirable buckling modes. The third constraint was to ensure that interaction between plate buckling and overall buckling would occur, in addition to checking the interaction index as defined in Equation [1.1]. The last constraint was intended to prevent excessive plate buckling deformation due to plasticity. Design checks were based on buckling stresses calculated using the DNV equations (DNV 1995).

Table 2.2 summarizes the geometry, lateral load and damage of all specimens based on the final design using actual plate thickness. The specimens were fabricated using hot-rolled structural steels with a specified minimum yield stress of 300 or 350 MPa. Stiffeners of the SP-A and SP-C series were made of two steel plates; but the SP-B series used a 127 x 102 mm structural tee as the stiffener. Specimen dimensions are shown in Figure 2.2.

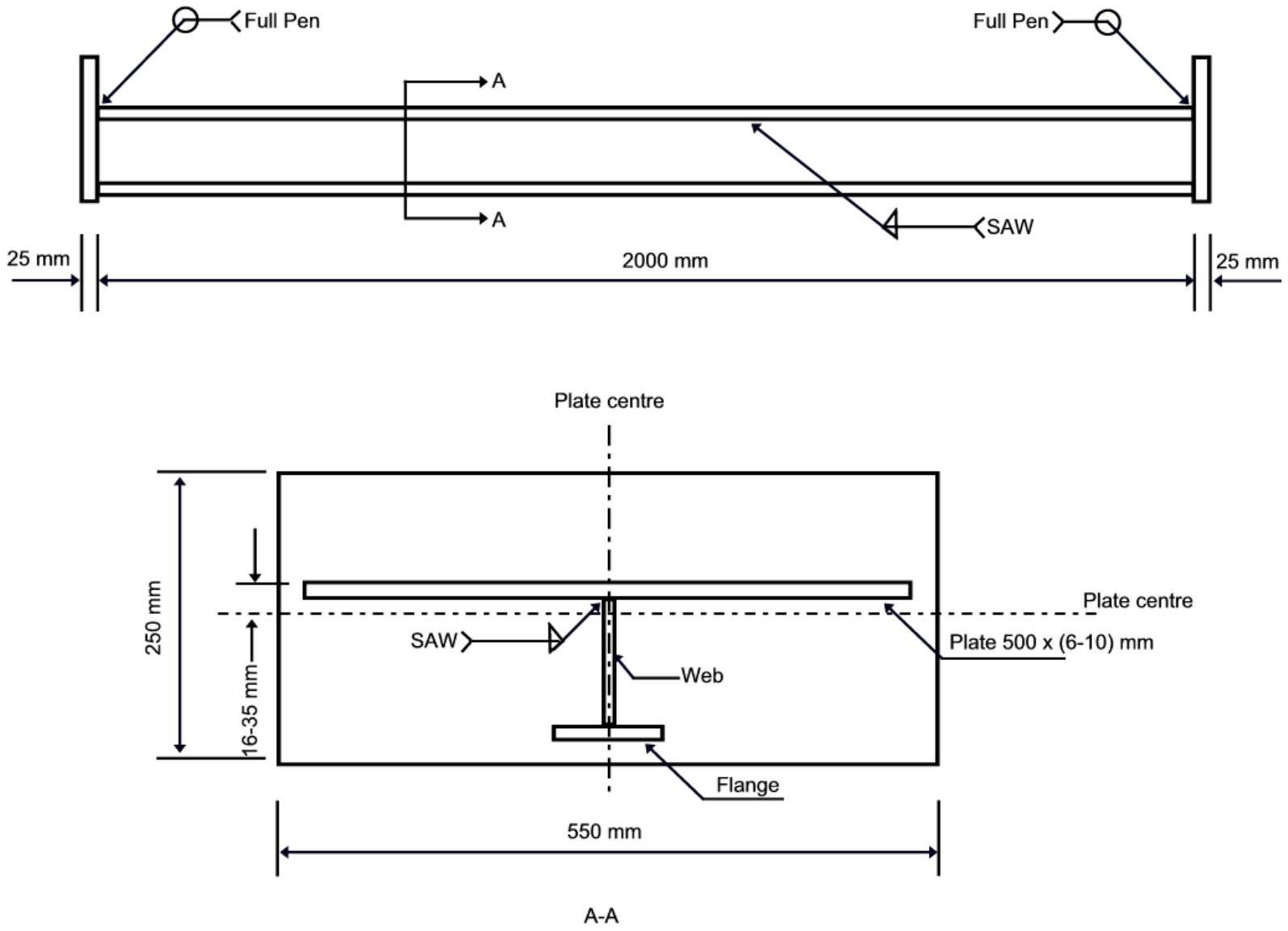

Figure 2.2 Schematic of Test Specimen

Specimen	Plate Size		Web Size		Flange Size		Interaction Index	Lateral Load (kN)	Damage
	b	t	h_w	t_w	b_f	t_f			
SP-A1	500	7.9	98	6.4	40	12.7	1.03	0	As-built. No damage
SP-A2	500	7.9	98	6.4	40	12.7	1.03	30	As-built. No damage
SP-A3	500	7.9	98	6.4	40	12.7	1.03	40	As-built. No damage
SP-B1	500	9.7	119	6.5	104	8.1	0.57	40	As-built. No damage
SP-B2	500	9.7	119	6.5	104	8.1	0.57	60	As-built. No damage
SP-B3	500	9.7	119	6.5	104	8.1	0.57	75	As-built. No damage
SP-C1	500	6.4	86	4.8	55	6.4	1.47	0	As-built. No damage
SP-C2	500	7.9	107	6.4	70	7.9	0.77	0	As-built. No damage
SP-DA	500	7.9	98	6.4	40	12.7	1.03	0	Metal loss defect in the web
SP-DB	500	9.7	119	6.5	104	8.1	0.57	40	Initial lateral deflection by pre-bending

Note: All dimensions are in mm.

Table 2.2 Final Design of Test Specimens

The magnitude of the lateral loads was selected so that the plastic bending moment capacity of the test specimen would not be exceeded without a significant axial compressive force and the associated P-δ effect. For the SP-B series, lateral loads between 40 and 75 kN were selected because smaller lateral loads (from zero to 25 kN) were tested in SSC-399.

Series SP-D consisted of two damaged specimens. Specimen SP-DA had the same geometry and material as the SP-A series, except for a machined through-the-thickness defect in the web (Figure 2.3). The defect location was chosen because it was more relevant to the interaction of plate buckling and overall buckling than other defect locations, based on test results from SSC-399. Specimen SP-DB was identical to SP-B1, except for pre-bending deformation that placed the plate in flexural compression.

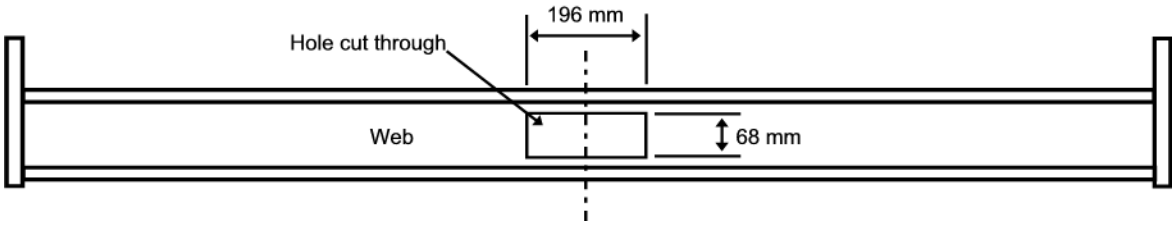

Figure 2.3 Design of Specimen SP-DA

The final designs shown in Table 2.2 met the requirements that failure modes other than plate and overall buckling would not take place. As shown in Table 2.3, stresses calculated based on the DNV equations indicated that these two buckling modes would occur at a similar load level.

In addition, plate buckling was expected to be elastic, as the associated buckling stresses were significantly lower than the specified yield stress.

Specimen	Specified Plate Yield Stress (MPa)	Local Plate Buckling Stress (MPa)	Overall Column Buckling Stress (MPa)
SP-A series	300	180	175
SP-B series	350	240	243
SP-C1	350	135	126
SP-C2	300	180	182

Table 2.3 Predicted Buckling Stresses Based on DNV (1995)

The test specimens were fabricated according to C-FER's specifications by a local steel fabricator. In order to ensure the welding quality and control geometric imperfections, the fabrication procedure was reviewed by C-FER and site visits were carried out during the fabrication.

In order to minimize plastic deformations and residual stresses along the plate edges, hydraulic jets were used to cut the steel plates. Prior to welding the web, the flange and plate were clamped together and tack welded to bracing members, such that the desired specimen configuration could be maintained during welding. A submerged arc welding procedure was used for the longitudinal welds, which were completed in stages on alternating sides of the web to prevent the distortion associated with consecutive welding on one side.

2.3 Initial Imperfections

Before being tested, all specimens except for SP-DB were comprehensively surveyed to determine the initial configuration within a global three-dimensional reference frame. Pre-deformed specimen SP-DB was not surveyed because the initial imperfections were insignificant compared to the imposed plastic deformations.

The measurement of initial geometric imperfections focused on the following deformations:

- out-of-flatness of the plate, which promotes local plate buckling;
- stiffener deflections perpendicular to the plate, which promotes overall buckling; and
- torsional deformation of the stiffener, which promotes stiffener tripping.

The measurement procedure employed a Nardini-SZ25120T lathe machine to provide a three-dimensional reference system. Electronic displacement gauges were mounted on the carriage of the lathe and traveled along gridlines on the specimen's surface to obtain a geometric profile. The measurement grid included nine longitudinal gridlines (five on the plate, two on the web, and two on the flange) intersected by twenty-two cross sections. The selected grid size was fine

enough to capture all significant imperfections that would influence plate buckling or other buckling modes.

The recorded data was later converted to the X-Y-Z coordinates of the mid-surface of the three plate components. A procedure was employed to find the best-fit plane of the plate. Out-of-plane deflections were then determined based on coordinates relative to the best-fit plane. Centroid positions based on the best-fit cross-sections were used for specimen alignment in the test set-up.

Figure 2.4 shows the plate imperfection profile for specimen SP-A1. The profiles for the other specimens are presented in Appendix A. Table 2.4 summarizes the analysis results of initial imperfections, with the following highlights as shown in Figure 2.5:

- maximum out-of-straightness deflection of the stiffener (u_1) was 4.7 mm;
- maximum plate deflection from the best-fit plane (u_2) was 4.2 mm;
- maximum torsional displacement of the web to flange junction (u_3) was 1.7 mm; and
- maximum out-of-straightness deflection of the web to plate junction (u_4) was 2.8 mm.

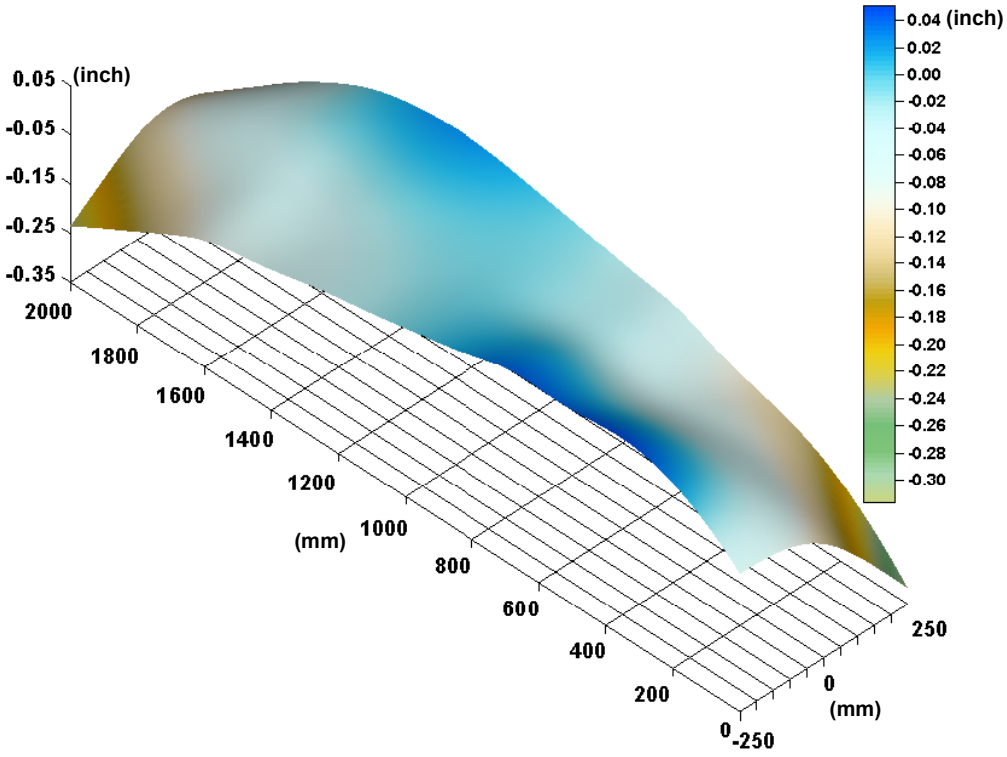

Figure 2.4 Initial Plate Profile of Specimen SP-A1

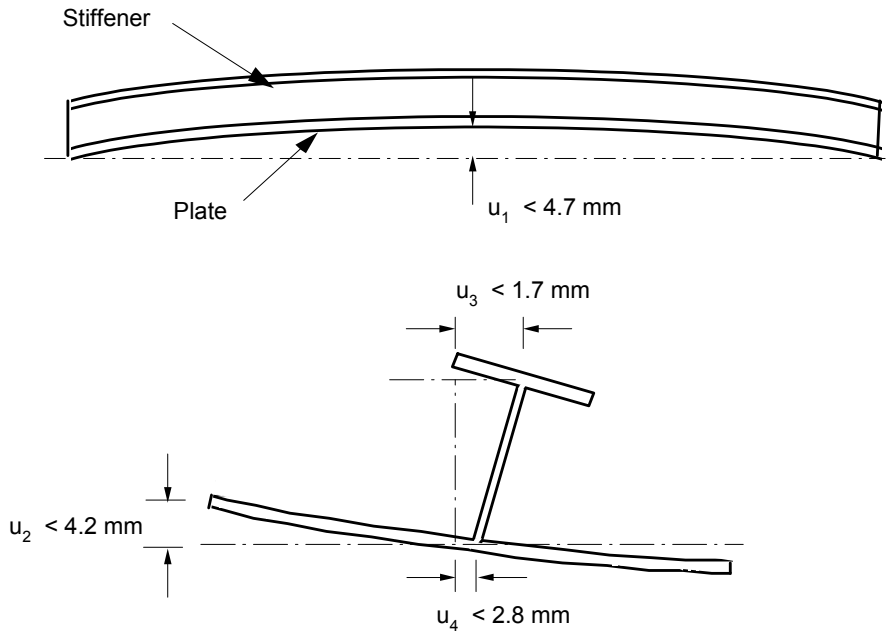

Figure 2.5 Maximum Imperfections

Specimen	u_1 (mm)	u_2 (mm)	u_3 (mm)	u_4 (mm)
SP-A1	-2.2 to -0.2	-4.9 to 2.1	0 to 0.7	-0.5 to 0.8
SP-A2	-0.5 to 0.6	-2.6 to 1.8	0 to 0.8	-0.4 to 0.9
SP-A3	-2.9 to -0.1	-4.9 to 1.4	0 to 0.8	-0.2 to 1
SP-B1	0.1 to 1.5	-4.3 to 1.7	0 to 1.1	0.2 to 1.7
SP-B2	0 to 1.8	-3.3 to 1.4	0 to 0.5	-5.2 to 1.6
SP-B3	-0.1 to 0.9	-3.9 to 1.2	0 to 0.5	0.3 to 3
SP-C1	-0.2 to 4.7	-2.4 to 4.2	0 to 0.7	-1.3 to 0.4
SP-C2	-0.4 to 4.6	-1.9 to 3.4	0 to 1.7	-4.9 to 1.4
SP-DA	-0.5 to 2	-3.3 to 2.3	0 to 1.7	-1.4 to 2.8

Table 2.4 Summary of Measured Initial Imperfections

2.4 Residual Stresses

Axial residual stresses primarily caused by welding were measured using a sectioning method and a mechanical extensometer. This procedure is based on the assumption that axial residual stresses are uniformly distributed through the thickness and along the length (except in the vicinity of the end plate), and will be released when a short section is cut into small longitudinal strips.

Measurements of the SP-A series specimens were made on a 350 mm long segment obtained from a full-size specimen fabricated using the same procedure. As shown in Figure 2.6, this short section was cut into 66 strips, after gauge marks were made on the surface of each strip. The distance between each pair of gauge marks was recorded before and after cutting, and the change in distance was used to determine the magnitude of the residual strain.

Measured axial strains were converted into axial stresses according to the elastic stress-strain relationship in a uniaxial stress condition. The results show that welded junctions had high tensile residual stresses, and the average compressive residual stress that spreads over the rest of the plate was approximately 37 MPa (Figure 2.7). Measured residual stresses in the web and the flange are shown in Figures 2.8 and 2.9. The magnitude and distribution of the residual stresses measured are considered representative for this type of welded structure.

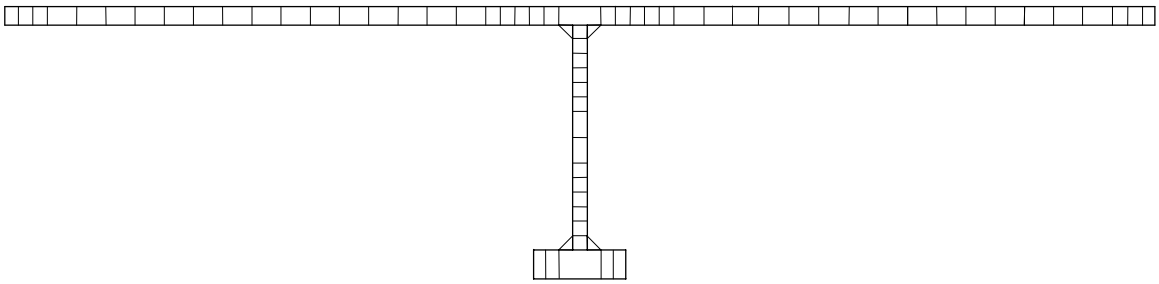

Figure 2.6 Section Pattern for Residual Stress Measurement

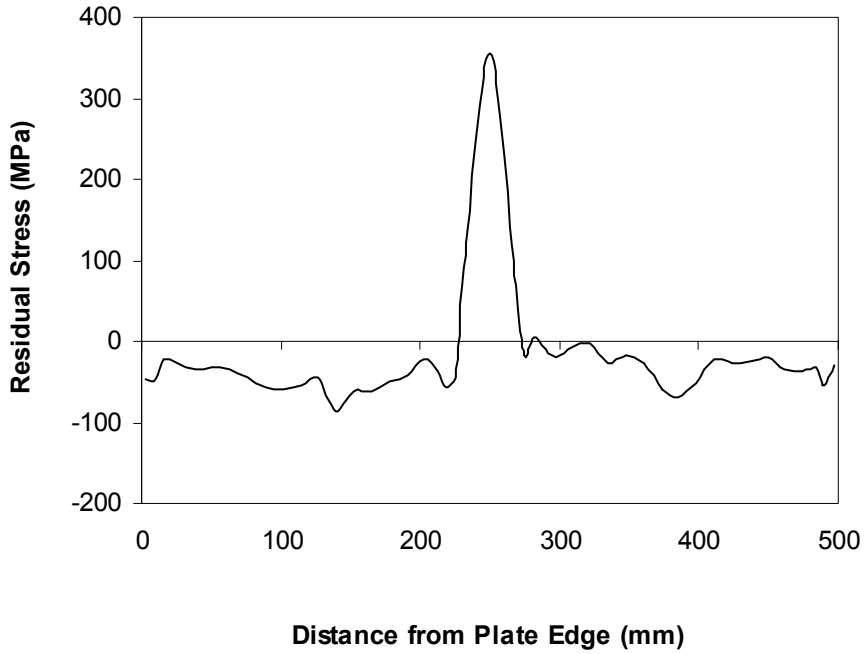

Figure 2.7 Residual Stress Distribution in the Plate

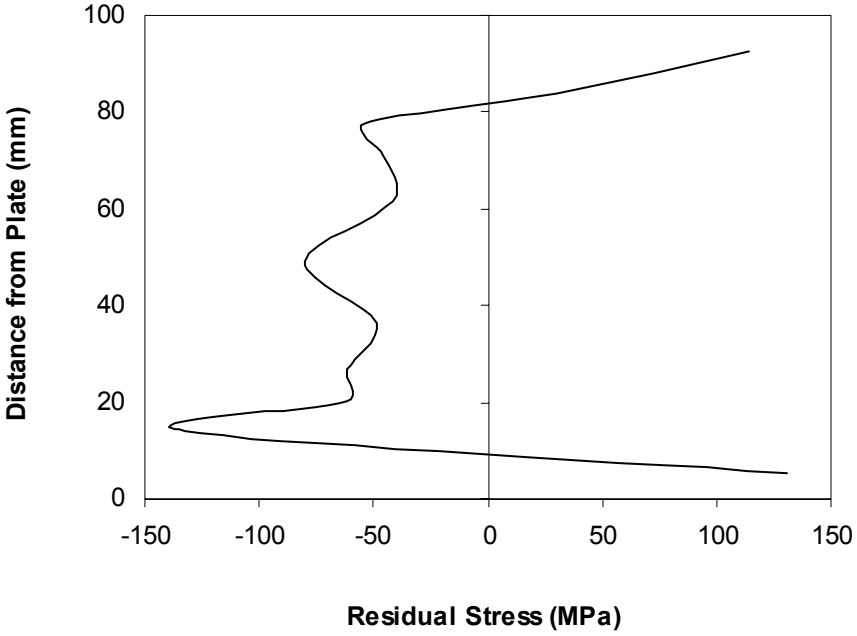

Figure 2.8 Residual Stress Distribution in the Web

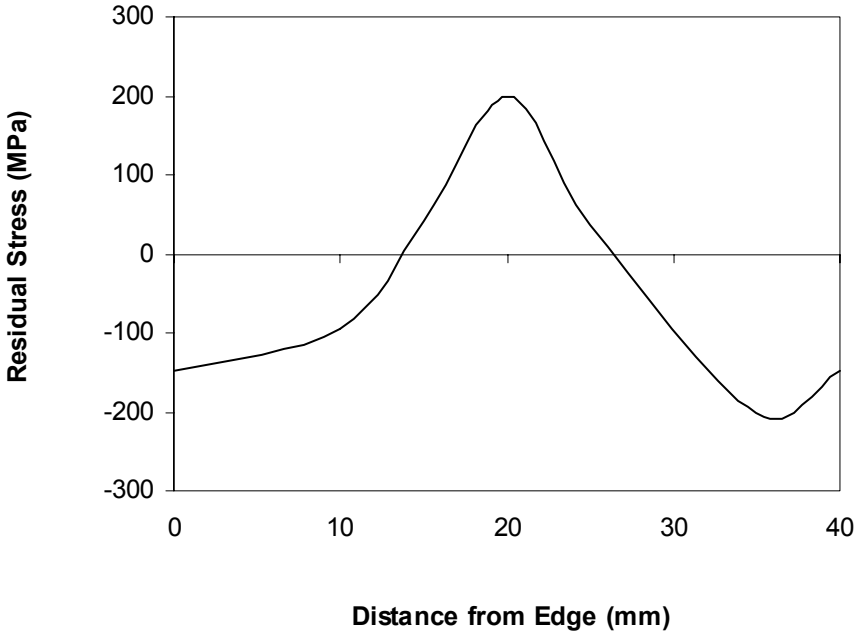

Figure 2.9 Residual Stress Distribution in the Flange

Residual stresses of an SP-B series specimen were measured during SSC-399 using a similar approach and are shown in Figure 2.10.

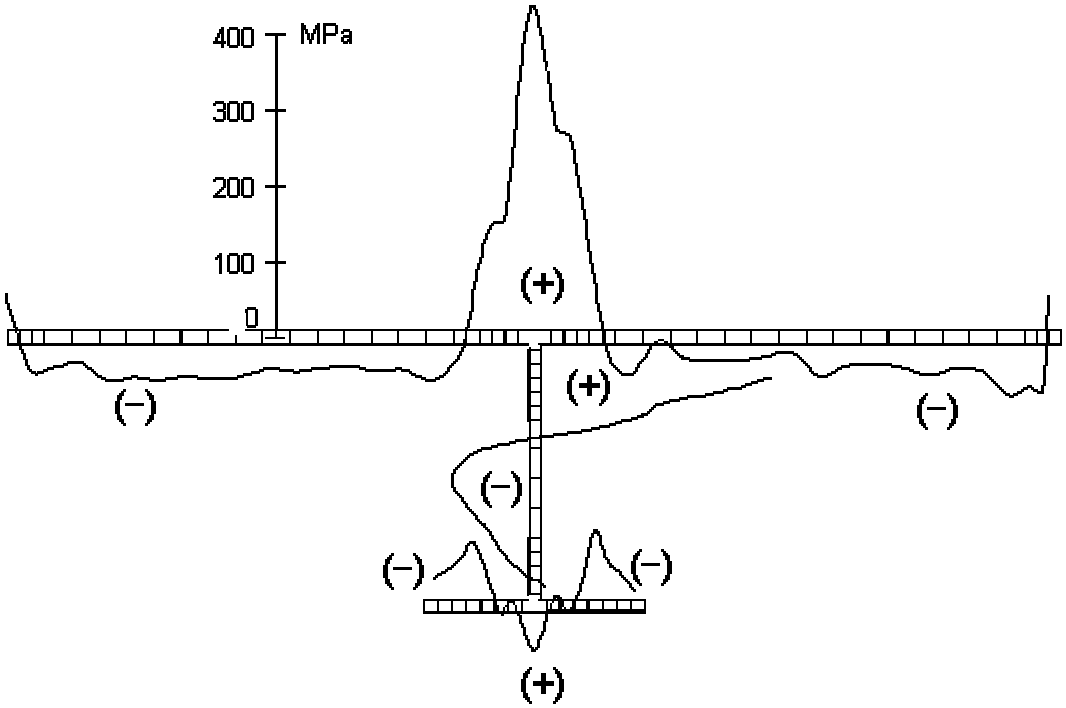

Figure 2.10 Residual Stresses Measured in SP-B Specimens

2.5 Material Properties

All specimens were made of hot-rolled structural steels with a specified minimum yield stress of 300 or 350 MPa. Tensile tests were conducted on coupons taken from the steel plates used to fabricate the test specimens. Table 2.5 summarizes average static yield stress and static ultimate tensile stress for the seven plate thickness used to fabricate the test specimens.

The stress versus strain curves are plotted in Figures 2.10 and 2.11. All stress-strain curves, except for the 12.7 mm plate used to make the flange of the SP-A specimens, show a distinctive yield plateau which is typical of hot-rolled steels.

Plate Sample	Application	Yield Stress (MPa)	Ultimate Tensile Stress (MPa)
4.8 mm plate	SP-C1 web	418	512
6.4 mm plate	SP-A web, SP-C1 plate & flange, SP-C2 web	399	517
6.5 mm plate	SP-B web	411	532
7.9 mm plate	SP-A plate, SP-C2 plate & flange	355	483
8.1 mm plate	SP-B flange	395	529
9.7 mm plate	SP-B plate	425	509
12.7 mm plate	SP-A flange	479	532

Table 2.5 Average Yield Stress and Ultimate Tensile Stress

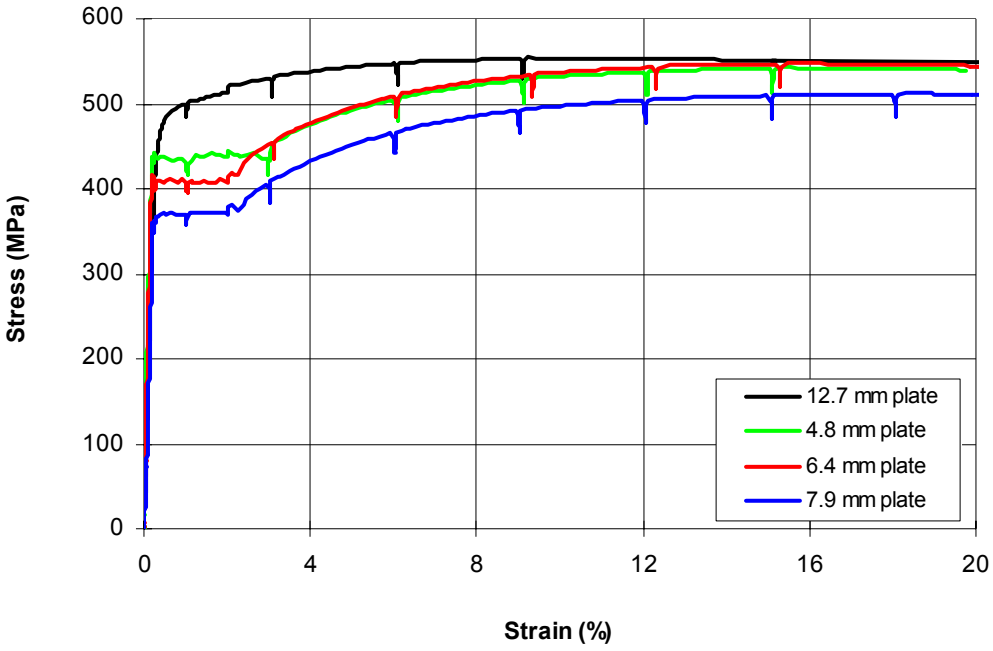

Figure 2.11 Stress-Strain Curves of SP-A and SP-C Specimens

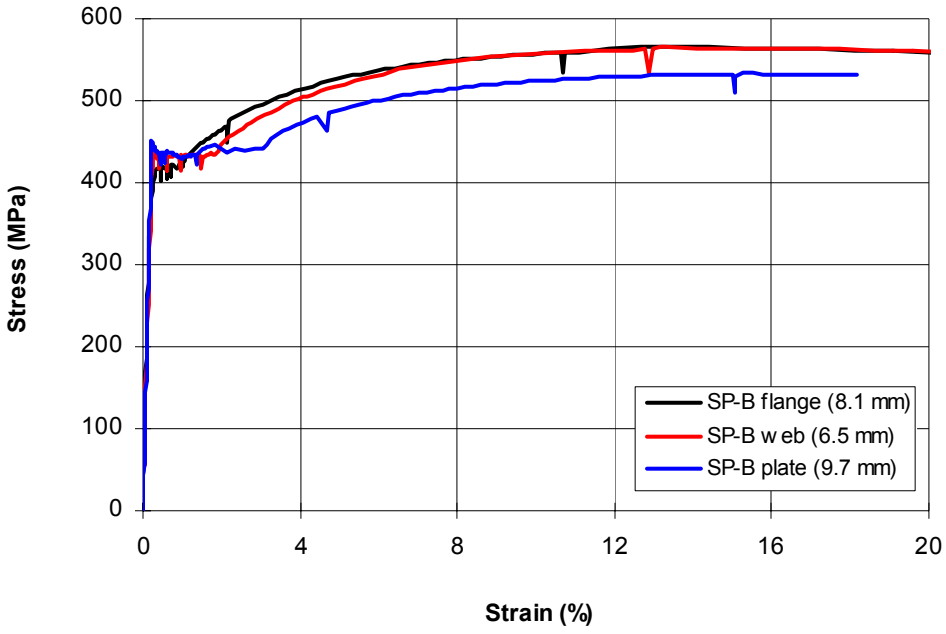

Figure 2.12 Stress-Strain Curves of SP-B Specimens

3. TESTING SYSTEM

3.1 Test Set-Up

All tests were carried out using a high capacity testing system developed during SSC-399 (Figure 3.1). The system was designed to study the multiple buckling modes of stiffened plates under combined in-plane and out-of-plane loads, while maintaining an accurate representation of the boundary conditions applicable to a unidirectional stiffened plate within a grillage system. This unique testing system consisted of several major components:

- the servo-hydraulic "TTS" testing machine to apply axial load;
- two hydraulic jacks attached to the back of the plate to apply lateral load;
- end fixtures to provide simple support at both ends; and
- a system of linear bearings and restraining devices to provide the required boundary conditions along plate edges.

The existing TTS (Tubular Testing System) at C-FER's laboratory is a high capacity testing system that has both axial and lateral load capabilities (Figure 3.2). The computer controlled servo-hydraulic loading system was manufactured by MTS Systems Corporation. It is integrated into a pre-stressed concrete strong wall, which provides lateral support to the steel rails that connect the upper and lower crossheads, and also serves as a reaction frame for lateral loading.

As shown in Figure 3.2, the test specimens were vertically positioned in the TTS. The TTS load actuator, located in the lower crosshead beneath the specimen, applied a compressive axial load. Lateral loads were applied at two points along the 2 m long span, using two hydraulic actuators fastened to the strong wall. The loading direction of the hydraulic actuators was reversible so that either the plate or the stiffener could be subjected to flexural compression. A servo-hydraulic control system connected to the lateral loading actuators enabled a constant force to be maintained throughout each test.

The end supports were designed to provide "pinned" connections; i.e. "simple" supports that do not restrict rotations. The design is similar to that previously used at Lehigh University for testing steel beam-columns (SSRC 1988). As shown in Figure 3.3, each support consisted of a half-cylinder bearing attached to the test specimen, and a thick base plate bolted to the TTS. Cement grout, placed between the specimen and the bearing, distributed contact stresses uniformly. As a specimen deformed, the cylindrical bearing rotated on the base plate, with the axial load always passing through the center of rotation (point O in Figure 3.3).

The design provided simple support boundary conditions to the test specimen, as both ends were free to rotate. Horizontal reactions were transferred through friction between the cylindrical bearing and the base plate.

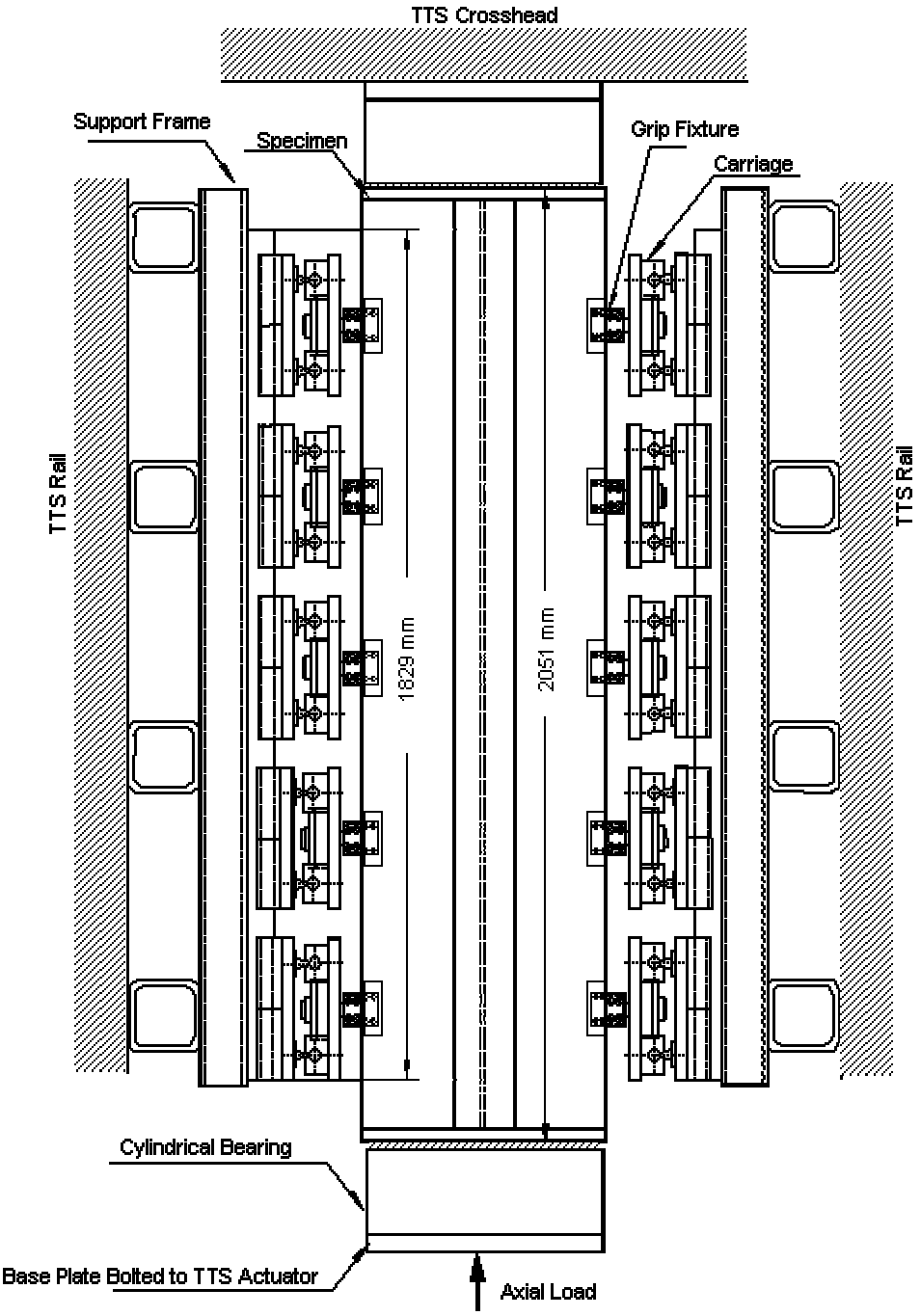

Figure 3.1 Stiffened Plate Testing System

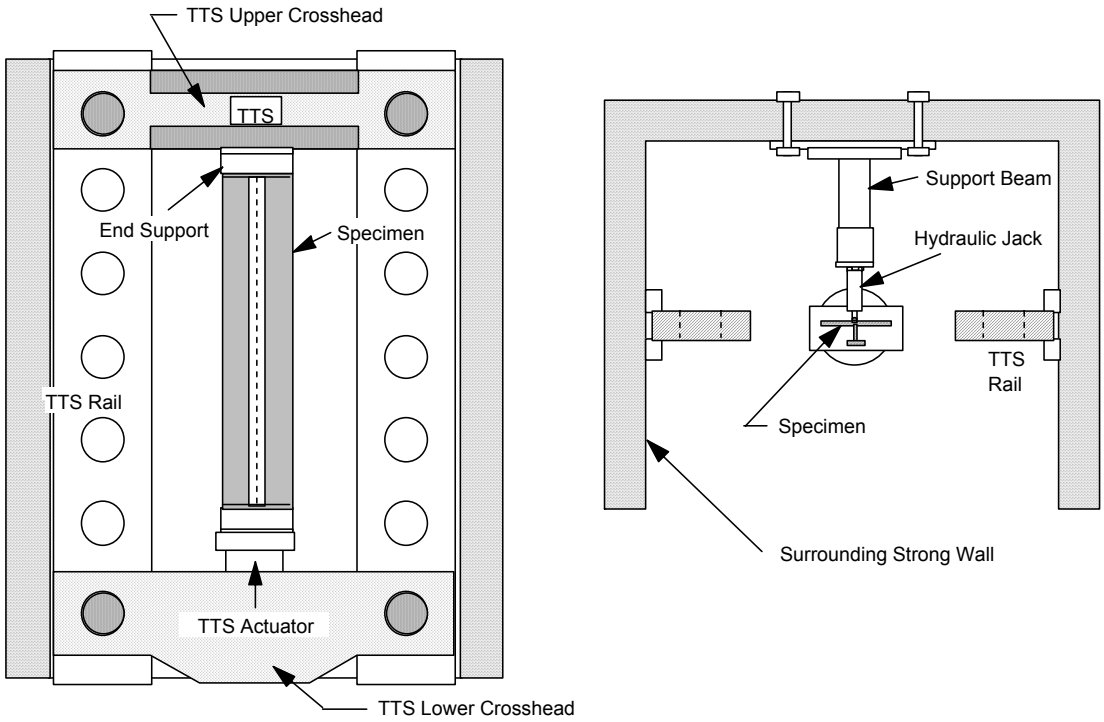

(a) Elevation View **(b) Plan View**

Figure 3.2 TTS Testing System
(without plate edge restraint system)

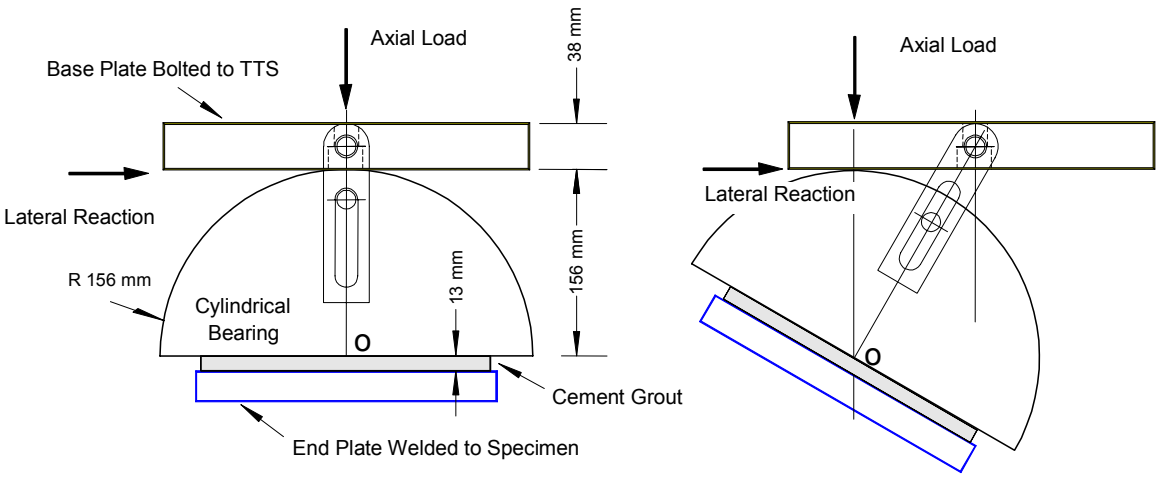

(a) Initial Configuration **(b) Deformed Configuration**

Figure 3.3 End Support

3.2 Plate Edge Restraints

Achieving proper boundary conditions along the unloaded edges of the stiffened plate specimens was considered an important aspect of the testing system, due to the influence of boundary conditions on buckling mode and failure load. For this reason, design and fabrication of the plate edge restrain system was given considerable attention during the previous project SSC-399.

Plate edge movements can be described in the coordinate system defined in Figure 3.4(a) with respect to the plate plane by three translational displacements (u_x, u_y and u_z) and three rotational displacements (θ_x, θ_y and θ_z). In order to duplicate the centerline between stiffeners in an actual ship structure, longitudinal edges of the test specimen should be restrained as symmetric boundaries, which allows free axial displacement (u_x), free lateral out-of-plane plate deflection (u_z), and free out-of-plane flexural rotation (θ_y). Lateral in-plane plate displacement (u_y), tangential rotation along the edge (θ_x), and in-plane rotation (θ_z) are restrained. Furthermore, numerical analysis using finite element models suggested that, in order to achieve the same buckling mode and failure load of a panel with continuously supported edges, at least four discrete supports were required at each side of the specimen.

As shown in Figure 3.1, the assembly of the plate edge restraint system developed for SSC-399 consisted of ten discrete supports (five on each side). The design used linear and angular spherical roller bearings to provide the required boundary conditions.

The design of the carriage is shown in Figure 3.4. Each carriage consisted of three major components:

- Carriage A traveled on shafts in the *x*-direction as the plate shortened under axial load. The shafts were approximately two meters long, extending the full length of the specimen.
- Carriage B traveled on shafts in the *z*-direction as the plate deflected out-of-plane. These shafts were fixed on Carriage A.
- Grip Fixture C held a 100 x 30 mm area of the plate edge to prevent the edge from rotating about an axis tangent to the plate edge. Rotation about the *y*-axis was free, since C was inserted into a pair of angular spherical roller bearings located at the center of Carriage B.

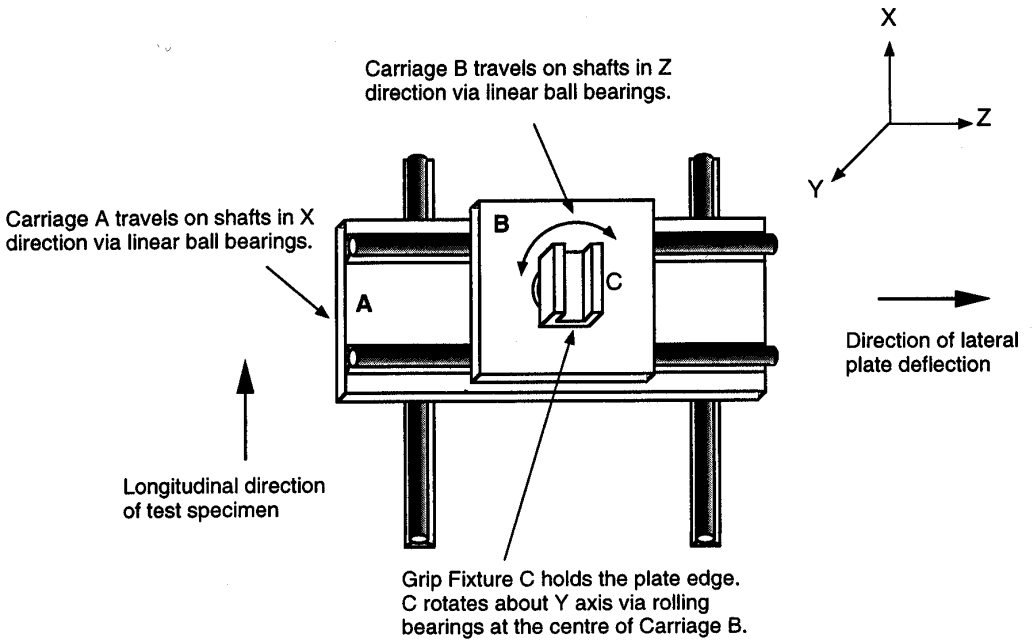

(a) Illustration of Design Concept

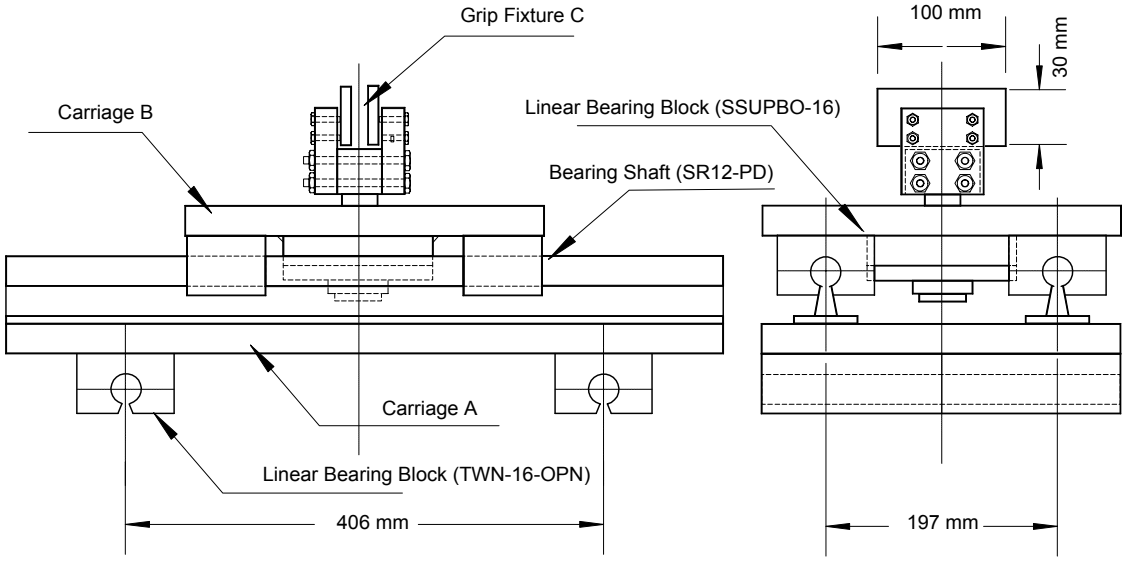

(b) Carriage Design

Figure 3.4 Plate Edge Restraint Carriage

3.3 Instrumentation

The instrumentation and data acquisition focused on the measurement of axial and lateral loads, and global displacements such as lateral deflections, axial shortening and end rotations. In addition, strain gauges were placed at the mid-span cross-section to detect plate buckling and to monitor axial strain distribution in the stiffener.

As shown in Figure 3.5, the instrumentation consisted of the following elements:

- eight displacement transducers for measuring end shortening, lateral deflection in the plane of the web, and torsional displacement of the stiffener;
- two rotation meters (clinometers) for measuring rotations at the simply supported ends;
- two load cells for measuring lateral loads (axial load was measured by the TTS piston pressure); and
- seven strain gauges for measuring axial strains at the mid-span cross-section.

At each load step beyond the elastic range, loads were held constant for two minutes prior to recording the data. This allowed the static response to be determined.

3.4 Test Procedure

Test specimen preparation involved pre-test measurements of specimen dimensions and initial imperfections, strain gauging, alignment in the TTS, and remaining instrumentation. To align specimens in the TTS, a geometrical method (SSRC 1988) was used, whereby reference coordinates were selected based on the three-dimensional configuration of the specimen, determined from pre-test measurements. This alignment method enabled the axial load to be applied through the centroid of the end cross-sections and parallel to the *x*-*y* plane (Figure 2.1), which was defined by the plate geometric survey as the mid-surface of the best-fit plane. Plate edge restraints and instruments were mounted on the specimen after it was positioned in the TTS.

The specimens were tested under axial compression, or the combination of axial compression and bending. For tests in which lateral loading was required, an axial load was applied prior to applying lateral loads to generate frictions at both ends. Lateral loads were then maintained at the prescribed level while applying axial load using displacement control, which permitted the post-ultimate strength response range to be captured.

After passing the ultimate load point, the test continued until axial shortening reached approximately 10 mm. This was deemed sufficient to adequately characterize the post-peak response.

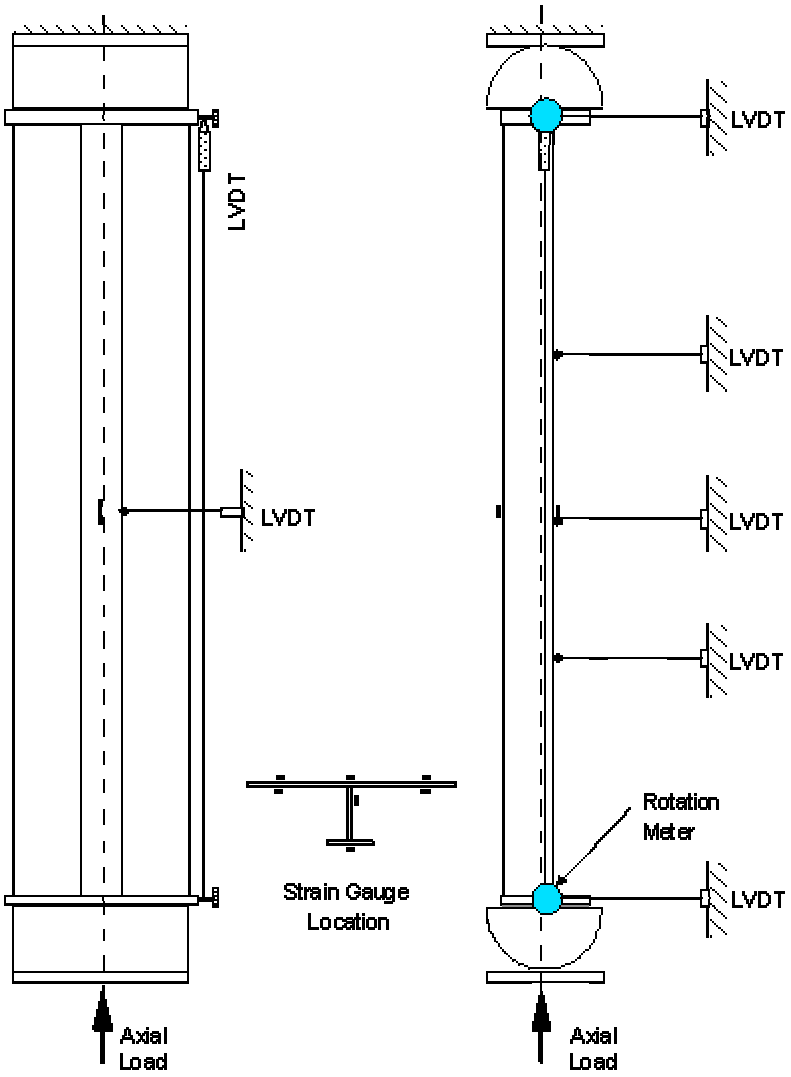

Figure 3.5 Instrumentation of Test Specimen

4. TEST RESULTS

4.1 Failure Mode

Table 4.1 presents the observed failure modes and test variables. The mid-section bending moment shown in the table is the uniform moment distributed between the lateral loading points. It is calculated using the constant lateral load and the shear span. This moment is the first-order design moment based on the undeformed configuration. Second-order moments related to factors such as the P-δ effect are not included.

Test	Interaction Index	Damage	Eccentricity (mm)	Lateral Load (kN)	Mid-Section Moment (kN-m)	Failure Mode
SP-A1	1.03	None	3 (1)	0	0	LPB + OCB(2)
SP-A2	1.03	None	0	30	25.9	LPB + OCB
SP-A3	1.03	None	0	40	34.6	LPB + OCB
SP-B1	0.57	None	0	41.5	35.7	LPB + OCB
SP-B2	0.57	None	0	61.9	53.2	LPB + OCB
SP-B3	0.57	None	0	73.8	63.5	Overall bending
SP-C1	1.47	None	0	0	0	LPB + OCB
SP-C2	0.77	None	0 (3)	0	0	LPB + Stiffener tripping
SP-DA	1.03	Web defect	3 (1)	0	0	LPB + Short section failure
SP-DB	0.57	Pre-bent	0	41	35.3	Overall bending

(1) The eccentricity toward the plate was intended to lessen stiffener compression and prevent stiffener tripping.

(2) LPB + OCB = Local plate buckling followed by overall column buckling.

(3) An undetected small eccentricity put the stiffener in flexural compression and caused stiffener tripping.

Table 4.1 Failure Mode and Test Variables

Interaction of local plate buckling and overall column buckling was observed in six of the eight tests of the as-built specimens. Plate buckling occurred in specimens SP-C2 and SP-DA before ultimate failure by other modes. Interaction of plate buckling and other failure modes in all four groups indicates that interactive buckling could take place at various levels of bending moment and interaction index, as well as in locally damaged specimens.

The development of buckling waves in the plate and the interaction with overall buckling followed a similar pattern. Generally, local plate buckling waves first appeared at the mid-span with a half wave on each side. As the axial load continued to increase, plate buckling waves amplified while the wave length shortened. With the increase of axial load, additional waves became visible. However, as the specimen developed overall buckling, plate buckling waves away from the mid-span gradually diminished. At the end of the test, the specimen exhibited large deformations due to the overall buckling. Plate buckling waves away from the mid-span were no longer noticeable.

Table 4.2 summarizes the characteristic loads that represent the load carrying capacity of the test specimens. The loads are static values recorded after the displacements had been held constant for two minutes. The mid-span moment consists of the uniform mid-section moment (Table 4.1) and the P-δ effect resulting from the axial load applied to the deflected specimen. For tests with significant lateral loads (SP-A2, SP-A3 and the SP-B series), the uniform mid-section moment was the dominant component. Because of the P-δ effect associated with the increasing deflection, the mid-span moment continued to rise after the axial load declined from its maximum.

Test	Axial Load at Plate Buckling Initiation (kN)	Maximum Axial Load (kN)	Mid-Span Displacement at Max. Axial Load (mm)	Mid-Span Moment at Max. Axial Load (kN-m)	Max. Mid-Span Moment (kN-m)
SP-A1	790	1098	6.9	8.41	26.3(1)
SP-A2	590	795	19	40.6	48.7
SP-A3	440	590	24	49.0	54.2
SP-B1	1230	1334	12	52.8	70.8(1)
SP-B2	900	992	21	72.3	80.1
SP-B3	Plate buckling not detected / observed	547(2)	30	80.9	82.0
SP-C1	420	864	7.1	6.61	14.6
SP-C2	770	1129	-11(3)	-12.0(3)	-28.3(3)
SP-DA	690	1036	4.3	1.76	1.89
SP-DB	Plate buckling not detected / observed	832	57	83.1	87.7

(1) Maximum moment at the time the test was terminated.

(2) Constant axial load level when the specimen failed under lateral loading.

(3) Negative deflection or moment refers to the bending direction in which the flange is in flexural compression.

Table 4.2 Static Loads and Deformations Measured during Tests

The axial load corresponding to the onset of plate buckling presented in Table 4.2 was detected by the strain gauges mounted on the plate surface. The ratio between the plate buckling load and the maximum axial load is plotted against the interaction index in Figure 4.1, which shows an approximately linear correlation between these two variables. The trend shown in Figure 4.1 suggests that plate buckling tends to take place later in relation to overall buckling failure for specimens with small interaction index values (e.g. the SP-B series).

Summary sheets of all ten tests are included in Appendix B. Each sheet presents the test summary with a schematic of the set-up, a load versus displacement plot, and a brief summary of the test observations. Summaries of each test series are given in the following sub-sections.

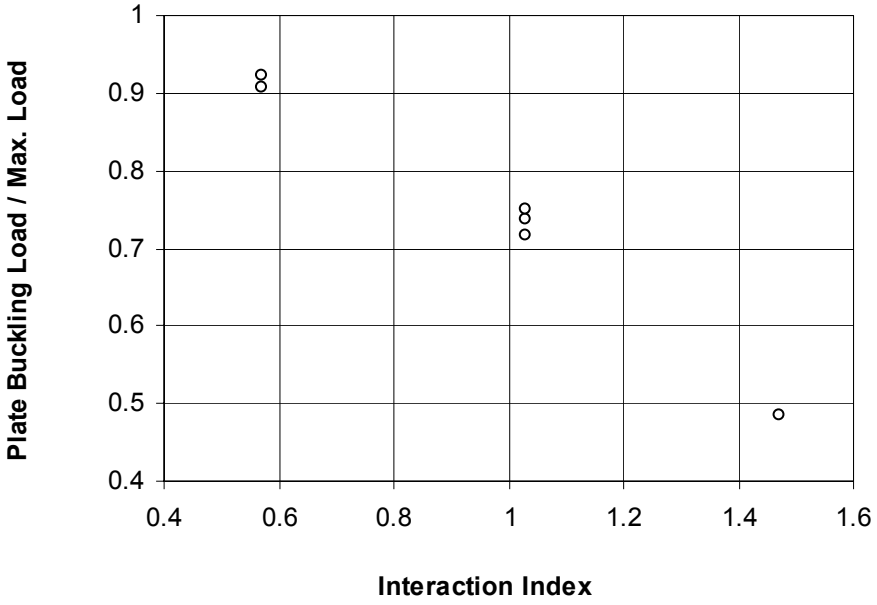

Figure 4.1 Correlation Between Interaction Index and the Ratio of Plate Buckling Load vs. Maximum Load

4.2 SP-A Series

The SP-A series consisted of three tests designed to study the effect of bending moment on specimens with an interaction index of 1.03. While SP-A1 had no lateral load, SP-A2 and SP-A3 were tested with 30 and 40 kN of lateral loads, respectively. The uniform mid-section uniform moment was 26 kN-m for SP-A2 and 35 kN-m for SP-A3, both were less than the 40 kN-m plastic moment derived from measured dimensions and yield stresses. Deformed shapes are shown in Figure 4.2, in which local plate buckling waves are clearly visible at the mid-span.

Strains measured during test SP-A1 are plotted against axial load in Figure 4.3. It shows that compressive strains in the plate were higher than that in the flange. This was related to a 3 mm eccentricity towards the plate, imposed in the axial load alignment to prevent stiffener tripping.

Figure 4.3 shows that axial strains at various plate surface locations started to diverge at a load level of 790 kN, indicating that the plate started to bend due to local buckling. During the test, plate buckling waves became visible at an axial load of approximately 900 kN.

The axial load versus shortening responses of the three tests are plotted in Figure 4.4. Because lateral loads were applied to SP-A2 and SP-A3, the maximum axial loads of these two tests were lower than that of SP-A1, which was tested in axial compression only.

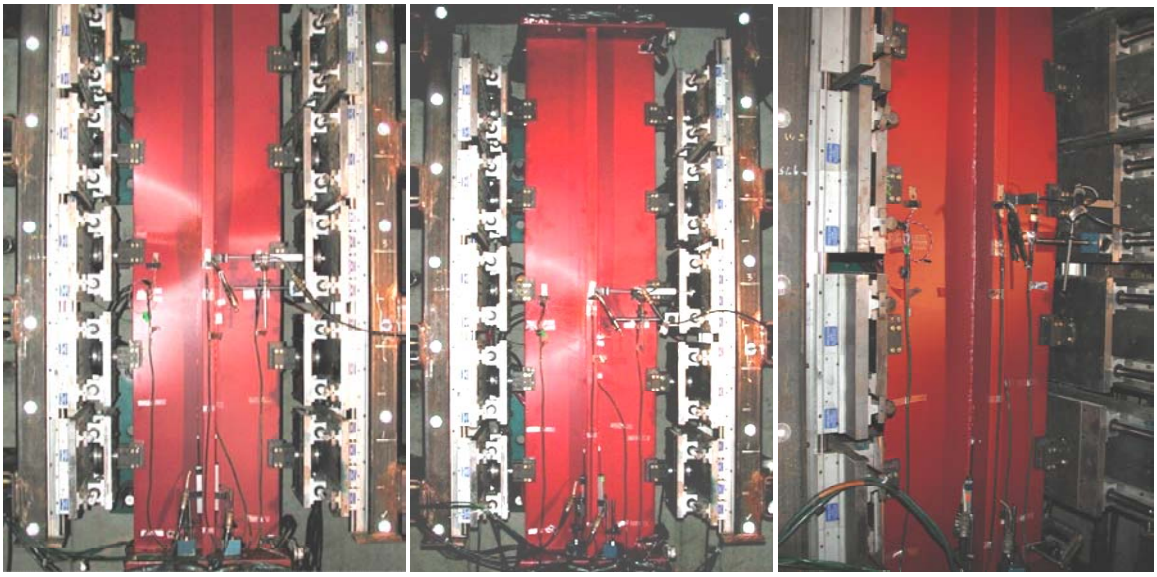

(a) SP-A1 (b) SP-A2 (c) SP-A3

Figure 4.2 Deformed Shapes of Series SP-A Specimens

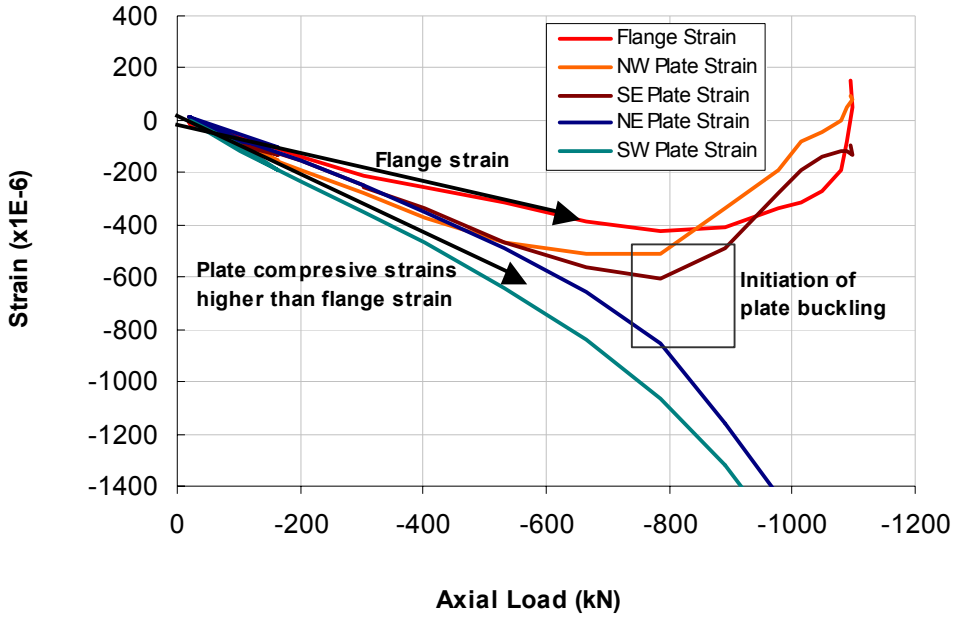

Figure 4.3 Strains Measured during Test SP-A1

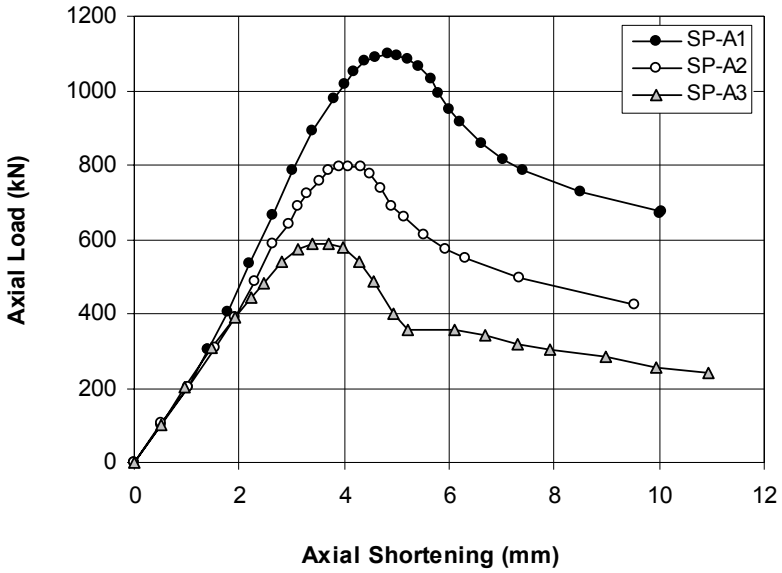

Figure 4.4 Axial Load vs. Shortening Responses of SP-A Series

The mid-span moment versus displacement relationships are plotted in Figure 4.5. For SP-A2 and SP-A3, the peak moments at the plateau were considerably higher than the 40 kN-m plastic moment, because of axial compression and strain hardening in the plastic range. It is noted that test SP-A1 did not reach its maximum moment capacity, as lateral load was not applied during this test and it was not feasible to achieve the maximum moment capacity solely by the P-δ effect.

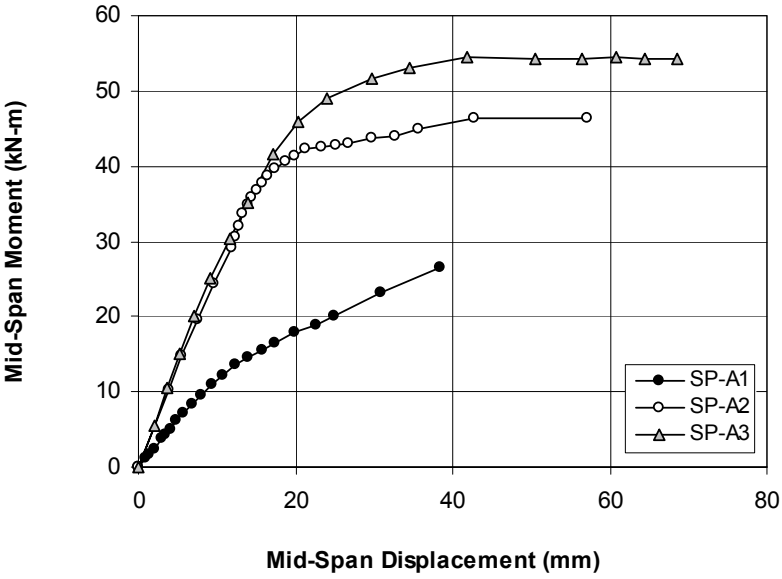

Figure 4.5 Moment versus Displacement Responses of SP-A Series

4.3 SP-B Series

The SP-B specimens have the same dimensions and materials as those tested in SSC-399. The lateral loads applied in the SSC-399 testing program were between zero and25 kN. For the three new tests (i.e. SP-B1, SP-B2 and SP-B3), higher lateral loads of 40, 60 and 75 kN were selected, and the associated uniform mid-section moments corresponded to 50%, 80% and 100% of the plastic moment of 64 kN-m. It is noted that SP-B3 failed by overall bending during lateral loading, when lateral loads reached 73.8 kN and the axial load was held constant at 550 kN.

In Figure 4.6(a), the deformed shape of SP-B1 shows the most evident plate buckling deformation. The picture of SP-B2 in Figure 4.6(b) was taken at about 60% of the maximum axial load when plate buckling waves became visible along the longitudinal edges of the plate. As shown in Figure 4.6(c), specimen SP-B3 failed in bending and axial compression without visible plate buckling deformations. Strain gauge readings plotted in Figure 4.7 show that plate strains of SP-B3 did not diverge as was expected for plate buckling, until overall bending became significant and the flange was in flexural tension. The mid-span moment versus deflection responses of these three tests are shown in Figure 4.8. Similar to the SP-A series, the maximum moment of SP-B2 and SP-B3 at over 80 kN-m was considerably higher than the plastic moment of 64 kN-m based on measured dimensions and yield stresses. Test SP-B1 had a relatively small mid-section moment, and it did not reach its full moment capacity.

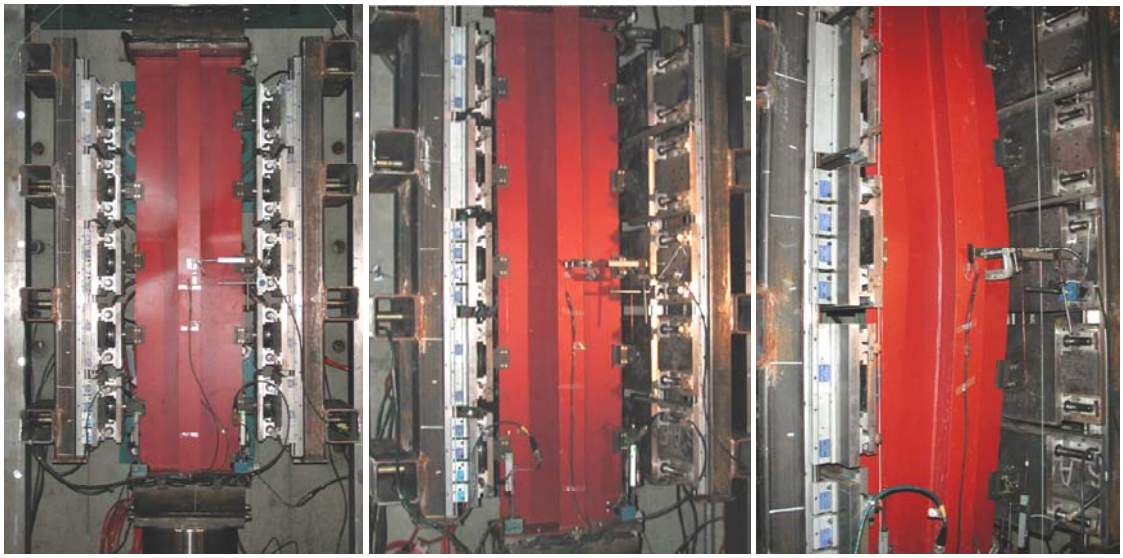

(a) SP-B1 **(b) SP-B2** **(c) SP-B3**

Figure 4.6 Deformed Shapes of New SP-B Tests

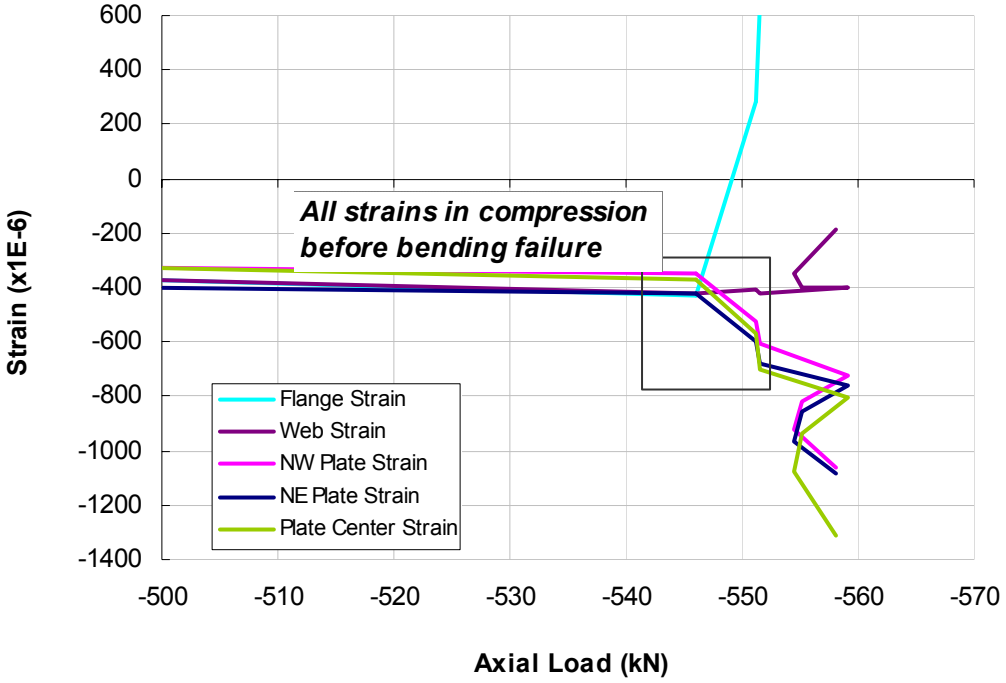

Figure 4.7 Strains Measured during Test SP-B3

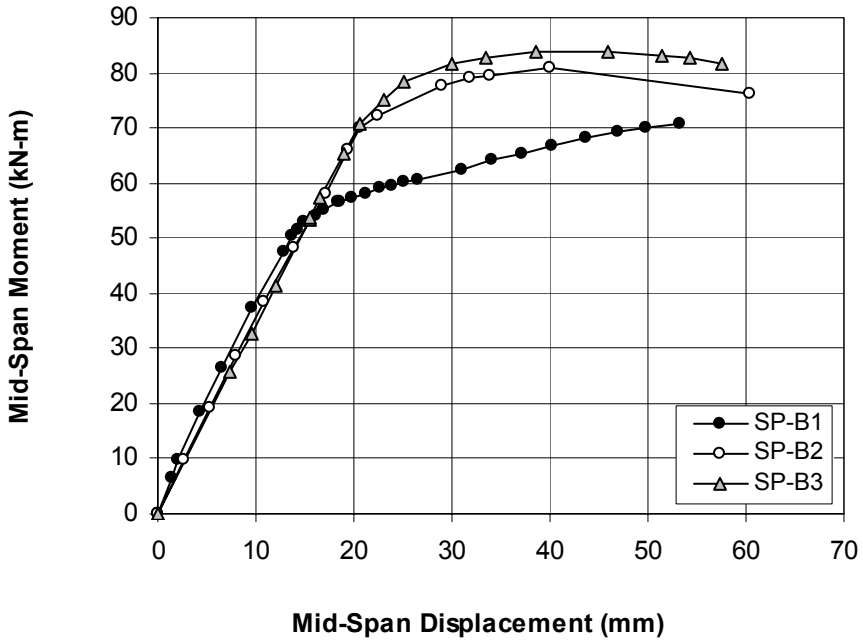

Figure 4.8 Moment vs. Displacement Responses of SP-B Series

Figure 4.9 plots the maximum axial force and the corresponding mid-span moment of all tests in the SP-A and SP-B series, including three tests from SSC-399. Specimens in the SP-B series had higher capacities than those of the SP-A series because of their large cross-sections and higher yield stresses; however, both series show a similar pattern, with the maximum axial force decreasing with the increase of bending moment. Once the maximum axial force and moment are normalized (with respect to the axial load capacity and the plastic moment) these two series merge together and can be represented by a single correlation between normalized axial force and moment (Figure 4.10). The axial load capacity used to normalize the axial force was derived using the column design equations of CSA S16-01 (2001). The correlation shown Figure 4.10 resembles the interaction diagram used for beam-column design.

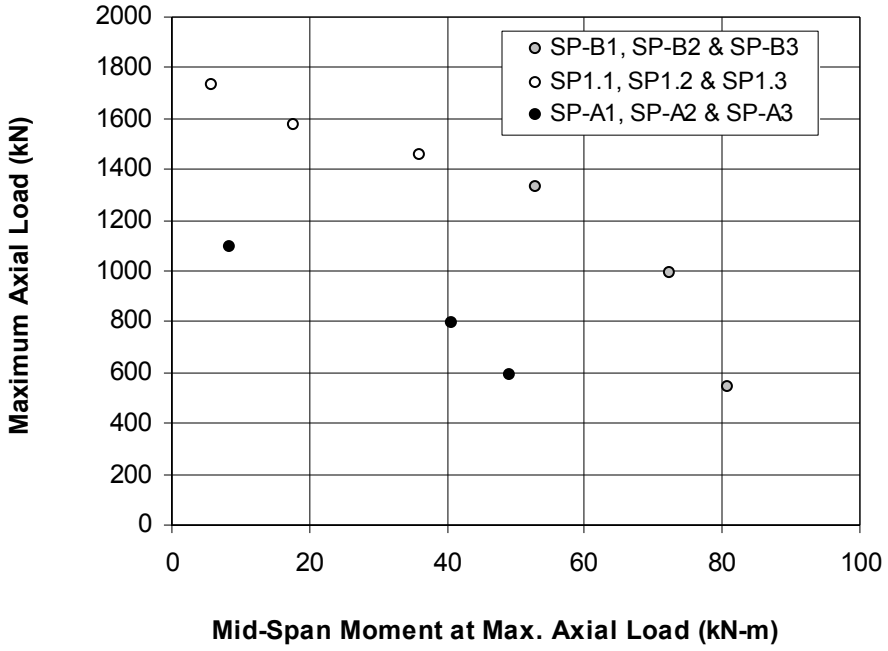

Figure 4.9 Moment vs. Axial Load Diagram of SP-A and SP-B Series

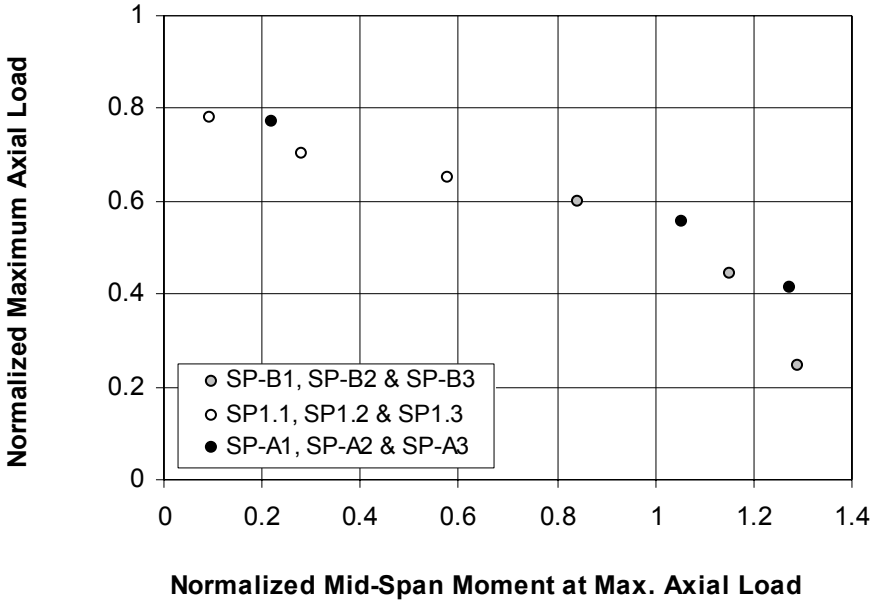

Figure 4.10 Normalized Axial Load vs. Moment Diagram of SP-A and SP-B Series

4.4 SP-C Series

All tests in this series were subjected to axial compression without lateral load. The specimens were different in size and material strength, resulting in interaction indices varying from 0.57 to 1.47. Specimens SP-C1 and SP-C2, which had respective interaction index values of 1.47 and 0.77, were new tests in this series. Other tests in this series included SP-A1 and SP1.2 of the SP-B series.

Pictures in Figure 4.11 show the deformed shapes of SP-C1 and SP-C2. During the test of SP-C1, plate local buckling waves were seen before overall column buckling. Strain gauge readings plotted in Figure 4.12 indicate that plate buckling initiated at a load level of 420 kN, as strains across the plate diverged. Specimen SP-C2 failed by a combination of plate buckling and stiffener tripping. Torsional deformation of the stiffener and plate buckling waves can be seen in the deformed shape in Figure 4.11(b).

Strains measured in SP-C2, as plotted in Figure 4.13, indicate that plate buckling initiated at about 770 kN. This coincided with the change in direction of lateral flange displacement as shown in Figure 4.14. The reversal in flange displacement represented the onset of stiffener tripping, which occurred as the stiffener carried additional compression following plate buckling. Subsequently, as shown in Figure 4.14, stiffener deflection continued to increase as stiffener tripping escalated.

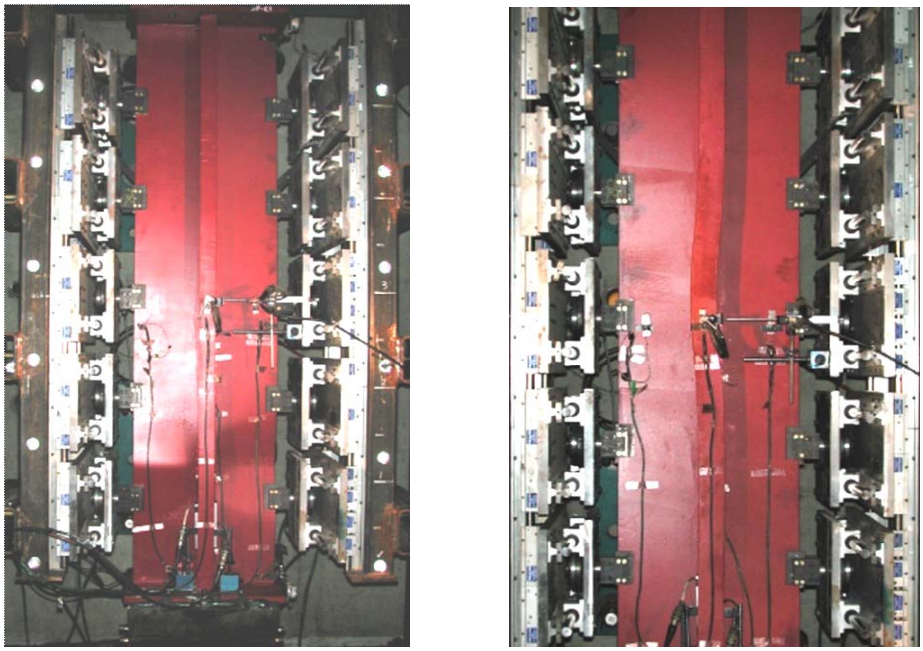

(a) SP-C1 (b) SP-C2

Figure 4.11 Deformed Shapes of New SP-C Tests

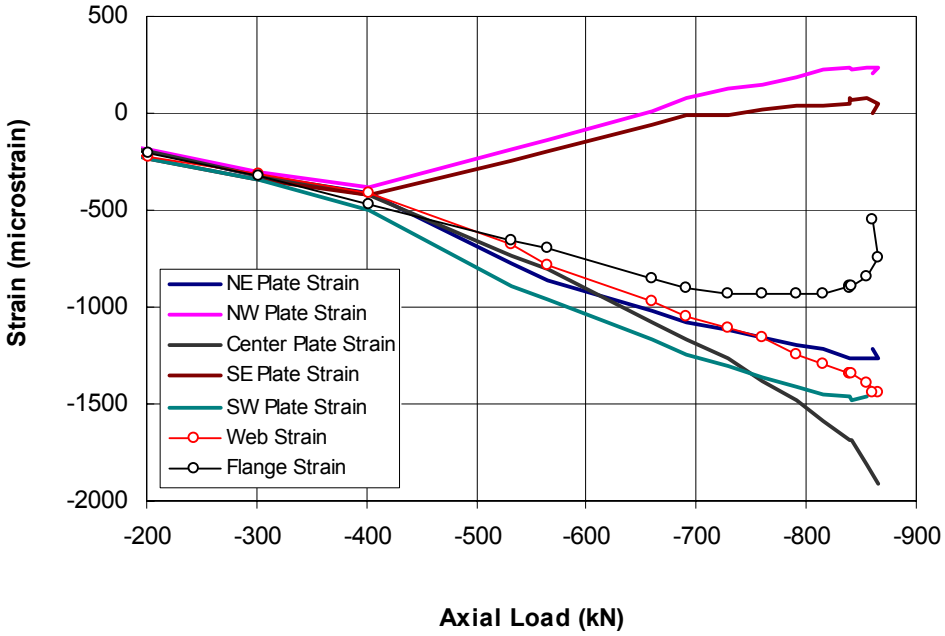

Figure 4.12 Strains Measured during Test SP-C1

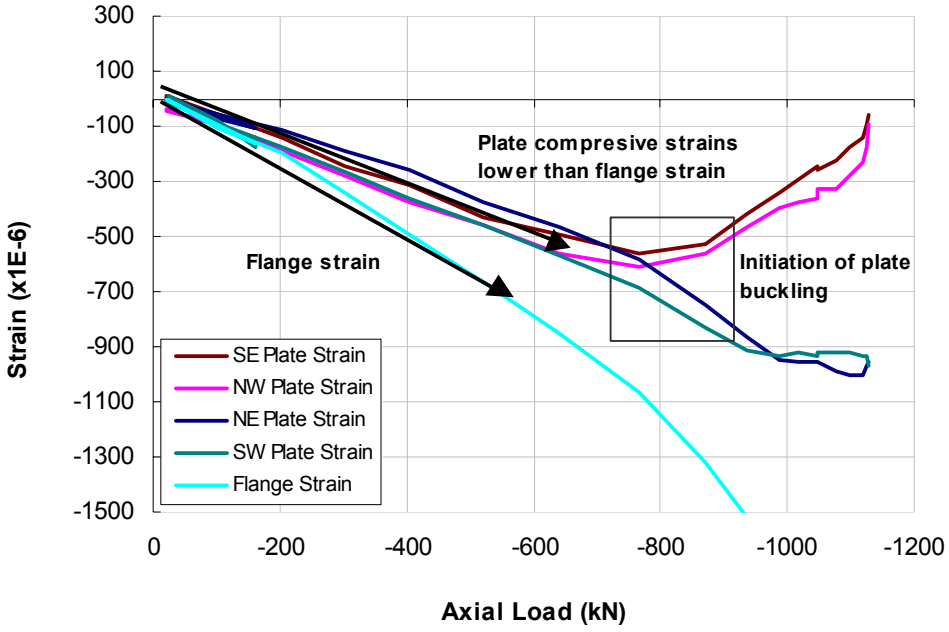

Figure 4.13 Strains Measured during Test SP-C2

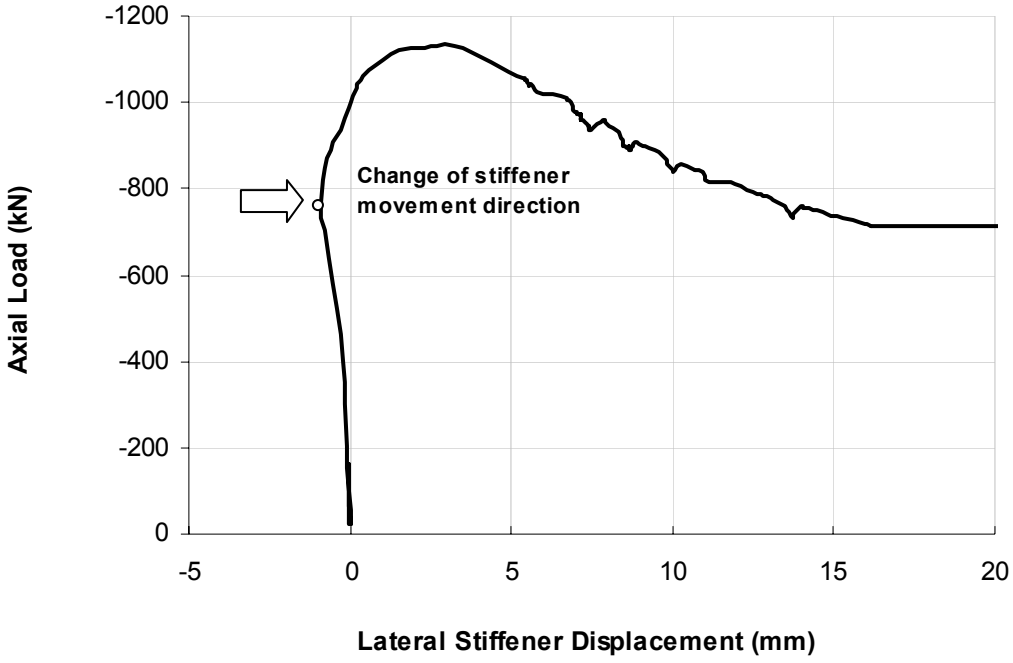

Figure 4.14 Stiffener Deflection during Test SP-C2

The cause of stiffener tripping for SP-C2 can be identified from the strain history shown in Figure 4.13. The compressive strain in the flange was higher than the plate strains, suggesting that there was an eccentricity towards the stiffener, which placed the stiffener in flexural compression. The difference between the strains in the flange and in the plate continued to increase with axial load, and reached a strain differential of 4.5×10^{-6}, which corresponded to a stress differential of 95 MPa, when plate buckling and stiffener tripping occurred. It is estimated that this differential stress corresponds to a mid-span, off-center displacement of 7 mm, which includes initial deflection, load eccentricity and mid-span lateral deflection at this load level.

The axial load versus shortening responses for the four tests in this series are shown in Figure 4.15. The specimen SP 1.2 had the highest load-carrying capacity because of its relatively large size. The load versus displacement plots are normalized in Figure 4.16, using the ultimate load and displacement. Responses of the three tests (SP-A1, SP-C1 and SP1.2) that involved the interaction of plate and overall buckling are similar. Specimen SP-C2, which failed by plate buckling and stiffener tripping, shows a more abrupt post-ultimate behavior than that of other tests. Observations in past experiments suggests that stiffener tripping typically exhibits a sudden loss of axial load capacity after having reached the ultimate.

The impact of the interaction index is further examined in Figure 4.17, which uses the axial load capacity normalized according to the axial load that causes the plate to yield. The six tests are presented as two groups: one for the three tests carried out at C-FER and the other for three tests by the University of Alberta. Interaction between plate buckling and overall buckling was observed in all six tests. However, the tests at C-FER generally exhibited more gradual post-buckling behavior than the University of Alberta tests. Figure 4.17 shows that for both groups there is a linear correlation between interaction index and normalized axial load, although the associated slopes are considerably different for these two groups.

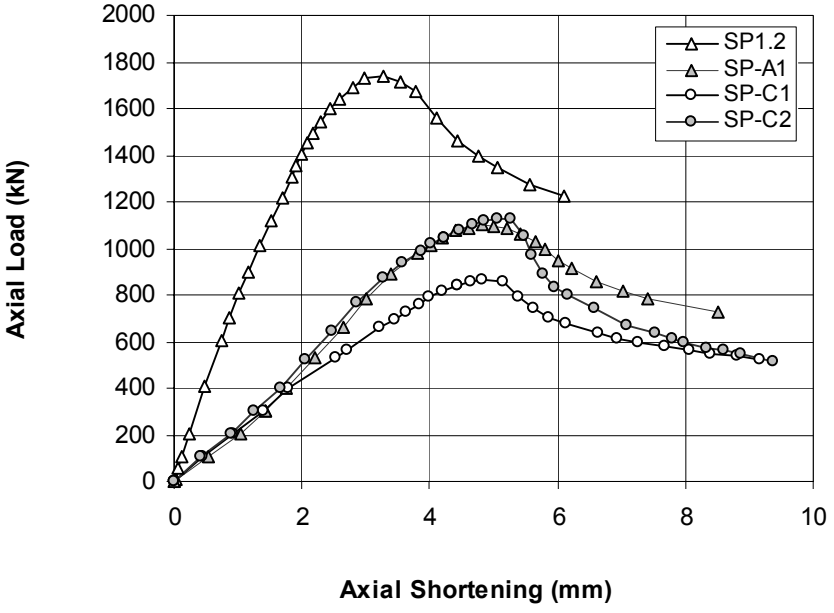

Figure 4.15 Axial Load vs. Shortening Responses of SP-C Series

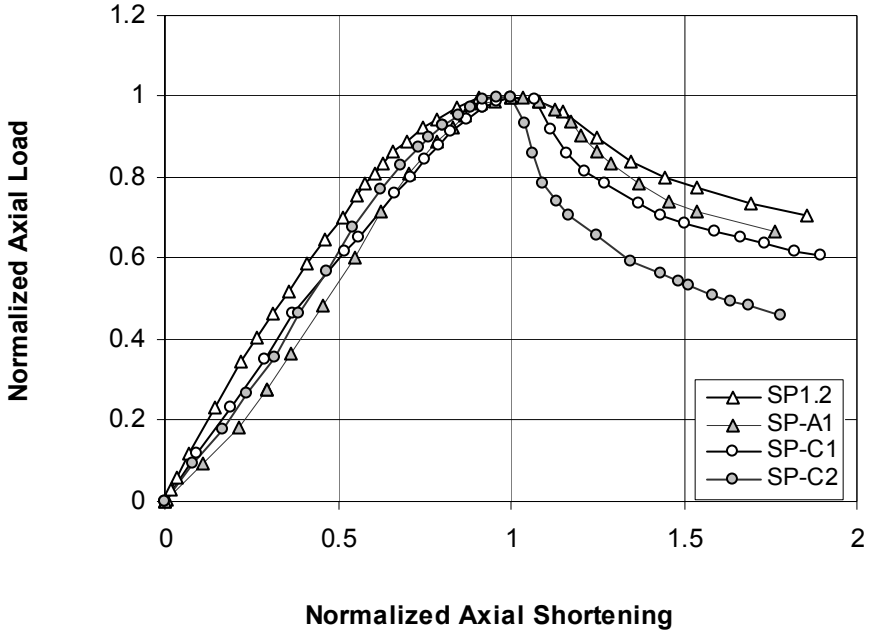

Figure 4.16 Normalized Axial Load vs. Shortening Responses of SP-C Series

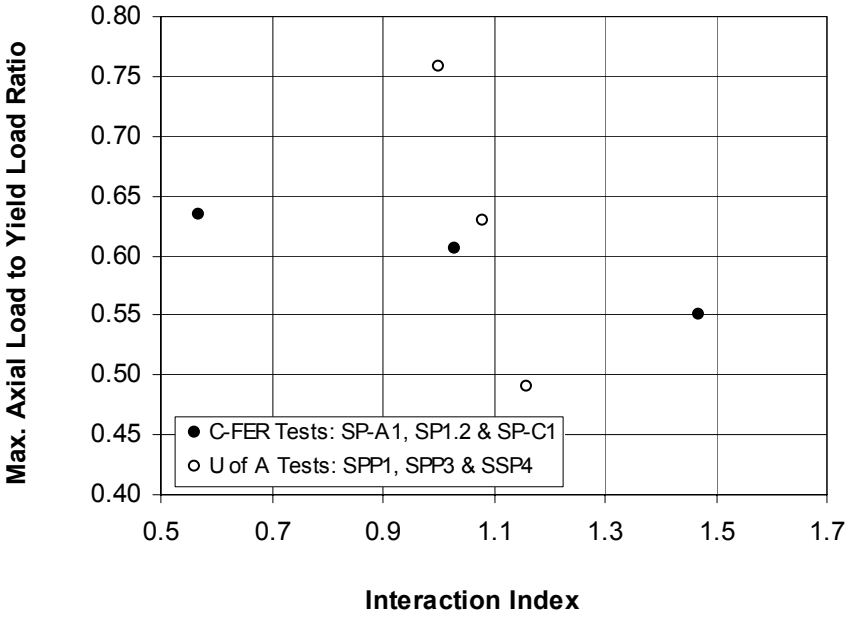

Figure 4.17 Correlation between Normalized Axial Load and Interaction Index

4.5 SP-D Series

Specimens SP-DA and SP-DB had the same dimensions, materials and load conditions as SP-A1 and SP-B1, respectively, except for the imposed damage. A 196 mm x 68 mm rectangular hole was machined in the web of SP-DA (Figure 2.3), which was then tested in axial compression. SP-DB was pre-bent in the test set-up to a 36 mm permanent deflection at the mid-span, and was subjected to axial compression in addition to 40 kN lateral loads.

Figure 4.18(a) shows the deformed shape of SP-DA, which failed in shear at the defect location (Figure 4.18(b)). The specimen exhibited plate buckling at the 690 kN load level, followed by failure of a short section where the web defect reduced the cross-sectional area considerably. The failure occurred suddenly with an abrupt decline in axial load. The load versus displacement response of SP-DA was very similar to SP-A1 until the sudden failure took place (Figure 4.19). It is believed that plate buckling caused the stiffener to carry additional compression, which led to failure of the weakened section. In comparison to SP-A1, the load-carrying capacity was reduced by only 6% because of the web defect; but the post peak response exhibited a far more severe softening behavior than that of SP-A1.

As shown by the deformed shape in Figure 4.18(c), SP-DB failed by overall bending without plate buckling. Comparison in Figure 4.20 with the equivalent as-built specimen SP-B1 indicates that pre-bending deformations reduced the maximum axial load by about 38% under the same lateral load. However, the maximum bending moment of 83 kN-m is comparable to those achieved by as-built specimens SP-B2 and SP-B3, suggesting that the reduced axial load capacity due to pre-bending deformation is caused by the increase of P-δ moment due to initial deflection.

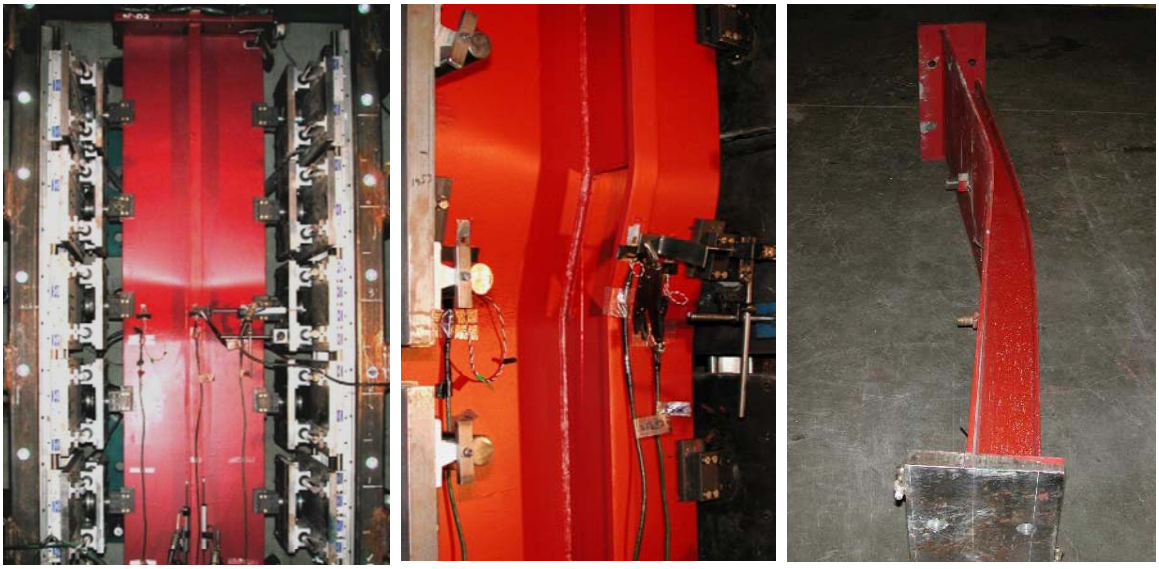

(a) SP-DA **(b) Mid-Span of SP-DA** **(c) SP-DBC2**

Figure 4.18 Deformed Shapes of Series SP-D Tests

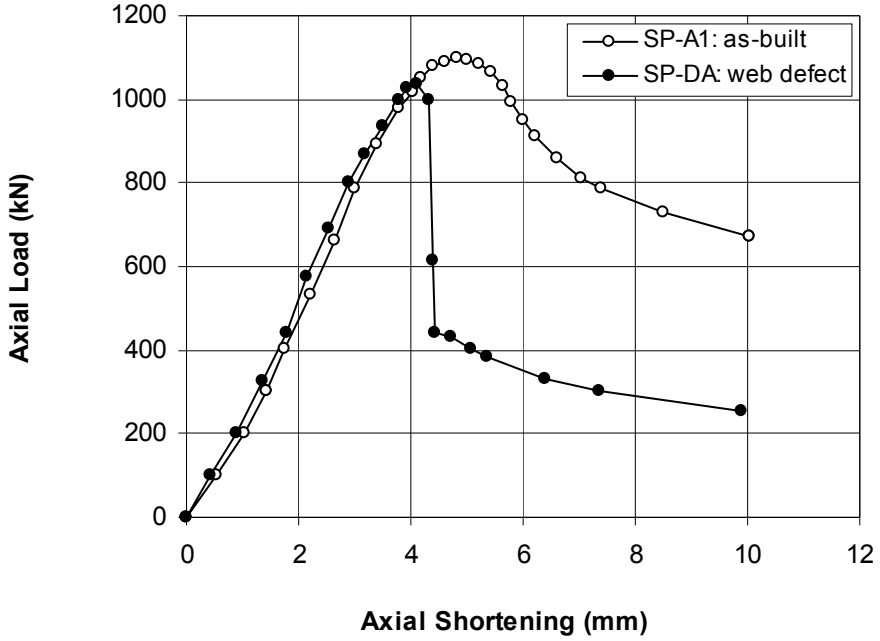

Figure 4.19 Comparison of Load-Displacement Responses of SP-DA and SP-A1

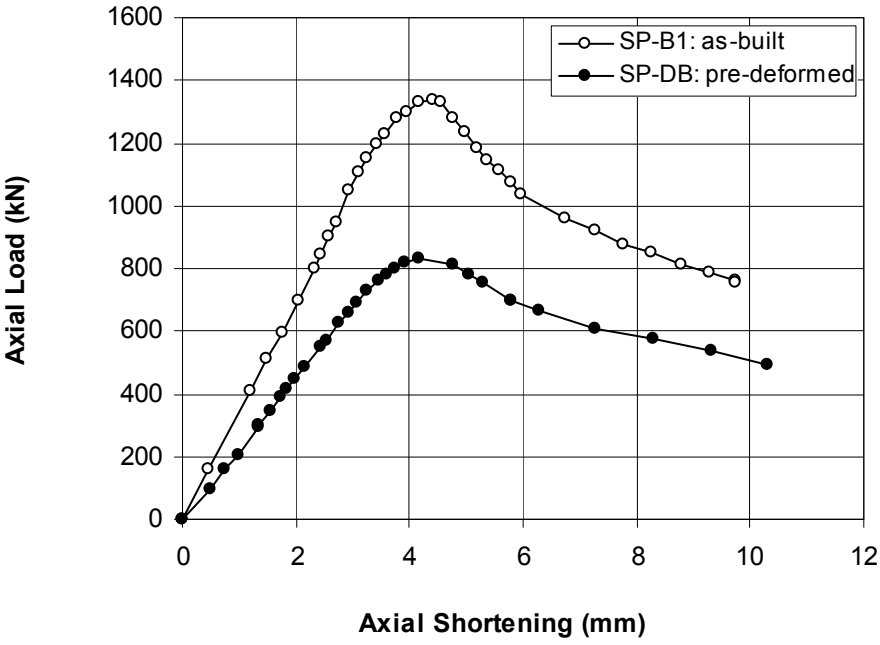

Figure 4.20 Comparison of Load-Displacement Responses of SP-DB and SP-B1

In total, seven damaged specimens were tested in this project and SSC-399. Table 4.3 presents a comparison of failure mode and axial load capacity between damaged and as-built specimens. The largest reductions in axial load capacity occurred with pre-deformed specimens.

In several cases, the specimens with localized metal loss defects exhibited failure modes which were different from those exhibited by the comparable as-built specimens. This is because the buckling mode that interacts with plate buckling differs from overall buckling. For example, failure of specimens SP-DA and SP3.1 occurred in a short section at the mid-span where the web defect was located, opposed to the overall buckling failure of equivalent as-built specimens SP-D1 and SP1.2. An asymmetric flange defect in SP3.3 caused the stiffener to trip, despite the fact that both SP1.2 (as-built) and SP3.2 (damaged with symmetric flange defects) failed by overall buckling. Because localized defects led to short section failure and stiffener tripping, the associated post-ultimate behavior in these cases involved a sudden decline of axial load (e.g. SP-DA in Figure 4.29). This may warrant an appropriate increase of safety margin when assessing the remaining capacity of damaged specimens susceptible to unstable failures, even though the reduction of capacity due to localized defects was as small as 3-6%.

As-Built			Damaged				
Specimen	**Failure Mode**	**Max. Load (kN)**	**Specimen**	**Damage**	**Failure Mode**	**Max. Load (kN)**	**Capacity Reduction**
SP-A1	LPB+OCB(1)	1098	SP-DA	Web defect	LPB + local web failure	1036	6%
SP-B1	LPB + OCB	1334	SP-DB	36 mm deflection	Overall bending	832	38%
SP1.2	LPB + OCB	1736	SP 2.1	20 mm deflection	LPB + OCB	1331	23%
			SP 2.2	35 mm deflection	LPB + OCB	1116	36%
			SP 3.1	Web defect	LPB + local web failure	1636	6%
			SP 3.2	Symmetric flange defects	LPB + OCB	1773	No reduction
			SP 3.3	One flange defect	LPB + stiffener tripping	1683	3%

(1) LPB + OCB = Local plate buckling followed by overall column buckling.

Table 4.3 Comparison of Damaged and As-Built Specimens

5. DESIGN METHOD

5.1 Review of Design Standards

5.1.1 Effective Width Calculation

Interaction between overall buckling and local buckling has received considerable attention in the treatment of thin wall components such as cold-formed steel structures (Yu 2000). The capacity of structural members, for which local buckling occurs before an overall instability failure, is determined using the effective width concept. The effective width concept was introduced in the early 1930s by von Karman et al. (1932) and has been used extensively to calculate the post-buckling capacity of plates. Although the concept is implemented in different design standards and guidelines, differences exist between these standards and guidelines. The following presents the effective width used in different sources.

CSA–S136–01

The concept, implemented in this North American cold-formed steel standard, is based on replacment of the actual cross-section by an effective cross-section using the following equation to obtain the effective width, B_e, of the plate.

$$B_e = \rho\, b \qquad [5.1]$$

where ρ is the effective width factor given as:

$$\rho = \frac{\lambda - 0.22}{\lambda^2} \quad \text{if} \lambda > 0.673 \qquad [5.2a]$$

or

$$\rho = 1 \quad \text{if } \lambda \le 0.673 \qquad [5.2b]$$

The parameter λ is the slenderness parameter defined as:

$$\lambda = \sqrt{\frac{f}{F_{cr}}} \qquad [5.3]$$

where f is the stress applied on the plate and F_{cr} is the elastic buckling stress of the plate given as:

$$F_{cr} = k\frac{\pi^2 E}{12\left(1-\nu^2\right)}\left(\frac{t}{b}\right)^2 \qquad [5.4]$$

where b and t are as defined in Figure 2.1, E is the modulus of elasticity, ν is the Poisson's ratio, f is the applied uniform stress in the plate, and k is a plate buckling coefficient, which accounts for support boundary conditions and plate loading conditions. For plates simply supported all around and subjected to a nominal uniform uniaxial stress, the buckling coefficient is taken as 4.0. This condition applies for a plate stiffened with multiple stiffeners as considered in this study.

DNV 1995

The 1995 edition of the DNV Classification Note 30.1 calculates the effective width of a plate differently depending on whether overall buckling of the stiffened panel is induced by the plate or by the stiffener. For plate induced overall buckling, the effective plate width is given as:

$$B_e = \left(\frac{1.8}{\beta_1} - \frac{0.8}{\beta_1{}^2}\right) b \qquad \text{if } \beta_1 \geq 1 \qquad [5.5a]$$

or

$$B_e = b \qquad \text{if } \beta_1 < 1 \qquad [5.5b]$$

where β_1 is the plate slenderness defined in equation [1.2]. For an axially loaded stiffened plate, the maximum stress applied on the effective plate width, f_{max}, corresponds to the overall buckling stress, which is obtained using the full cross-section properties and a column buckling equation.

DNV 2002

The new DNV guideline for plated structures uses the same effective plate width as CSA-S136-01, except that the reference stress level is taken as the material yield strength rather than the applied stress, f, in [5.3]. The plate effective width predicted in DNV 2002 will therefore tend to be smaller than that predicted by CSA–S136–01.

API 2000

As opposed to other design guides, the American Petroleum Institute Bulletin 2V limits the plate capacity to its buckling capacity. An effective plate width is therefore not calculated.

5.1.2 Axial Compression

The uniaxial compression capacity of stiffened steel plates, determined by the allowable stress within the effective area, is generally obtained using the cross-section properties and a column curve. Various design guidelines and standards have adopted different column curves for this calculation. The column curves are intended to account for the effects of yielding, initial imperfections and residual stresses. The following describes some of the column equations that have been investigated for this project.

CSA–S136–01

The column curve adopted for cold formed steel columns reflects the unique residual stresses in cold formed steel members and takes the following form of:

$$f_u = \left(0.658\,\lambda_c^2\right) F_y \qquad \text{if } \lambda \le 1.5 \qquad [5.6a]$$

or

$$f_u = \left(\frac{0.877}{\lambda_c^2}\right) F_y \qquad \text{if } \lambda > 1.5 \qquad [5.6b]$$

The parameter λ_c is given by

$$\lambda_c = \sqrt{\frac{F_y}{F_e}} \qquad [5.7]$$

where F_y is the yield strength of the material and F_e is the elastic buckling capacity given as:

$$F_e = \frac{\pi^2\, E}{\left(KL/r\right)^2} \qquad [5.8]$$

The radius of gyration, *r*, is defined for the full cross-section and *KL* is the effective length of the stiffened steel plate.

CSA–S16–01

For a stiffened steel plate made of hot rolled steel plates, the Structural Stability Research Council (SSRC) column curve 2 is a more suitable choice, considering that residual stresses in welded steel members are different from those in cold-formed steel members. Although the original SSRC column curve was given in five parts, the modified form implemented in CSA-S16–01 is expressed by a single equation:

$$f_u = F_y \left(1 + \lambda_c^{2.68}\right)^{-1/1.34} \qquad [5.9]$$

where the terms are as defined earlier.

DNV 1995 and 2000

The procedure outlined in DNV 1995 is more laborious than the procedures outlined above. The critical stress for plate induced buckling is given as follows:

$$f_u = F_y \qquad \text{if } \lambda \le 0.2 \qquad [5.10a]$$

or

$$f_u = F_y \left(\frac{1 + \mu + \lambda_c^2 - \sqrt{\left(1 + \mu + \lambda_c^2\right)^2 - 4\lambda_c^2}}{2\lambda_c^2} \right) \qquad \text{if } \lambda > 0.2 \qquad [5.10b]$$

where

$$\mu = \frac{\omega Z_p}{r_e{}^2} \qquad [5.11]$$

$$\omega = \delta + 0.7 Z_p \left(1 - \frac{A_e}{A}\right) \qquad [5.12]$$

and λ_c is as defined in equation [5.7].

The variable r_e is the radius of gyration of the reduced cross-section, Z_p is the distance from the centroid of the reduced section to the plate mid-thickness, A_e is the area of the reduced section, and A is the area of the full section. Initial deflection, δ, is the maximum admissible out-of-straightness for compression elements, and is usually taken as $\delta = 0.0015\, L$.

API 2000

The American Petroleum Institute has adopted an approach proposed by Faulkner (1975) for deriving the average failure stress of uniaxially stiffened plate panels in end compression. The approach ignores the interaction between adjacent stiffener fields, namely, it is assumed that flexural failure is plate-induced overall buckling with simple support conditions at the transverse edges. The allowable axial stress is given by:

$$f_u = F_y \qquad \text{if } \bar{\lambda} \le 0.5 \qquad [5.13a]$$

$$f_u = (1.5 - \bar{\lambda})F_y \qquad \text{if } 0.5 < \bar{\lambda} \le 1.0 \qquad [5.13b]$$

or

$$f_u = F_y / 2\bar{\lambda} \qquad \text{if } \bar{\lambda} > 1.0 \qquad [5.13c]$$

where $\bar{\lambda}$ is a dimensionless slenderness parameter, equal to the square root of the ratio between the yield stress and the elastic plate buckling stress.

$$\bar{\lambda} = \frac{b}{t}\sqrt{\frac{F_y 12\left(1-\nu^2\right)}{E\,\pi^2\,k}} \qquad [5.14]$$

The plate buckling coefficient k is taken as the minimum of k_R and k_F. For a single stiffened plate panel $k_R = 4.0$ and k_F is given as follows:

$$k_F = \frac{\left(1+\alpha^2\right)^2 + n\gamma}{\alpha^2\left(1+n\gamma\right)} \quad \text{for} \quad \alpha \le \left(1+n\gamma\right)^{1/4} \qquad [5.15a]$$

$$k_F = \frac{2\left(1+\sqrt{1+n\gamma}\right)}{\left(1+n\gamma\right)} \quad \text{for} \quad \alpha \ge \left(1+n\gamma\right)^{1/4} \qquad [5.15b]$$

The term γ is the stiffness ratio between stiffener and the plate and is given as:

$$\gamma = \frac{E\,I_s}{b\,D} \qquad [5.16]$$

where I_s is the moment of inertia of the stiffener about an axis parallel to plate surface at the base of the stiffener, and D is the bending rigidity for a unit width of plate given as

$$D = \frac{E\,t^3}{12\left(1-\nu^2\right)} \qquad [5.17]$$

5.1.3 Axial Compression and Bending

Stiffened steel plates are often subjected to a combination of in-plane and out-of-plane forces. This was the case for six of the ten specimens tested in this project. The general approach to take into account the combined effect of in-plane forces and bending of structural elements is to use an interaction equation of the form:

$$\frac{P}{P_u} + \frac{U_1 M}{M_u} \leq 1.0 \qquad [5.18]$$

where P and M are the applied axial force and bending moment, respectively, P_u is the axial load capacity, M_u is the bending moment capacity generally taken as the yield moment capacity. The moment amplification factor U_1 accounts for the P-δ effect, or the second order effect of the axial load acting on the deformed member, and is given as:

$$U_1 = \frac{1}{1 - \frac{P}{P_{eu}}} \qquad [5.19]$$

where P_{eu} is the elastic overall buckling capacity of the stiffened panel. The moment resistance, M_u, in equation [5.18] corresponds to the elastic moment that causes yielding of the extreme fibers in the plate, or the plate buckling stress in the case of API Bulletin 2V. It should be noted that the moment resistance, M_u, based on yielding of the plate would typically be larger than the yield moment since the centroid of the cross-section lies close to the plate. Because the bending moment in the test specimens was applied to cause compression in the plate, the bending moment and axial load terms in [5.18] are both positive. The moment resistance is calculated on the reduced section in all guidelines investigated in this study, except in API Bulletin 2V where the moment resistance is calculated on the full section.

5.1.4 Comparison with Test Results

Tables 5.1 and 5.2 show a summary of the calculated values of equation [5.18], referred to as the interaction value, for seven tests in this program and three earlier tests by the University of Alberta (SSP1, SSP3 and SSP4). Tests that involved stiffener tripping (i.e. SP-C2 and SSP2) and simulated damages (i.e. SP-DA and SP-DB) were not included. For each of the design guidelines presented above, the table lists the values of the axial load resistance, P_u, the bending moment resistance, M_u, and the moment amplification factor, U_1. The amplification factor was calculated using equation [5.19] and the axial load, P, which was applied at failure of the test specimen. Similarly, the bending moment, M, used in the interaction equation [5.18] is equal to the bending moment applied during the test. The value of the left hand side of equation [5.18] is listed as the interaction value in Tables 5.1 and 5.2. An interaction value of 1.0 represents a prediction that matches perfectly with the test. If the interaction value is less (or greater) than unity, the design equations are unconservative (conservative) as they overestimate (or underestimate) the capacity.

Test Specimen	Test Results		DNV 1995				DNV 2002			
	Max. Axial Load P (kN)	Mid-Section Moment M (kN·m)	P_u (kN)	M_u (kN·m)	U_1	Interaction Value	P_u (kN)	M_u (kN·m)	U_1	Interaction Value
SP-A1	1098	3.29	986	70	1.68	1.19	934	70	1.68	1.25
SP-A2	795	25.92	986	70	1.41	1.33	934	70	1.41	1.38
SP-A3	590	34.56	986	70	1.28	1.23	934	70	1.28	1.26
SP-B1	1334	35.65	1656	136	1.30	1.15	1604	136	1.30	1.17
SP-B2	992	53.18	1656	136	1.21	1.07	1604	136	1.21	1.09
SP-B3	550	63.48	1656	136	1.11	0.85	1604	136	1.11	0.86
SP-C1	864	0.00	643	44	2.85	1.34	603	44	2.85	1.43
SSP1	1934	19.34	2232	225	1.27	0.98	2107	225	1.27	1.03
SSP3	1158	5.79	1155	84	2.36	1.17	934	84	2.36	1.40
SSP4	1866	9.33	1895	155	1.60	1.08	1630	155	1.60	1.24
Mean						**1.14**				**1.21**
COV						**0.13**				**0.15**

Table 5.1 Comparison of Test Results with DNV Guidelines

Test Specimen	Test Results		API 2000				CSA–S136–01			
	Max. Axial Load P (kN)	Mid-Section Moment M (kN·m)	P_u (kN)	M_u (kN·m)	U_1	Interaction Value	P_u (kN)	M_u (kN·m)	U_1	Interaction Value
SP-A1	1098	3.29	648	40	1.56	1.82	1015	70	1.68	1.16
SP-A2	795	25.92	648	40	1.35	2.10	1015	70	1.41	1.31
SP-A3	590	34.56	648	40	1.24	1.97	1015	70	1.28	1.21
SP-B1	1334	35.65	1092	82	1.26	1.77	1686	136	1.30	1.13
SP-B2	992	53.18	1092	82	1.18	1.68	1686	136	1.21	1.06
SP-B3	550	63.48	1092	82	1.09	1.35	1686	136	1.11	0.84
SP-C1	864	0.00	424	23	2.21	2.04	600	44	2.85	1.44
SSP1	1934	19.34	1440	339	1.25	1.41	2155	225	1.27	1.01
SSP3	1158	5.79	184	111	2.21	6.41	966	84	2.36	1.36
SSP4	1866	9.33	324	183	1.57	5.83	1755	155	1.60	1.16
Mean						**2.55**				**1.17**
COV						**0.70**				**0.15**

Table 5.2 Comparison of Test Results of API and CSA Standards

Table 5.2 indicates that the approach used in API Bulletin 2V is the most conservative of all the approaches presented in the table. The change in effective plate width between the 1995 and the 2002 editions of the DNV guideline results in only a very small change in predicted resistance as evidenced by the small change in mean and a coefficient of variation (COV) of the interaction value. CSA–S136–01 provides a prediction comparable to DNV. The interaction values based on DNV and CSA standards have a coefficient of variation (COV) of 13-15%, and on average are 14-21% higher than the test results.

5.2 Alternative Approach

An alternative prediction model based on the Perry-Robertson (Chen and Lui 1987) equation was examined. This approach has been used in the literature for predicting the overall buckling capacity of stiffened steel plates. The maximum axial stress is expressed as:

$$\sigma_{max} = \frac{P}{A}\left[1 + \frac{e\,c}{r_e^{\,2}}\frac{1}{1 - P/P_e}\right] \qquad [5.20]$$

where e is the axial load eccentricity, c is the distance from the centroid of the cross-section to the extreme fiber on the plate side, r_e is the radius of gyration of the reduced section, and the other variables are as described above. If the reduced cross-section is used for the calculations of the required section properties, the limiting value of the maximum stress, σ_{max}, is taken as the yield strength. Table 5.3 summarizes the predicted plate capacity for specimens tested in this series. The effective plate width used for the calculations presented in Table 5.3 was calculated based on CSA–S136–01. The eccentricity, e, is obtained by dividing the applied bending moment by the applied axial load at failure, as measured in the tests. Since no lateral loads were applied on the test specimens in the U of A test program, the measured load eccentricity was used directly in Equation [5.20]. The failure criterion was obtained by setting the maximum stress equal to the yield strength of the plate material. The predicted axial load capacity is the value of P that satisfies Equation [5.20]. The mean test to predicted ratio is equal to 0.97 and the COV is 0.11. It is noted that the Perry-Robertson equation, with an effective plate width predicted by the procedure outlined in CSA–S136–01, provides a suitable prediction of the test results. Of all the procedures investigated, this one provides the most accurate prediction of the test results.

Test Specimen	P_{test} (kN)	Effective e (mm)	$P_{predicted}$ (kN)	P_{test} / $P_{predicted}$
SP-A1	1098	3.0	1150	0.95
SP-A2	795	32.6	713	1.11
SP-A3	590	58.6	554	1.06
SP-B1	1334	26.7	1356	0.98
SP-B2	992	53.6	1049	0.95
SP-B3	550	115.4	705	0.78
SP-C1	864	3.0	791	1.09
SSP1	1934	10.0	2260	0.86
SSP3	1158	5.0	1195	0.97
SSP4	1866	5.0	1964	0.95
Mean				**0.97**
COV				**0.11**

Table 5.3 Predicted Maximum Axial Load using the Alternative Approach

6. SUMMARY

6.1 Testing Program

Typical buckling modes of stiffened steel plates include local plate buckling, overall column buckling, and stiffener tripping. Interaction of plate buckling and overall buckling was observed in past experiments. Numerical analyses and a limited number of previous tests suggested that interactive buckling occurred in axially compressed panels with an interaction index (defined in Equation [1.1]) that was equal to or greater than 1.0.

A test matrix consisting of four test series (i.e. SP-A, SP-B, SP-C and SP-D) was developed to examine the effect of bending moment, interaction index and damage on interactive buckling. Full-scale specimens which resembled stiffened plate panels in ship structures were fabricated using welded or hot-rolled T-stiffeners. Ten tests, including eight for "as-built" specimens and two for "damaged" specimens, were carried out in a high-capacity testing system. This unique system was developed during a previous SSC project (SSC-399) to study multiple buckling modes of stiffened plates under combined in-plane and out-of-plane loads, while maintaining an accurate representation of the boundary conditions applicable to a unidirectional stiffened plate within a grillage system.

In six tests of as-built specimens, plate buckling preceded and interacted with overall buckling. The other two as-built specimens, SP-B3 and SP-C2, failed by overall bending and interaction of plate buckling and stiffener tripping, respectively. Two specimens with simulated damage were also tested. The specimen with a web defect, SP-DA, sustained plate buckling and failed at the short section where the defect was located. The pre-deformed specimen SP-DB had an overall bending failure.

6.2 Effect of Test Variables

Effect of interaction index. Interaction of plate buckling and overall buckling was observed in the test of specimens with interaction indices varying from 0.6 to 1.5. Test results show that plate buckling initiated at about 70-75% of the ultimate failure load when the interaction index was approximately 1.0. For a lower interaction index, the difference between plate buckling load and ultimate load becomes smaller.

Effect of bending moment. Test results suggest that plate buckling tends to occur shortly before overall buckling for specimens subjected to high bending moments, even though the influence of bending moment is less significant in comparison to the interaction index. For example, specimen SP-B3 had the highest bending moment in the SP-B series and the plate did not buckle until bending failure took place. In addition, test results indicate that a consistent correlation between the normalized axial load and the bending moment exist for specimens with different sizes and materials. This relationship resembles the so-called interaction diagram used for beam-column design.

Effect of damage. The most significant reduction of axial load capacity occurred for pre-deformed specimens. As shown by SP-DB, an initial deflection of 1.8% span length led to a 38% reduction in the maximum axial load capacity. Comparison with as-built specimens suggests that the pre-deformed specimen achieved a similar maximum bending moment. The reduction of axial load is primarily attributed to the P-δ effect related to the initial deflection. Specimens with localized metal loss defects had a small reduction in load capacity; however, an unstable failure mode associated with a sudden decline of axial load was observed in the post-ultimate stage. This contrasted with the stable overall buckling failure of as-built specimens.

6.3 Design Issues

An evaluation of existing design methods concluded that the DNV design guidelines and the North America design standard for cold-formed structures, CSA-S136, provide an approach to deal with interactive buckling, by using a reduced plate width (effective width) to account for the effect of plate buckling when calculating the beam-column strength of a stiffened plate. Comparison with the test results demonstrated that predictions based on these guidelines are generally conservative and have a moderate COV of about 15%. In the case of SP-B3, the reduced width was overly conservative, as plate buckling did not occur during the test. Design guidelines that do not include plate width reduction cannot be applied to interactive buckling of stiffened plates, as illustrated by the evaluation of API Bulletin 2V.

On the basis of the above evaluation, an alternative design method that combines the reduced width due to plate buckling and the Perry-Robertson equation for beam-column design was proposed. A comparison with test results shows that, when predicting the ultimate axial load, the test-to-prediction ratio of this alternative approach has an average of 0.97 (i.e. prediction is 3% higher than test) and a COV of 11%.

All tests that involved interaction of plate buckling and overall buckling exhibited a gradual decline of axial load after the ultimate point. However, it is noted that two previous axial compression tests at the University of Alberta showed unstable post-ultimate behavior when the stiffened plates failed by interactive buckling. Also noted is the stiffener tripping failure of SP-C2 and SSP2, likely caused by a small inadvertent eccentricity or initial deflection that put the stiffener in flexural compression. Further investigation is recommended to identify conditions associated with these unstable failure modes, and to validate if such conditions exist in actual ship structures.

A literature search indicated that full-scale interactive buckling tests of hot-rolled stiffened plates have rarely been reported. Hence, test results presented in this document provide valuable data to verify ship structure design methods dealing with interactive buckling. Further experiments and numerical modeling are recommended for representative stiffener designs, steel grades, and load conditions.

With respect to the assessment of in-service structures, test results suggest that the reduced load capacity associated with pre-bending deformation can be addressed using existing design methods by including the P-δ effect. Localized metal loss defects may cause stiffened plates to fail by unstable buckling modes which are different from those of as-built structures. Further

study is required to develop assessment methods based on the validation of defect types and load conditions associated with such unstable failures.

7. REFERENCES

American Petroleum Institute (2000). API Bulletin 2V, Design of Flat Plate Structures. Second edition, American Petroleum Institute, Washington, D.C.

Canadian Standards Association (2001). S136–01, North American Specification for the Design of Cold-Formed Steel Structural Members. Canadian Standards Association, Toronto, Ontario.

Canadian Standards Association (2001). S16-01, Limit States Design of Steel Structures. Canadian Standards Association, Toronto, Ontario.

Chen, Q., DeGeer, D. and Kennedy, B.W. (1996). Strength and Stability Testing of Stiffened Plate Components. C-FER Report No. 95026, C-FER Technologies Inc., Edmonton, Alberta. September.

Chen, W.F. and Lui, E.M. (1987). Structural Stability – Theory and Implementation. Elsevier Science Publishing Co., New York.

Det Norske Veritas (1995). Classification Notes No. 30.1, Buckling Strength Analysis, Det Norske Veritas, Hovik, Norway.

Det Norske Veritas (2002). Recommended Practice DNV-RP-C201, Buckling Strength of Plated Structures, Det Norske Veritas, Hovik, Norway.

Faulkner, D. (1975). A Review of Effective Plating for use in the Analysis of Stiffened Plating in Bending and Compression, Journal of Ship Research, Vol. 19, No. 1, pp. 1 – 17.

Grondin, G.Y., E. Wang, and A.E. Elwi (2002), Interaction Buckling of Stiffened Steel Plates, 2002 Annual Technical Session and Meeting of the Structural Stability Research Council, April.

Sheikh, I.A., G.Y. Grondin, and A.E. Elwi (2000). Buckling of Stiffened Steel Plates Under Uniaxial Compression and Bending. CSCE Conference, London, Ontario, Canada, June.

SSRC 1988. Guide to Stability Design Criteria for Metal Structures. Structural Stability Research Council, ed. By T.V. Galambos, 4th ed., Wiley, New York.

von Karman, T., E.E. Sechler and L.H. Donnell (1932). The Strength of Thin Plates in Compression. *Transactions ASME*, Vol. 54, APM 54-5.

Yu, W.W. (2000). Cold-Formed Steel Design. Third Edition, John Wiley & Sons, Inc., New York.

APPENDIX A MEASURED PLATE IMPERFECTIONS

(All initial displacements in inches. All measurement grids in mm.)

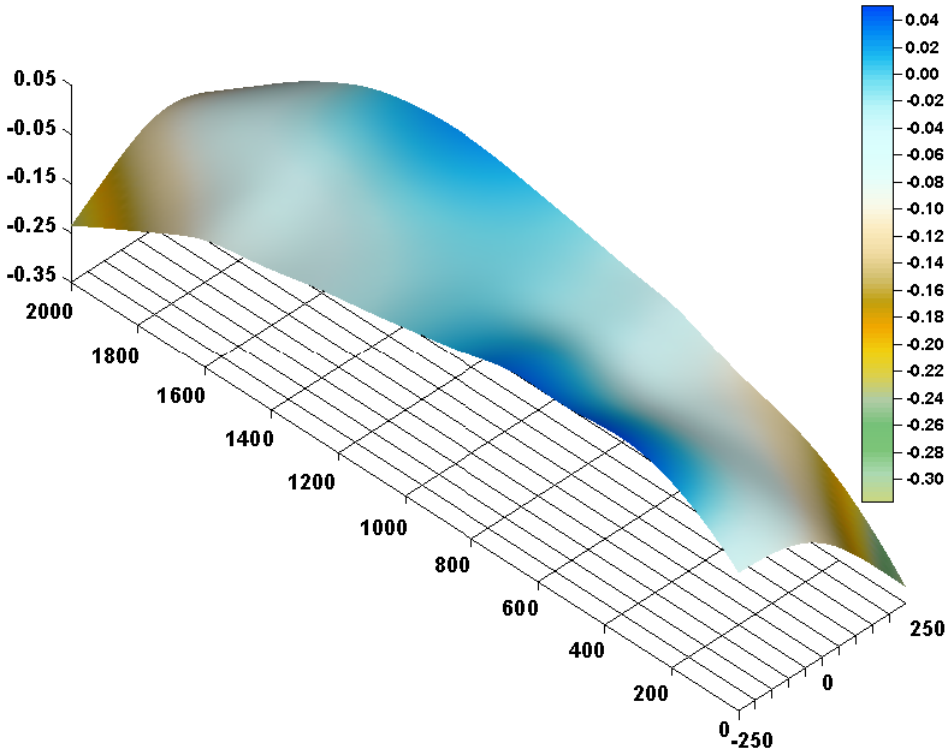

Figure A.1 Plate Imperfections of SP-A1

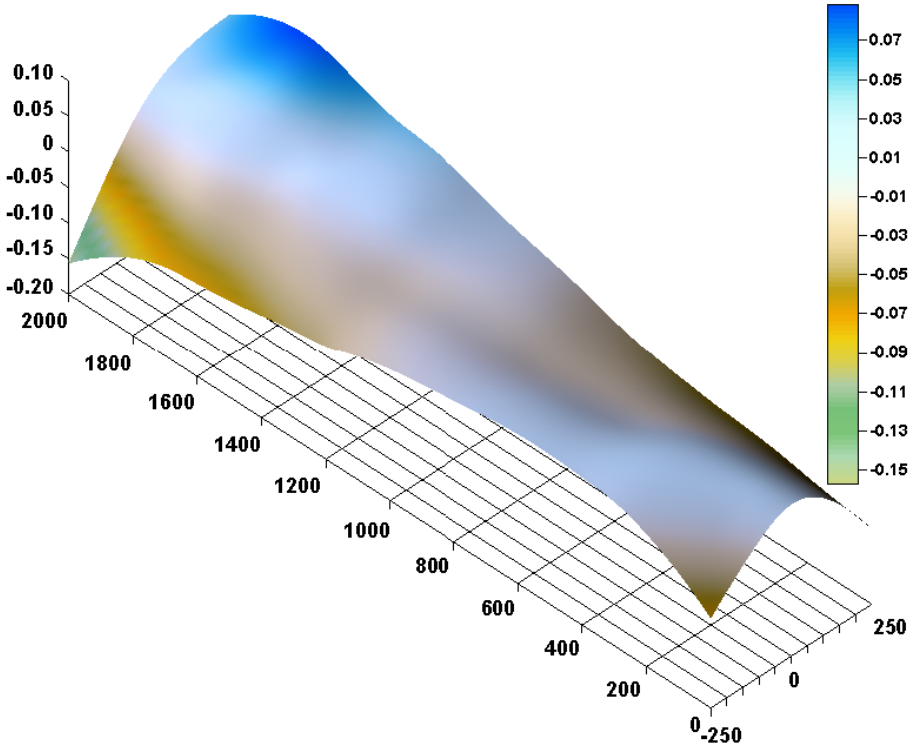

Figure A.2 Plate Imperfections of SP-A2

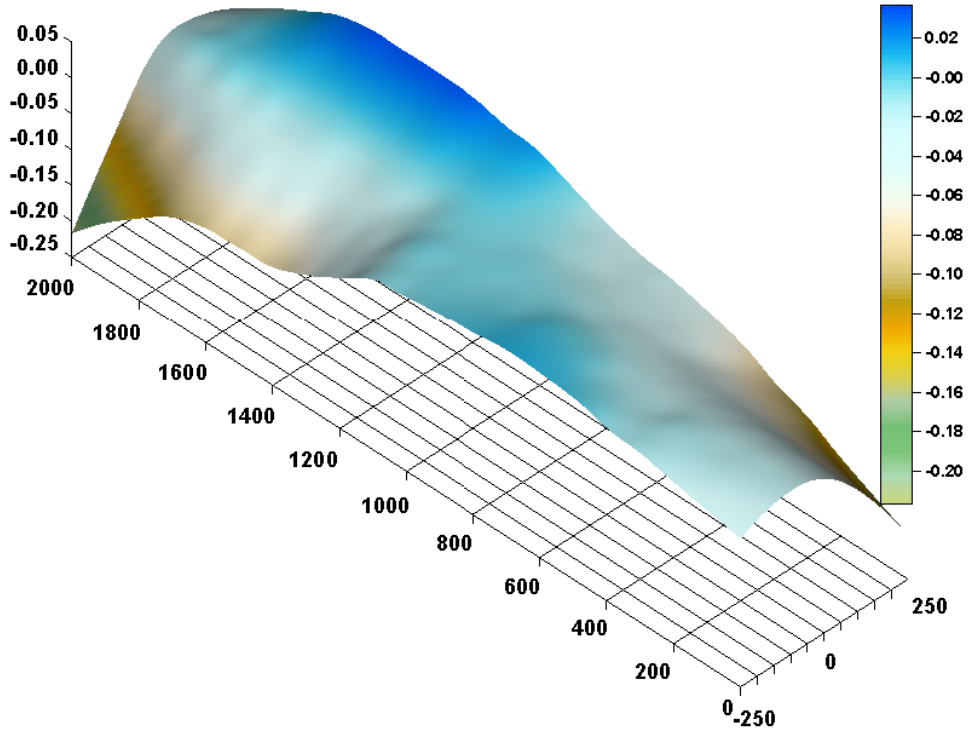

Figure A.3 Plate Imperfections of SP-A3

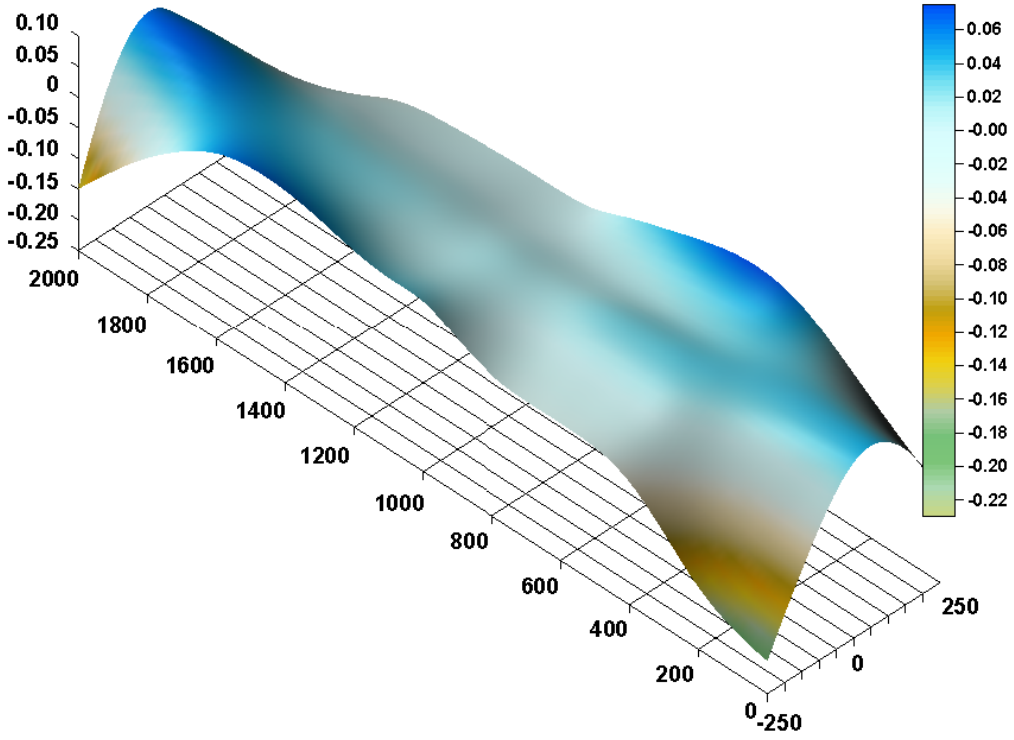

Figure A.4 Plate Imperfections of SP-B1

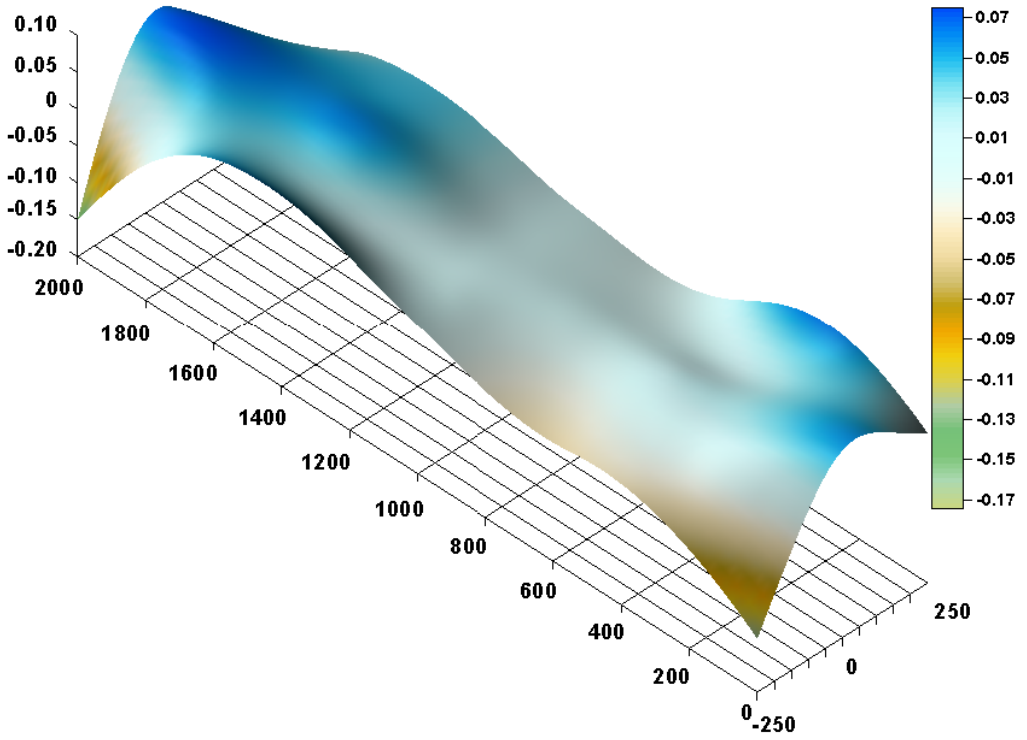

Figure A.5 Plate Imperfections of SP-B2

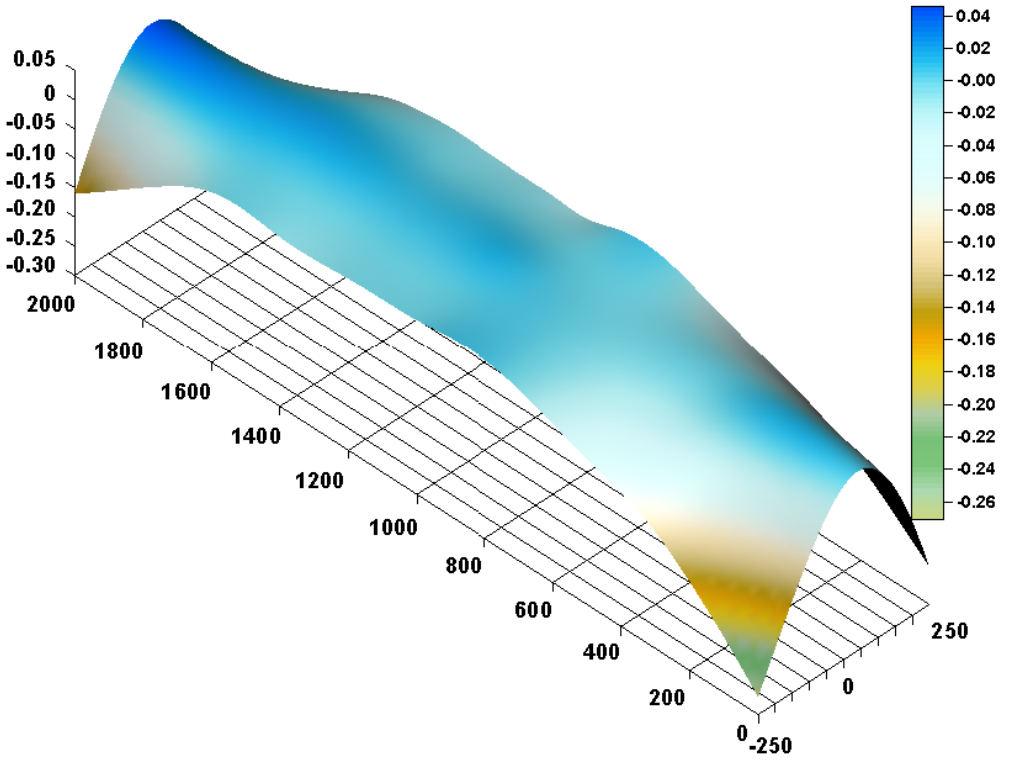

Figure A.6 Plate Imperfections of SP-B3

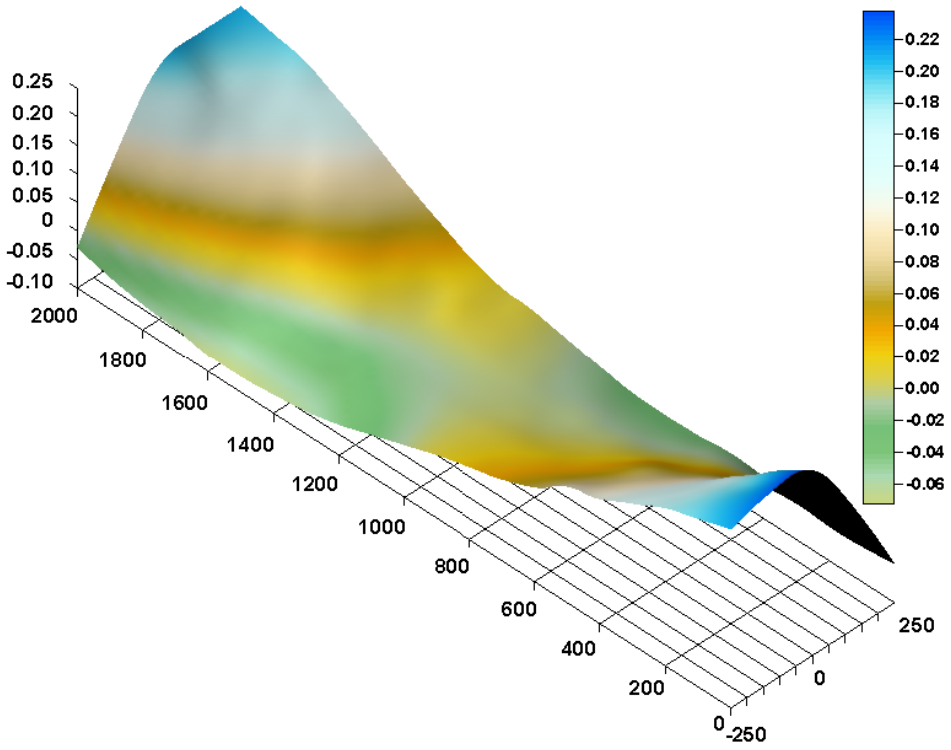

Figure A.7 Plate Imperfections of SP-C1

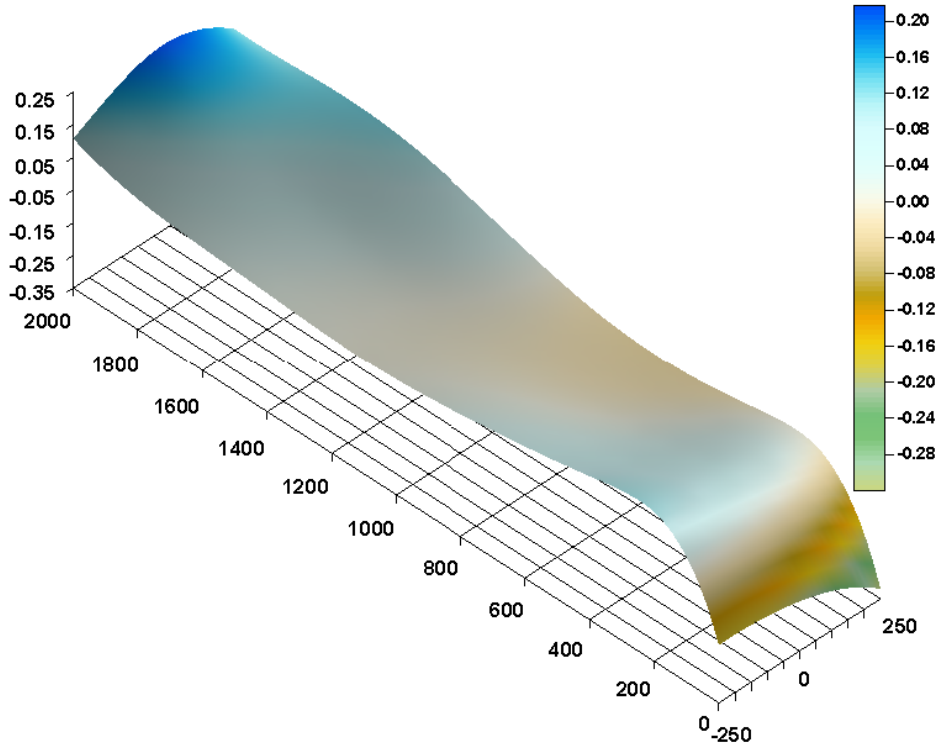

Figure A.8 Plate Imperfections of SP-C2

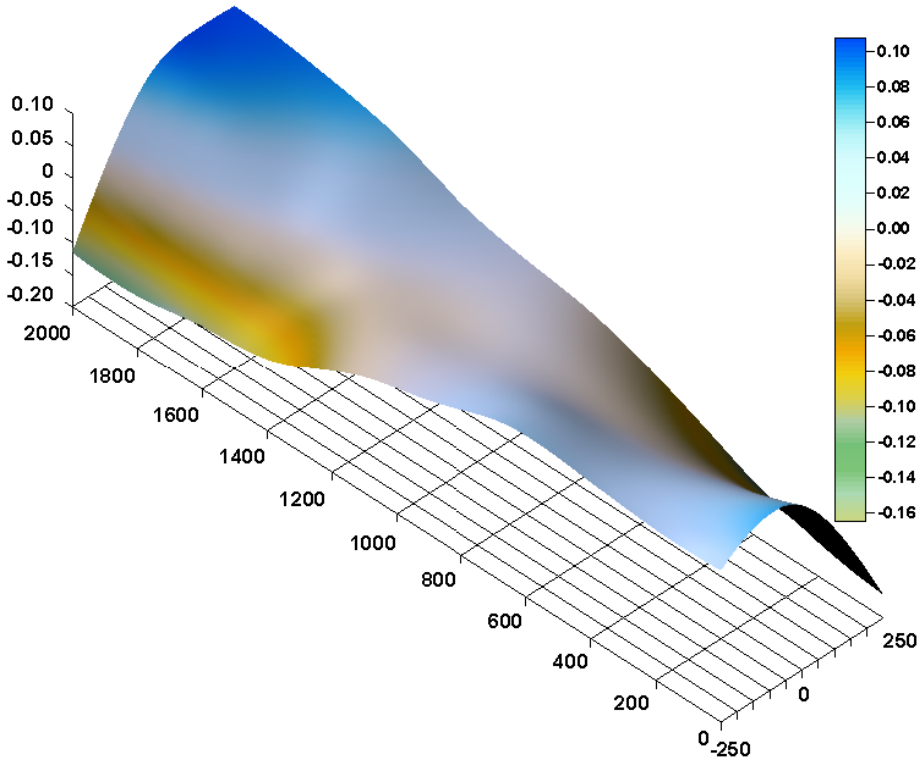

Figure A.9 Plate Imperfections of SP-DA

APPENDIX B TEST SUMMARY SHEETS

Specimen Type: As-Built

Type of Damage/Deformation: N/A

Load Configuration:
Axial compression only.

Failure Mode: Plate Buckling followed by Overall Buckling

Maximum Axial Load: 1118 kN
Mid-Span Moment at Max. Load: 8.4 kN-m

Test Summary

Pre-ultimate:
Plate buckling waves initiate and amplify gradually. Stiffener remains straight.

At ultimate:
No change in behavior at ultimate strength.

Post-ultimate:
Gradual loss in capacity. Continued amplification of Overall Buckling waves. Plate Buckling Waves diminish. Stiffener does not trip.

Schematic:

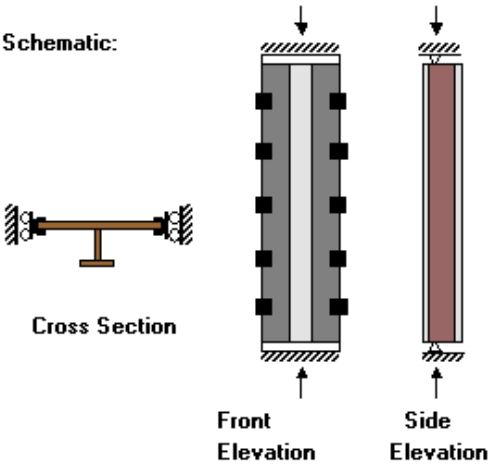

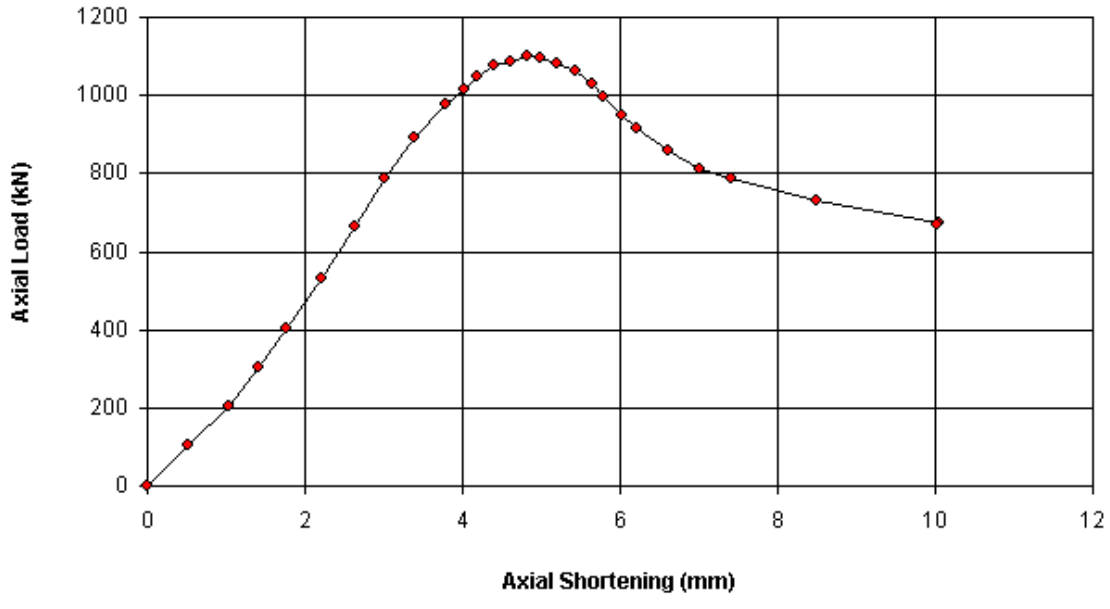

Load versus Axial Shortening Response

Figure B.1 Test Summary Sheet of SP-A1

Specimen Type: As-Built

Type of Damage/Deformation: N/A

Load Configuration:
Axial compression with two 30 kN
lateral loads. Plate in flexural compression.

Failure Mode: Plate Buckling followed by Overall Buckling

Maximum Axial Load: 830 kN
Mid-Span Moment at Max. Load: 40.6 kN-m

Test Summary

Pre-ultimate:
Plate buckling waves initiate and amplify gradually.
Stiffener remains straight.

At ultimate:
No change in behavior at ultimate strength.

Post-ultimate:
Gradual loss in capacity. Continued amplification of
Overall Buckling waves. Plate Buckling Waves diminish.
Stiffener does not trip.

Schematic:

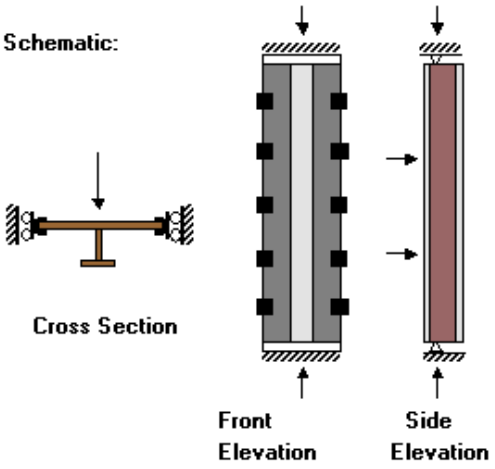

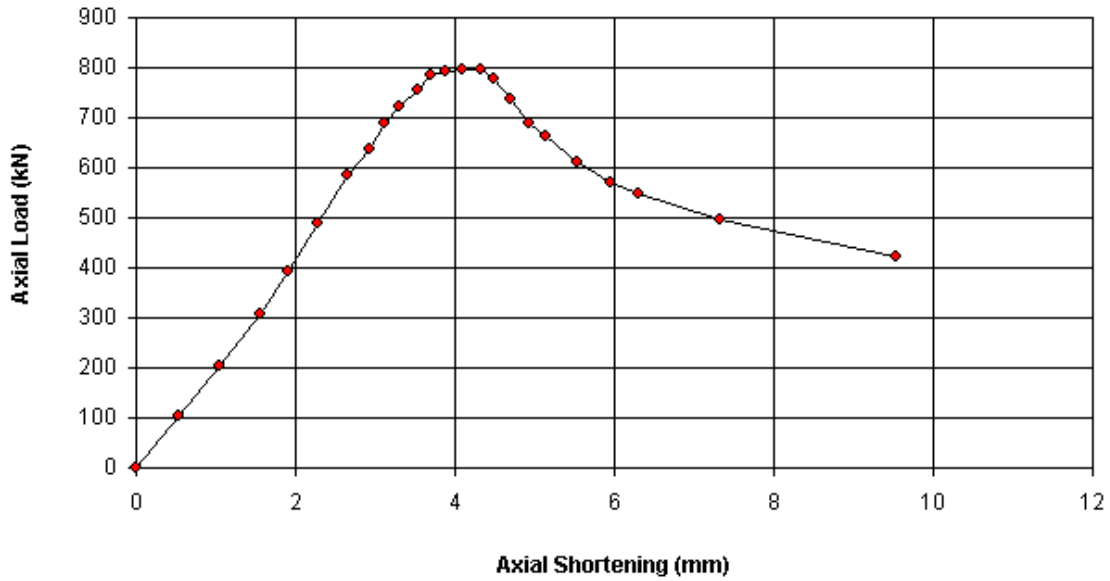

Load versus Axial Shortening Response

Figure B.2 Test Summary Sheet of SP-A2

Specimen Type: As-Built

Type of Damage/Deformation: N/A

Load Configuration:
Axial compression with two 40 kN
lateral loads. Plate in flexural compression.

Failure Mode: Plate Buckling followed by Overall Buckling

Maximum Axial Load: 621 kN
Mid-Span Moment at Max. Load: 49 kN-m

Test Summary

Pre-ultimate:
Plate buckling waves initiate and amplify gradually.
Stiffener remains straight.

At ultimate:
No change in behavior at ultimate strength.

Post-ultimate:
Gradual loss in capacity. Continued amplification of buckling waves. Stiffener does not trip.
Lateral Load reduced to 35 kN at 5.7 mm of axial shortening.

Schematic:

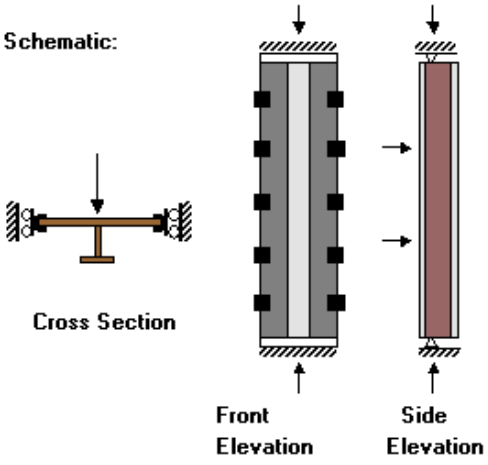

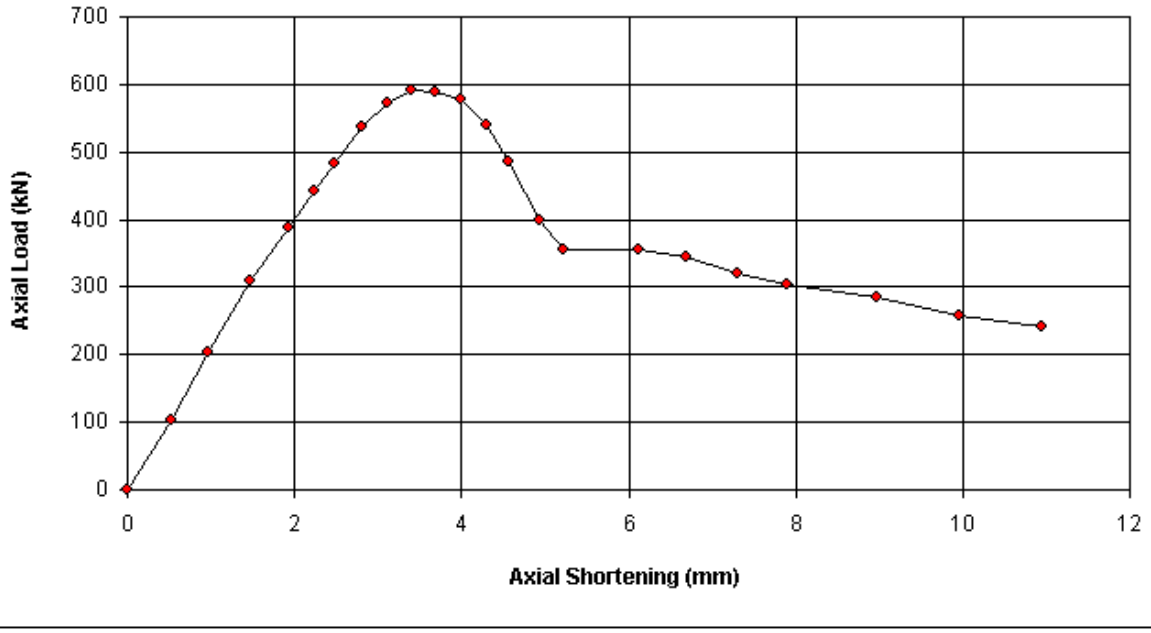

Load versus Axial Shortening Response

Figure B.3 Test Summary Sheet of SP-A3

Specimen Type: As-Built

Type of Damage/Deformation: N/A

Load Configuration:
Axial compression with two 40 kN lateral loads. Plate is in flexural tension.

Failure Mode: Plate Buckling followed by Overall Buckling

Maximum Axial Load: 1354 kN
Mid-Span Moment at Max. Load: 52.8 kN-m

Test Summary

Pre-ultimate:
Plate buckling waves initiate and amplify gradually. Stiffener remains straight.

At ultimate:
No change in behavior at ultimate strength.

Post-ultimate:
Gradual loss in capacity. Continued amplification of buckling waves. Stiffener does not trip.

Schematic:

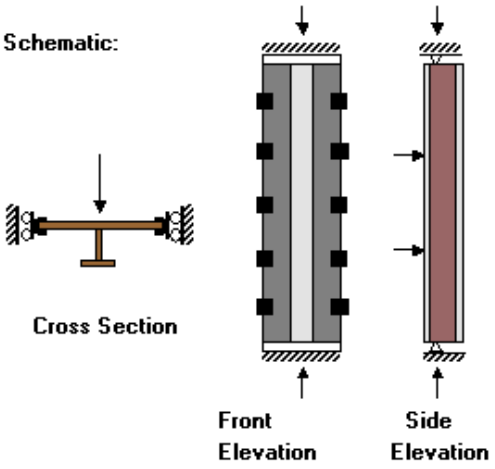

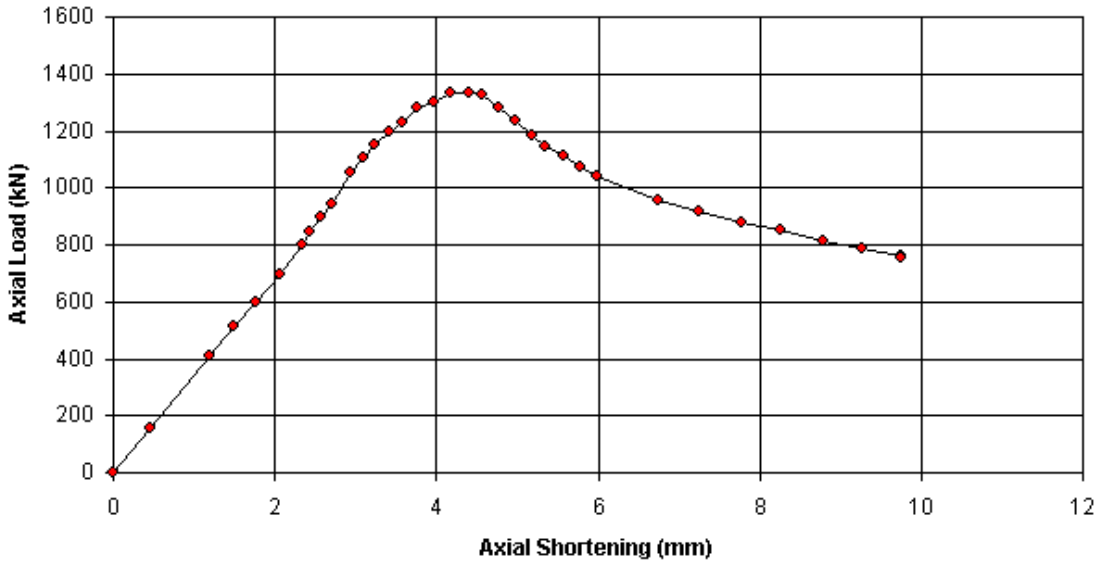

Load versus Axial Shortening Response

Figure B.4 Test Summary Sheet of SP-B1

Specimen Type: As-Built

Type of Damage/Deformation: N/A

Load Configuration:
Axial compression with two 60 kN lateral loads.
Plate in flexural tension

Failure Mode: Plate Buckling followed by Overall Buckling

Maximum Axial Load: 999 kN
Mid-Span Moment at Max. Load: 72.3 kN-m

Test Summary

Pre-ultimate:
Stiffener tripping initiates and amplifies gradually.
Plate remains flat.

At ultimate:
Sudden increase in tripping deformation accompanied by sudden, 30% loss in capacity.

Post-ultimate:
Gradual loss in capacity. Continued amplification of stiffener tripping. Plate does not buckle.

Schematic:

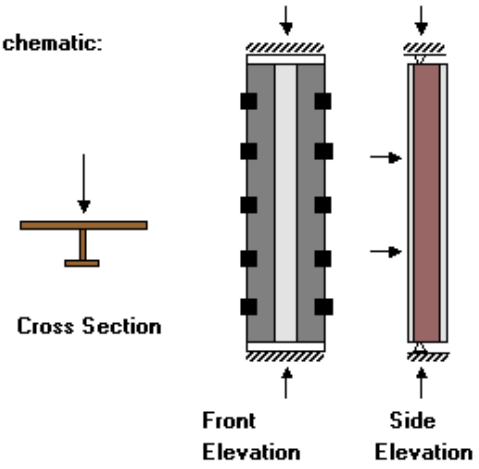

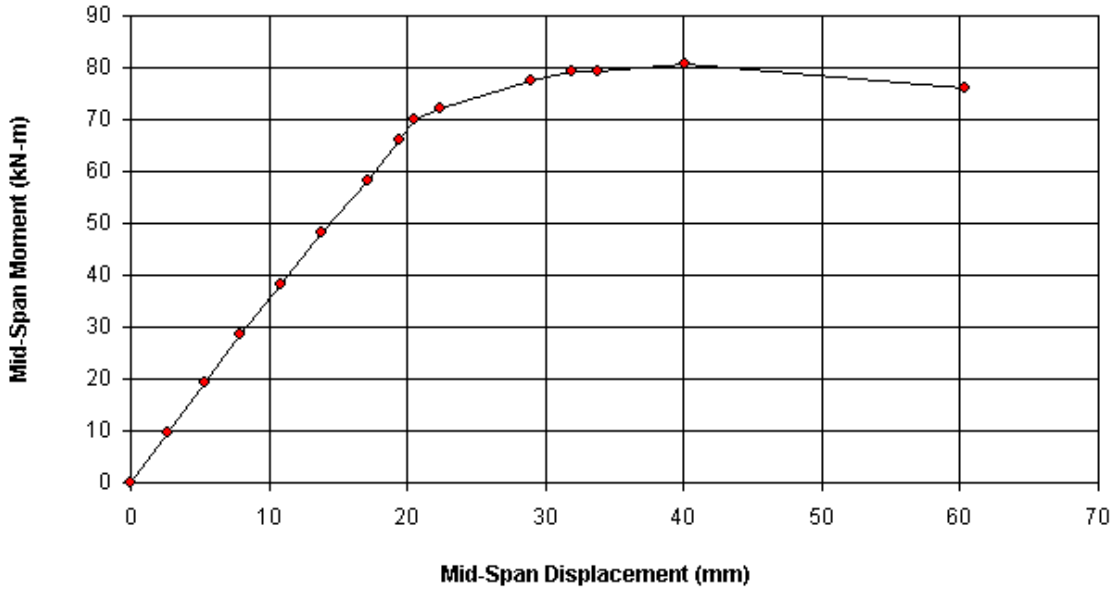

Load versus Displacement Response

Figure B.5 Test Summary Sheet of SP-B2

Specimen Type: As-Built

Type of Damage/Deformation: N/A

Load Configuration:
Axial compression with two 74 kN lateral loads. Plate is on the tension side.

Failure Mode: Overall Bending

Maximum Axial Load: 559 kN
Mid-Span Moment at Max. Load: 80.9 kN-m

Test Summary

Pre-ultimate:
Plate buckling followed by bending.

At ultimate:
Sudden increase in midspan displacement accompanied by sudden loss in capacity.

Post-ultimate:
Entire stiffener had yielded in plastic deformation
Plate does not show any physical signs of buckling.

Schematic:

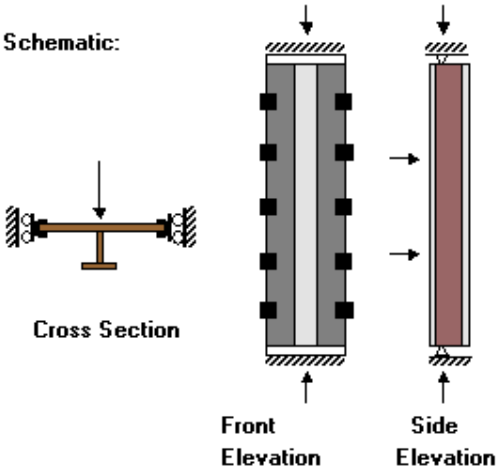

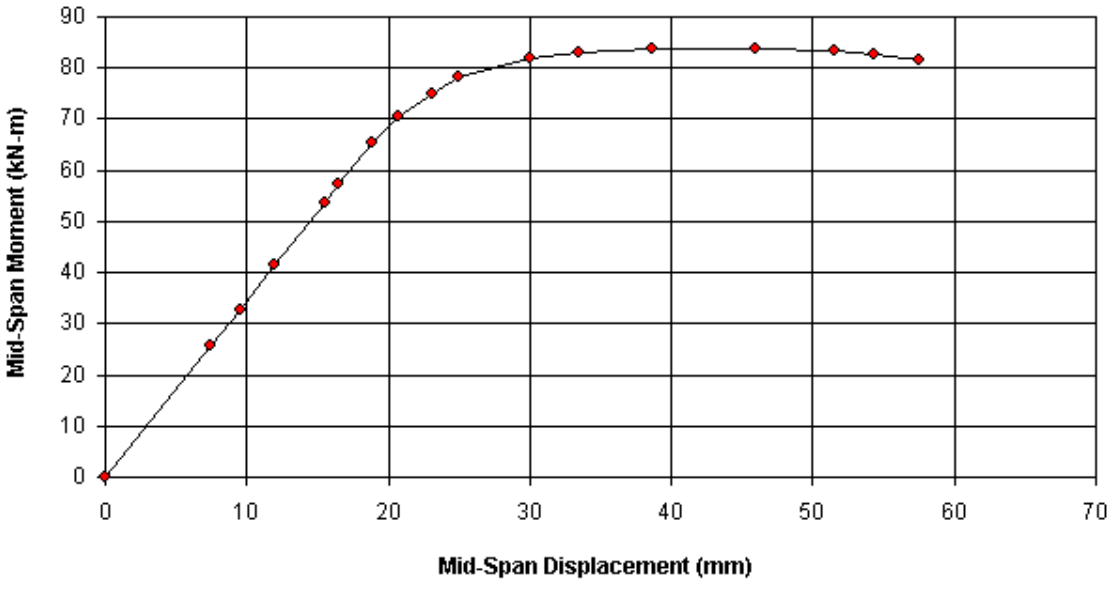

Load versus Displacement Response

Figure B.6 Test Summary Sheet of SP-B3

Specimen Type: As-Built

Type of Damage/Deformation: N/A

Load Configuration:
Axial compression only.

Failure Mode: Plate Buckling followed by Overall Buckling

Maximum Axial Load: 883 kN
Mid-Span Moment at Max. Load: 6.6 kN-m

Test Summary

Pre-ultimate:
Plate buckling waves initiate and amplify gradually. Stiffener remains straight.

At ultimate:
No change in behavior at ultimate.

Post-ultimate:
Gradual loss in capacity. Continued amplification of buckling waves. Stiffener does not trip.

Schematic:

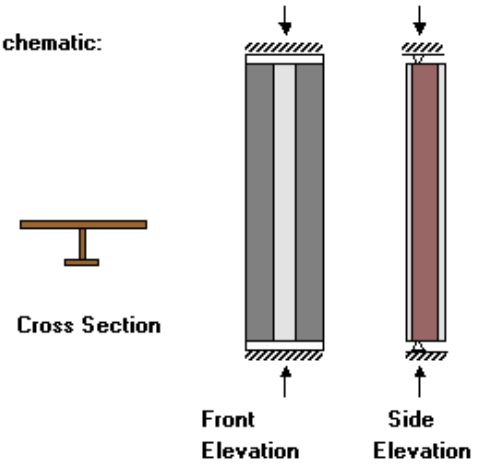

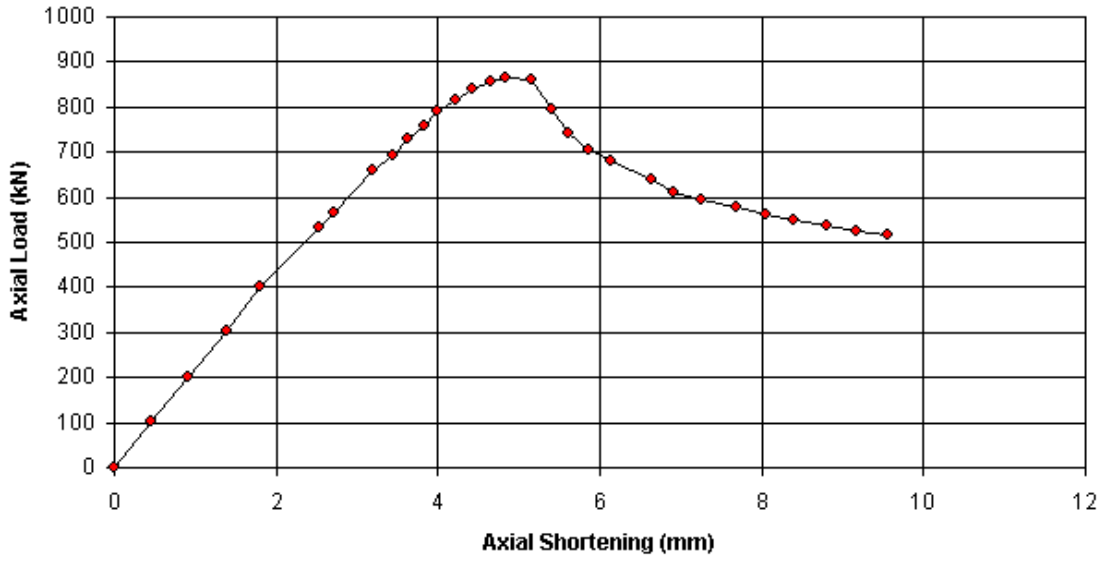

Load versus Axial Shortening Response

Figure B.7 Test Summary Sheet of SP-C1

Specimen Type: As-Built

Type of Damage/Deformation: N/A

Load Configuration:
Axial compression only.

Failure Mode: Plate Buckling followed by Stiffener Tripping

Maximum Axial Load: 1160 kN
Mid-Span Moment at Max. Load: 12 kN-m

Test Summary

Pre-ultimate:
Plate buckling waves initiate and amplify gradually. Stiffener trips.

At ultimate:
Stiffener trips resulting in a sudden loss of capacity.

Post-ultimate:
Gradual loss in capacity. Continued amplification of buckling waves. Stiffener continues to rotate.

Schematic:

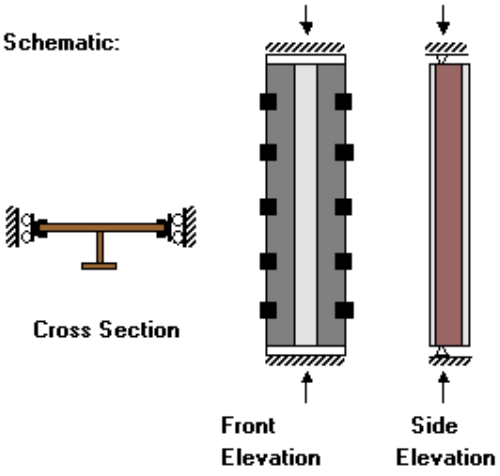

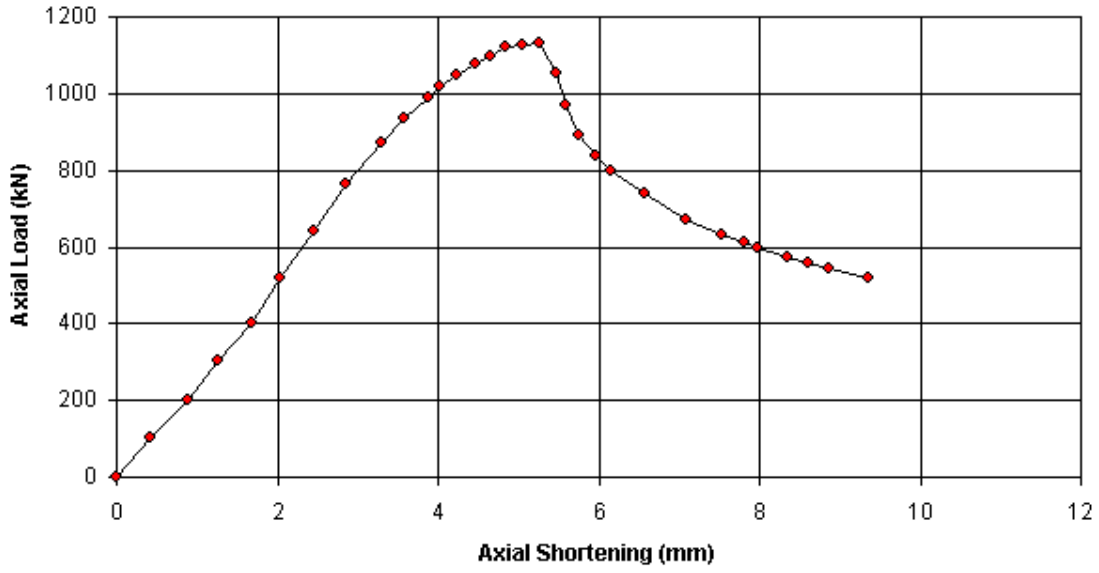

Load versus Axial Shortening Response

Figure B.8 Test Summary Sheet of SP-C2

Specimen Type: Damaged

Type of Damage/Deformation: Metal loss defect machined in stiffener web at midspan.

Load Configuration:
Axial compression only.

Failure Mode: Plate buckling followed by local stiffener failure (midspan portion buckles in the plane of the web).

Maximum Axial Load: 1036 kN
Mid-Span Moment at Max. Load: 1.8 kN-m

Test Summary

Pre-ultimate:
Plate buckling waves initiate and amplify gradually. Stiffener remains straight.

At ultimate:
Midspan portion (about 200 mm long) suddenly buckles in the plane of the web. Plate buckling waves disperse.

Post-ultimate:
Deformation concentrates at midspan in vicinity of web "damage". Specimen suffers dramatic loss in axial load capacity.

Schematic:

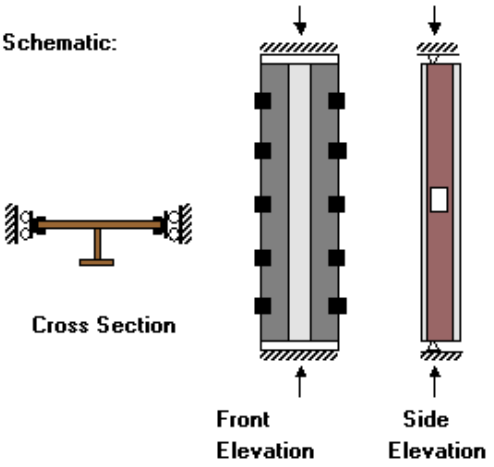

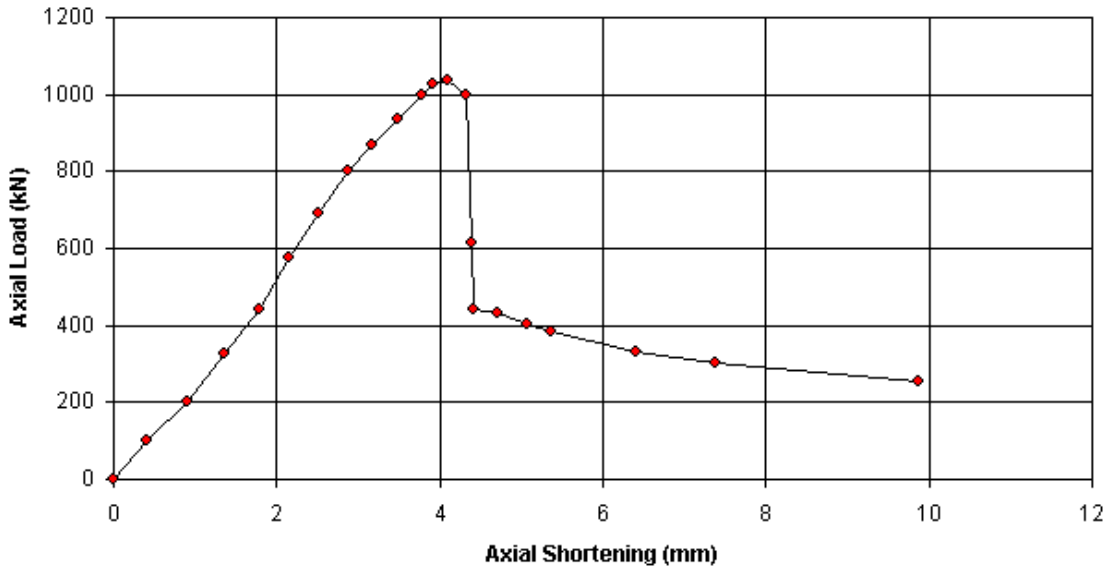

Load versus Axial Shortening Response

Figure B.9 Test Summary Sheet of SP-DA

Specimen Type: Deformed

Type of Damage/Deformation: Initial bending deformation with a mid-span defelection of 36 mm.

Load Configuration:
Axial compression with two 40 kN lateral loads. Plate is on the tension side.

Failure Mode: Overall Bending

Maximum Axial Load: 864 kN
Mid-Span Moment at Max. Load: 83.1 kN-m

Test Summary

Pre-ultimate:
Plate Bending
Stiffener remains straight.

At ultimate:
No change in behavior at ultimate.

Post-ultimate:
Gradual loss in capacity.
Stiffener does not trip.

Schematic:

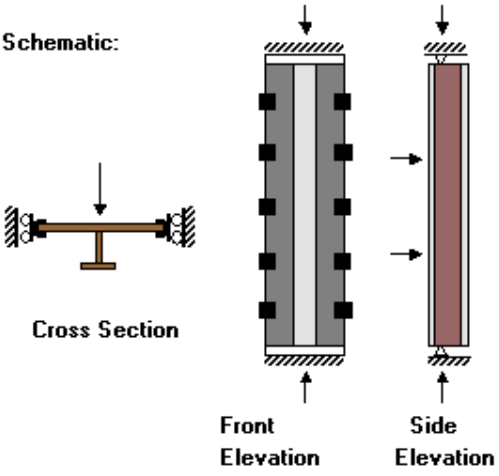

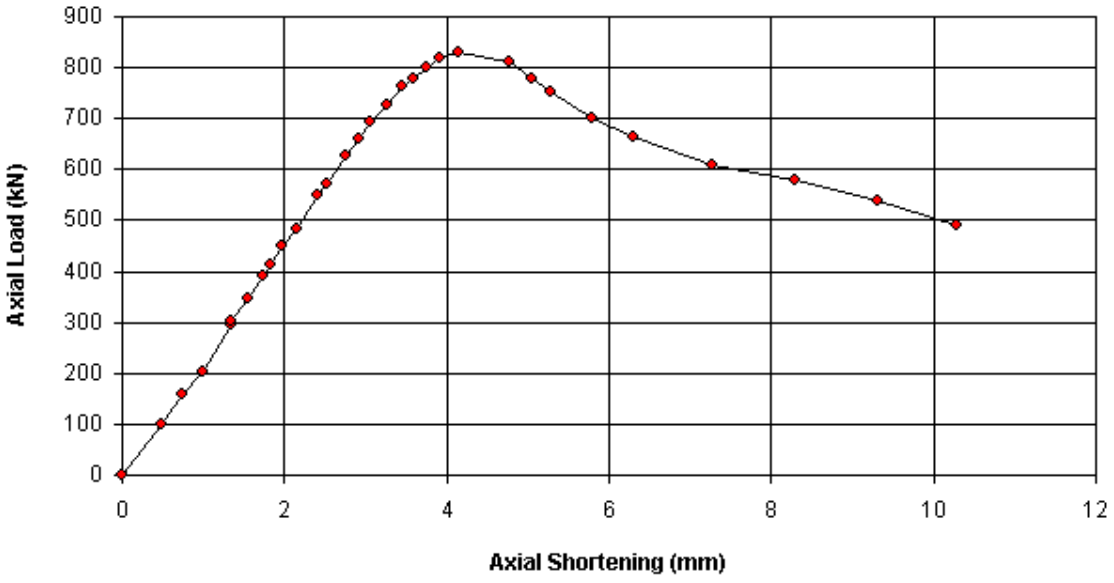

Load versus Axial Shortening Response

Figure B.10 Test Summary Sheet of SP-DB

SHIP STRUCTURE COMMITTEE PARTNERS AND LIAISON MEMBERS

PARTNERS

The Society of Naval Architects and Marine Engineers

Mr. Joe Cuneo
President,
Society of Naval Architects and Marine Engineers

Dr. John Daidola
Chairman,
SNAME Technical & Research Steering Committee

The Gulf Coast Region Maritime Technology Center

Dr. John Crisp
Executive Director,
Gulf Coast Maritime Technology Center

Dr. Bill Vorus
Site Director,
Gulf Coast Maritime Technology Center

LIAISON MEMBERS

American Iron and Steel Institute
American Society for Testing & Materials
American Society of Naval Engineers
American Welding Society
Bethlehem Steel Corporation
Canada Center for Minerals & Energy Technology
Colorado School of Mines
Edison Welding Institute
International Maritime Organization
International Ship and Offshore Structure Congress
INTERTANKO
Massachusetts Institute of Technology
Memorial University of Newfoundland
National Cargo Bureau
Office of Naval Research
Oil Companies International Maritime Forum
Tanker Structure Cooperative Forum
Technical University of Nova Scotia
United States Coast Guard Academy
United States Merchant Marine Academy
United States Naval Academy
University of British Columbia
University of California Berkeley
University of Houston - Composites Eng & Appl.
University of Maryland
University of Michigan
University of Waterloo
Virginia Polytechnic and State Institute
Webb Institute
Welding Research Council
Worchester Polytechnic Institute
World Maritime Consulting, INC

Mr. Alexander Wilson
Captain Charles Piersall (Ret.)
Captain Dennis K. Kruse (USN Ret.)
Mr. Richard Frank
Dr. Harold Reemsnyder
Dr. William R. Tyson
Dr. Stephen Liu
Mr. Dave Edmonds
Mr. Tom Allen
Dr. Alaa Mansour
Mr. Dragos Rauta
Mr. Dave Burke / Captain Chip McCord
Dr. M. R. Haddara
Captain Jim McNamara
Dr. Yapa Rajapaksie
Mr. Phillip Murphy
Mr. Rong Huang
Dr. C. Hsiung
Commander Kurt Colella
Dr. C. B. Kim
Dr. Ramswar Bhattacharyya
Dr. S. Calisal
Dr. Robert Bea
Dr. Jerry Williams
Dr. Bilal Ayyub
Dr. Michael Bernitsas
Dr. J. Roorda
Dr. Alan Brown
Dr. Kirsi Tikka
Dr. Martin Prager
Dr. Nick Dembsey
VADM Gene Henn, USCG Ret.

RECENT SHIP STRUCTURE COMMITTEE PUBLICATIONS

Ship Structure Committee Publications on the Web - All reports from SSC 392 and forward are available to be downloaded from the Ship Structure Committee Web Site at URL:
http://www.shipstructure.org
SSC 391 and below are available on the SSC CD-ROM Library. Visit the National Technical Information Service (NTIS) Web Site for ordering information at URL:
http://www.ntis.gov/fcpc/cpn7833.htm

SSC Report Number	Report Bibliography
SSC 432	**Adaptation of Commercial Structural Criteria to Military Needs** R.Vara, C.M. Potter, R.A. Sielski, J.P. Sikora, L.R. Hill, J.C. Adamchak, D.P. Kihl, J. Hebert, R.I. Basu, L. Ferreiro, J. Watts, P.D. Herrington 2003
SSC 431	**Retention of Weld Metal Properties and Prevention of Hydrogen Cracking** R.J. Wong 2003
SSC 430	**Fracture Toughness of a Ship Structure** A.Dinovitzer, N. Pussegoda, 2003
SSC 429	**Rapid Stress Intensity Factor Solution Estimation for Ship Structures Applications** L. Blair Carroll, S. Tiku, A.S. Dinovitzer 2003
SSC 428	**In-Service Non-Destructive Evaluation of Fatigue and Fracture Properties for Ship Structure** S. Tiku 2003
SSC 427	**Life Expectancy Assessment of Ship Structures** A. Dinovitzer 2003
SSC 426	**Post Yield Stability of Framing** J. DesRochers, C. Pothier, E. Crocker 2003
SSC 425	**Fatigue Strength and Adequacy of Weld Repairs** R.J. Dexter, R.J. Fitzpatrick, D.L. St. Peters 2003
SSC 424	**Evaluation of Accidental Oil Spills from Bunker Tanks (Phase I)** T. McAllister, C. Rekart, K. Michel 2003
SSC 423	**Green Water Loading on Ship Deck Structures** M. Meinhold, D. Liut, K. Weems, T. Treakle, Woe-Min Lin 2003
SSC 422	**Modeling Structural Damage in Ship Collisions** Dr. A.J. Brown 2003
SSC 421	**Risk Informed Inspection of MarineVessels** Dr. B.M. Ayyub, U.O. Akpan, P.A. Rushton, T.S. Koko, J. Ross, J. Lua 2003